



3 1293 00993 0979



This is to certify that the

thesis entitled

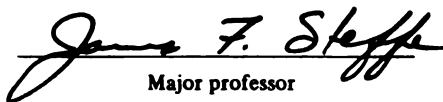
NON-NEWTONIAN SHEAR RATE APPROXIMATIONS AND
OPTIMAL EXPERIMENTAL CONDITIONS IN BACK
EXTRUSION TESTING

presented by

Nelly J. Marte Guzman

has been accepted towards fulfillment
of the requirements for

M.S. degree in Food Engineering


Major professor

Date 7 July 87



RETURNING MATERIALS:
Place in book drop to
remove this checkout from
your record. FINES will
be charged if book is
returned after the date
stamped below.

NOV 11 6 32 00 PM '11		
-----------------------	--	--

**NON-NEWTONIAN SHEAR RATE APPROXIMATIONS AND OPTIMAL
EXPERIMENTAL CONDITIONS IN BACK EXTRUSION TESTING**

By

Nelly J. Marte Guzman

A THESIS

**Submitted to
Michigan State University
in partial fulfillment of the requirements
for the degree of**

MASTER OF SCIENCE

Department of Food Science and Human Nutrition

1987

ABSTRACT

NON-NEWTONIAN SHEAR RATE APPROXIMATIONS AND OPTIMAL EXPERIMENTAL CONDITIONS IN BACK EXTRUSION TESTING

By

Nelly J. Marte Guzman

Newtonian approximation for power law fluids and power law approximation for Herschel-Bulkley fluids, as well as optimal experimental conditions in back extrusion or annular pumping testing were considered in this study.

The results obtained with the back extrusion device were in good agreement with those obtained with the Haake viscometer. Best results were obtained with the back extruder using a plunger to cup radius ratio between 0.77 and 0.85 and a plunger velocity combination in the ratio of 4.0 to 5.0. Under those optimal experimental conditions the power law approximation for Herschel-Bulkley fluids works in excellent agreement with actual values. The Newtonian approximation for power law fluids also works well but may vary with the rheological properties.

To avoid end effects in back extrusion testing, the plunger bottom should be separated from the container bottom a minimum distance equivalent to the inner container diameter at the end of the experiment.

To: my parents David and Lindin,
my daughter Nellie Grace,
my sister Nana and
my husband Miguel Angel.

ACKNOWLEDGMENTS

The author wishes to thank Dr. Ronnie Morgan, Dr. Robert Ofoli and Dr. Mark Uebersax, members of the committee, for their helpful comments. Special recognition to Dr. James Steffe who serves as Major Advisor for his guidance and confidence.

Sincere thanks also to The Partners of the Americas for its financial contribution in support of the program.

Finally, thanks to all those friends who offered their time and expertise, especially Melania Molina, Fernando Osorio and Fernando Hirujo.

TABLE OF CONTENTS

	<u>Page</u>
List of Tables	vii
List of Figures	ix
Nomenclature	xii
 <u>CHAPTERS</u>	
1. Introduction	1
2. Literature Review	3
2.1 Newtonian Model	3
2.2 Non-Newtonian Models	4
2.2.1 The Power Law Fluid Model	5
2.2.2 The Bingham Plastic Model	6
2.2.3 The Herschel-Bulkley Model	7
2.3 Viscometers and Rheometers	7
2.3.1 Back Extrusion Technique	8
3. Theoretical Development	10
3.1 Basic Theories	10
3.1.1 Back Extrusion of Newtonian Fluids	10
3.1.2 Back Extrusion of Power Law Fluids	13
3.1.3 Back Extrusion of Herschel-Bulkley Fluids	17
3.1.4 Procedure for the Determination of Rheological Properties of a Herschel- Bulkley Fluid	23
3.2 Computer Programs for Non-Newtonian Fluids	24
4. Experimental Procedure Applications	26
4.1 Equipment, Materials and Methods	26

4.2	Effect of Plunger Velocity and Plunger Radius ..	27
4.3	Newtonian Approximation for Power Law Fluids Based on Simulated Data	29
4.4	Power Law Approximation for Herschel- Bulkley Fluids Based on Simulated Data	32
4.5	Newtonian Approximation for Power Law Fluids Based on Experimental Data	37
4.6	Power Law Approximation for Herschel- Bulkley Fluids Based on Experimental Data	42
4.7	End Effects	44
5.	Results and Discussion	48
5.1	Shear Rate Approximations Based on Theoretical Data	48
5.1.1	Newtonian Approximation for Power Law Fluids	48
5.1.2	Power Law Approximation for Herschel- Bulkley Fluids	58
5.2	Shear Rate Approximation Based on Experimental Data	72
5.2.1	Newtonian Approximation for Power Law Fluids	72
5.2.2	Power Law Approximation for Herschel Bulkley Fluids	85
5.3	End Effect Evaluation	92
6.	Conclusions	99
7.	Practical Guidelines for Conducting Back Extrusion Testing	101
8.	Suggestions for Future Research	102
9.	References	104
10.	Appendices	
A:	RHEO - Programs for Non-Newtonian Fluids in Back Extrusion Testing	107

B:	Calculation example for the power law shear rate at the wall as an approximation to the shear rate at the wall for Herschel-Bulkley fluids, based on simulated data	113
C:	1. Calculation example for the determination of rheological properties of a power law fluid using the back extrusion device	118
	2. Calculation example for shear stress and shear rate at the wall of Herschel-Bulkley fluid and approximated to power law values	121
D:	Table of Results	125

LIST OF TABLES

Table	Page
1 Rheological properties and experimental conditions for power law fluids used in the Newtonian approximation based on simulated data	33
2 Rheological properties and experimental conditions for Herschel-Bulkley fluids used in the power law approximation based on simulated data	38
3 Shear rate at the wall for Newtonian fluids from Morgan's equation	49
4 Shear rate at the wall ranges for different flow behavior indices corresponding to different power law fluids	53
5 Rheological properties of power law fluids determined using the Haake viscometer data over a shear rate range of 10 - 100 s ⁻¹	74
6 Shear stress and shear rate values for 1.0 % Methocel obtained using the Haake viscometer	75
7 Shear stress and shear rate values for 2.0 % Methocel obtained using the Haake viscometer	76
8 Shear stress and shear rate values for 1.0 % guar gum obtained using the Haake viscometer	77
9 Shear stress and shear rate values for 1.5 % guar gum obtained using the Haake viscometer	78
10 Shear stress and shear rate values for high sucrose corn syrup obtained using the Haake viscometer	79
11 Values of the experimental parameters for 1.25 %, 1.5 % and 2.0 % Kelset samples using the back extruder	86
12 Shear stress and shear rate values for 1.25 % Kelset obtained using the Haake viscometer	87
13 Shear stress and shear rate values for 1.5 % Kelset obtained using the Haake viscometer	88

14	Shear stress and shear rate values for 2.0 % Kelset obtained using the Haake viscometer	89
15	Experimental data, collected from the back extrusion device for 1.0 % Methocel, used in the end effect evaluation	93
16	Experimental data collected from the back extrusion device of 1.0 % Methocel at three plunger velocities	94
17	Experimental rheological parameters for 1.0 % Methocel for $V_{p1} = 45.00 \times 10^{-4}$ m/s, $V_{p2} = 62.00 \times 10^{-4}$ m/s and $R_i = 1.2$ cm	95
18	Experimental rheological parameters for 1.0 % Methocel for $V_{p1} = 45.00 \times 10^{-4}$ m/s, $V_{p2} = 16.67 \times 10^{-4}$ m/s and $R_i = 1.2$ cm	96
19	Experimental rheological parameters for 1.0 % Methocel for $V_{p1} = 45.00 \times 10^{-4}$ m/s, $V_{p2} = 83.33 \times 10^{-4}$ m/s and $R_i = 1.2$ cm	97

LIST OF FIGURES

Figure	Page
1 Geometry of the annular back extrusion device	11
2 Schematic representation of coordinates describing axial flow in a back extrusion device (Osorio, 1985)	20
3 Newtonian shear rate approximation of power law fluids based on simulated data	31
4 Power law shear rate approximation of Herschel-Bulkley fluids based on simulated data	34
5 Newtonian shear rate approximation of power law fluids based on experimental data	39
6 Diagram of force versus distance obtained from the Instron to recorder for 1.5 % Methocel with plunger velocity of 8.33×10^{-3} m/s and a chart speed of 5.0×10^{-4} m/s (Osorio, 1985)	41
7 Power law shear rate approximation of Herschel-Bulkley fluids based on experimental data	45
8 End effect evaluation	46
9 Shear rate at the wall for Newtonian fluids, based on Morgan's equation (Equation 6)	50
10 Shear rates difference versus annular gap, at different plunger velocities, for 1.5% guar gum ...	54
11 Shear rates difference versus annular gap, at different plunger velocities, for 2.0 % Methocel ..	55
12 Shear rates difference versus annular gap, at different plunger velocities, for 1.5 % Methocel ..	56
13 Shear rates difference versus annular gap, at different plunger velocities, for corn syrup	57

14	Shear rate at the wall versus annular gap, at different plunger velocities, for 1.5 % guar gum ..	59
15	Shear rate at the wall versus annular gap, at different plunger velocities, for 2.0 % Methocel ..	60
16	Shear rates difference versus annular gap, at different plunger velocities, for 1.0 % Kelset	62
17	Shear rates difference versus annular gap, at different plunger velocities, for 1.5 % Kelset	63
18	Shear stresses difference versus annular gap, at different plunger velocities, for 1.0 % Kelset	65
19	Shear stresses difference versus annular gap, at different plunger velocities, for 2.0 % Kelset	66
20	Shear rate at the wall versus annular gap, at different plunger velocities, for 2.0 % Kelset	68
21	Effect of the dimensionless annular gap (K) on the power law approximation of a Herschel-Bulkley fluid (2.0 % Kelset)	89
22	Effect of the plunger velocity (Vp) on the power law approximation of a Herschel-Bulkley fluid (2.0 % Kelset)	70
23	Effect of the dimensionless annular gap (K) on the power law approximation of a Herschel-Bulkley fluid (1.5 % Kelset)	71
24	Rheograms for 1.0 % Methocel, considering the power law data from the back extruder, the Newtonian approximation of the power law fluid, and Haake viscometer data	80
25	Rheograms for high sucrose corn syrup, considering the power law data from the back extruder, the Newtonian approximation of the power law fluid, and Kaake viscometer data	81
26	Rheograms for 1.5 % guar gum, considering the power law data from the back extruder, the Newtonian approximation of the power law fluid, and Haake viscometer data	82
27	Rheograms for 1.0 % guar gum, considering the power law data from the back extruder, the Newtonian approximation of the power law fluid, and Haake viscometer data	83

28	Rheograms for 1.25 % Kelset, considering data obtained from the Haake viscometer, the back extruder, and the power law approximation	90
29	Rheograms for 1.5 % Kelset, considering data obtained from the Haake viscometer, the back extruder, and the power law approximation	91

NOMENCLATURE

- C_{sp} = chart speed of the recorder, m/s
- F = force applied to the plunger, N
- F_b = buoyancy force, N
- F_{cb} = force corrected for buoyancy, N
- F_T = recorded force while plunger is traveling down, N
- F_{Te} = recorded force after the plunger is stopped, N
- G = acceleration due to gravity, m/s²
- K = ratio of radius of plunger to that of outer cylinder, dimensionless
- L = vertical length of wetted plunger surface, m
- l_{cm} = chart length obtained for recorder, m
- n = flow behavior index, dimensionless
- O = initial level of fluid when the plunger has not been forced down in the sample, m
- P = pressure drop per unit of length, Pa/m
- PL = pressure in excess of hydrostatic pressure at the plunger base, Pa
- r = radial coordinate from common axis of cylinder forming annulus, m
- R_1 = radius of the plunger, m
- R_o = radius of outer cylinder of annulus, m
- s = reciprocal of n , dimensionless
- T = dimensionless shear stress, defined in Equation (18)
- To = dimensionless yield stress, defined in Equation (19)

Tw = dimensionless shear stress at the plunger wall,
defined in Equation (22)

V = velocity, m/s

V_p = plunger velocity, m/s

GREEK SYMBOLS

ζ	= sample density, Kg /m ³
η	= consistency coefficient for power law fluids, Pa s ⁿ
η_B	= plastic viscosity, Pa s
η_H	= Herschel-Bulkley consistency coefficient, Pa s ⁿ
λ	= value of dimensionless radial coordinate for which shear stress is zero
λ_- , λ_+	= limits of plug region in Herschel-Bulkley flow
μ	= Newtonian viscosity, Pa s
$\rho = r/R$	= dimensionless radial coordinate
τ	= shear stress, Pa
τ_o	= yield stress, Pa
τ_w	= shear stress at the plunger wall, Pa
$\tau_w \text{ New}$	= shear stress at the wall as a Newtonian fluid, Pa
$\tau_w \text{ pl}$	= shear stress at the wall as a power law fluid, Pa
$\tau_w \text{ HB}$	= shear stress at the wall as a Herschel-Bulkley fluid, Pa
$\dot{\gamma}$	= shear rate, sec ⁻¹
$\dot{\gamma}$	= shear rate at the plunger wall, sec ⁻¹
$\dot{\gamma}_w \text{ New}$	= shear rate at the wall as a Newtonian fluid
$\dot{\gamma}_w \text{ pl}$	= shear rate at the wall as a power law fluid
$\dot{\gamma}_w \text{ HB}$	= shear rate at the wall as a Herschel-Bulkley fluid
$\Delta \dot{\gamma}_{w_1}$	= difference between the shear rate at the wall for the power law fluid and the shear rate at the wall approximated to Newtonian, defined in Equation (29)

- $\dot{\Delta\gamma}_{w_2}$ = difference between the shear rate at the wall for the Herschel-Bulkley fluid and the shear rate at the wall approximated to power law, defined in Equation (30)
- $\Delta\tau_{w_2}$ = difference between the shear stress at the wall for the Herschel-Bulkley fluid and the shear stress at the wall approximated to power law, defined in Equation (31)
- Φ = dimensionless flow rate defined in Equation (21)
- ϕ = dimensionless velocity defined in Equation (14)
- α = dimensionless geometric coefficient defined in Equation (5)

Chapter 1

INTRODUCTION

Rheological properties are critical in proper process and equipment design. They are also useful as indicators for detecting physico-chemical changes in food materials. Hence, they are key parameters required to solve food industry problems in numerous areas.

The back extrusion, or annular pumping geometry, has been used for characterizing relative flow properties of various food materials. These devices may vary in size and shape, but usually operate in a similar manner. The sample is first placed in a vertical container. Then a plunger, traveling at a constant velocity, is forced down into the material causing a positive displacement of the sample. The sample flows upward through an annular space between the plunger and inner wall of the container. Force on the plunger is usually the measured parameter and is correlated as a relative rheological property (Morgan, 1979).

To date, analytical expressions to obtain rheological properties of Newtonian fluids (Morgan, 1979) and non-Newtonian fluids (Osorio, 1985) in a back extrusion device have been developed. However, those expressions based on non-Newtonian rheological models such as the Herschel-Bulkley case are very complicated and their application in resolving real problems is

very time consuming. Simple analytical methods or approximations, as well as optimum experimental conditions must be considered.

The objectives of this work were: 1) To determine the effect of plunger velocity (V_p) and plunger radius (R_i), in determining the rheological properties of the power law and Herschel-Bulkley fluids according with the expressions developed by Osorio, 1985. 2) To consider the use of the power law and the Newtonian approximations for determining shear rate when dealing with Herschel-Bulkley and power law fluids respectively. 3) To study the end effect error in the determination of the rheological properties from back extrusion data. 4) To experimentally validate the results.

Chapter 2

LITERATURE REVIEW

Many industries, government research establishments and university research groups are concerned with a wide range of fluids which can be broadly classified as non-Newtonian. Polymer melts and polymer solutions come readily to mind in this connection, but the complete list is seemingly endless. So, rheometry plays a major role in the experimentalists approach to non-Newtonian fluid mechanics because those who are practically concerned with the flow behavior of these fluids invariably require measurements of their mechanical properties (Walters, 1975).

2.1 Newtonian Model

For many fluids, measurements of shear stress and shear rate (at various magnitudes of both) indicate a direct proportionality between the variables: $\tau = \mu \dot{\gamma}$. Such materials, for which the ratio of shear stress to shear rate, or viscosity, is constant (i.e., independent of the magnitude of shear stress or shear rate), are called Newtonian. Most fluids of simple structure, composed of relatively simple molecules in a single phase, behave as Newtonian fluids (Darby, 1976).

Water, and most aqueous solutions, organic liquids, silicones and liquid metals behave, within experimental accuracy, as Newtonian fluids. The model may be adequate, although not exact, for the dilute suspensions, emulsions, and solutions of moderately long chain molecules (Whorlow, 1980).

2.2 Non-Newtonian Models

All those fluids for which the flow curve (shear stress versus shear rate) is not linear through the origin at a given temperature and pressure are said to be non-Newtonian. These fluids are commonly divided into three broad groups, although in reality these classifications are often by no means distinct or sharply defined.

1. Time-independent fluids are those for which the rate of shear at a given point is solely dependent upon the instantaneous shear stress at that point. (These materials are sometimes referred to as 'non-Newtonian viscous fluids' or alternatively as 'purely viscous fluids').

2. Time-dependent fluids are those for which the shear rate is a function of both the magnitude and the duration of shear and possibly of the time lapse between consecutive applications of shear stress.

3. Viscoelastic fluids are those that show partial elastic recovery upon the removal of a deforming shear stress. Such

materials possess properties of both fluids and elastic solids (Skelland, 1967).

Because of the wide variation in their structure and composition, foods exhibit flow behavior ranging from simple Newtonian to time dependent non-Newtonian and viscoelastic. Furthermore, a given food may exhibit combinations of classical behaviors, depending on its origin, concentration, and previous history. Flow properties of food are used for a number of purposes, such as quality control (Kramer and Twigg, 1970), insights to physicochemical structure (Sherman, 1966), process engineering applications (Boger and Tiu, 1974; Rao and Anantheswaran, 1982; Steffe and Morgan, 1986), and correlation with sensory evaluation (Szczesniak and Farkas, 1962).

Non-Newtonian fluids may be distinctly classified by the way in which the shear stress varies with the shear rate, or in terms of the variation of apparent viscosity with shear stress or shear rate (Darby, 1976).

Some of the most common rheological models, which have been used in axial laminar flow in a concentric annulus are the power law, the Bingham plastic, and the Herschel-Bulkley fluid models.

2.2.1 The Power Law Fluid Model

This model, usually attributed to Ostwald but proposed independently by de Waele and others, is used to represent the behavior of many polymer solutions and melts, and sometimes of other systems. The equation for the model may be written as

$$\tau = \eta \dot{\gamma}^n \quad (1)$$

where η is a constant sometimes referred to as the consistency index, and n may have any positive value.

When n is greater than unity the material becomes less fluid as the shear rate increases. This is known as shear-thickening, or sometimes as dilatant behavior. When n is less than unity it is known as shear thinning or sometimes pseudoplastic behavior. When n is 1, of course, the flow curve corresponds to a Newtonian liquid. This model has proved very useful for approximating fluid behavior over a fixed range of shear rate values. However, it has limitations for small and very large shear rates.

2.2.2 The Bingham Plastic Model

This material behaves as an ideal rigid solid (no deformation) when subjected to a shear stress smaller than a certain (yield) value (yield stress). For stresses above the yield value, the Bingham plastic flows as a fluid, with the shear stress being a linear function of shear rate. Although it is doubtful that any real material actually behaves precisely in this manner, the behavior of many materials, notable pastes, suspensions, slurries, paints, etc. may often be adequately approximated by this model over a suitable range of conditions (Darby, 1976). This model is expressed as a two parameter model,

$$\tau = \tau_0 + \eta_B \dot{\gamma} \quad (2)$$

where τ_0 is the yield stress and η_B is the plastic viscosity.

2.2.3 The Herschel-Bulkley (H-B) Model

One of the most popular modifications of the Bingham model is to insert the power law term for the viscous component:

$$\tau = \tau_0 + \eta_H \dot{\gamma}^n \quad (3)$$

where τ_0 is the yield stress, η_H is the H-B consistency index, and n is the flow behavior index. The Herschel-Bulkley model has the merit that it describes a flow curve in a small number of parameters and often is found to give a reasonably good representation of an experimentally determined curve. It does, however, suffer from the disadvantage that, unlike the simple power law, it is less easy to fit to the observed data because it usually involves an extrapolation in order to arrive at the value of yield stress (Prentice, 1984). Since Bingham plastic, power law and Newtonian behavior may be regarded as special cases of the Herschel-Bulkley model, the model represents the behavior of a large number of materials without being unduly difficult to handle mathematically (Whorlow, 1980).

2.3 Viscometer and Rheometers

Under any conditions of motion and stress, a constant viscosity coefficient is sufficient to determine the behavior of incompressible Newtonian liquids. The measurement of this viscosity coefficient involves the use of a Viscometer defined simply as 'an instrument for the measurement of viscosity'. The viscosity of non-Newtonian elastic liquids may be shear rate dependent, the viscometer is therefore inadequate to characterize the behavior of these materials and has to be replaced by a rheometer defined as 'an instrument for measuring rheological properties' (Walters, 1974).

There are two basic objectives in Rheometry. The first involves a straightforward attempt to characterize the behavior of non-Newtonian liquids in a number of simple (rheometrical) flow situations using suitable defined material functions. The second objective involves the construction of rheological equations of state for the liquids which can be later used in the solution of flow problems of practical importance (Walters, 1974).

2.3.1 Back Extrusion Technique

Back extrusion apparatuses have been used for characterizing relative flow properties of various food materials (Morgan, 1979). In the back extrusion technique the following two facts are involved: 1) a plunger is forced down in a fluid, and 2) the fluid flows upward through a concentric annular space (Osorio, 1985).

Some of the unique characteristics of this rheological apparatus is that it allows quick and easy measurements of small volume samples contained in standard glass test tubes. This provides for a wide range of variations in sample preparation and pre-treatment processes. This instrument should prove useful in quality control of the manufacturing of fluid foods (Steffe and Osorio, 1987).

Several works have been developed in the area of the back extrusion technique.

Morgan et al. (1979) developed mathematical relations for calculating shear stress, shear rate and velocity profiles for annular counter flow of a Newtonian fluid in a simple back extrusion device. Viscosity standards were used for experimental validation of the equations.

Osorio (1985) developed mathematical expressions to describe the behavior of non-Newtonian fluids in a back extrusion device using the Herschel-Bulkley fluid model. With the mathematical model developed, expressed in form of dimensionless terms, it is possible to determine the rheological properties of Newtonian, power law, Bingham plastic, and Herschel-Bulkley fluids. In addition, shear stress and shear rate at the wall may also be calculated.

Chapter 3

THEORETICAL DEVELOPMENT

3.1 Basic Theories

3.1.1 Back Extrusion of Newtonian Fluids

Morgan (1979) developed mathematical relationships for describing the operation of an annular back extrusion device, including equations which can be used for determining viscosity at known shear rates and certain viscoelastic properties. Newtonian viscosity standards were used to validate mathematical relationships.

Geometry of the annular back extrusion device used for this study is shown in Figure 1. As the plunger is lowered into the sample, fluid will begin to flow upward through the annulus. If the plunger velocity is constant, total plunger force will be the sum of shear forces on the plunger wall and the static pressure pushing upward on the bottom surface of the plunger. Static force at the base of the plunger is composed of buoyancy force, and that responsible for fluid flow in the upward direction. Buoyancy effects can easily be accounted for by simple calculation of the hydrostatic head.

Assuming Newtonian flow, from the plunger force balance and the conservation of momentum equation the following expressions were developed by Morgan (1979):

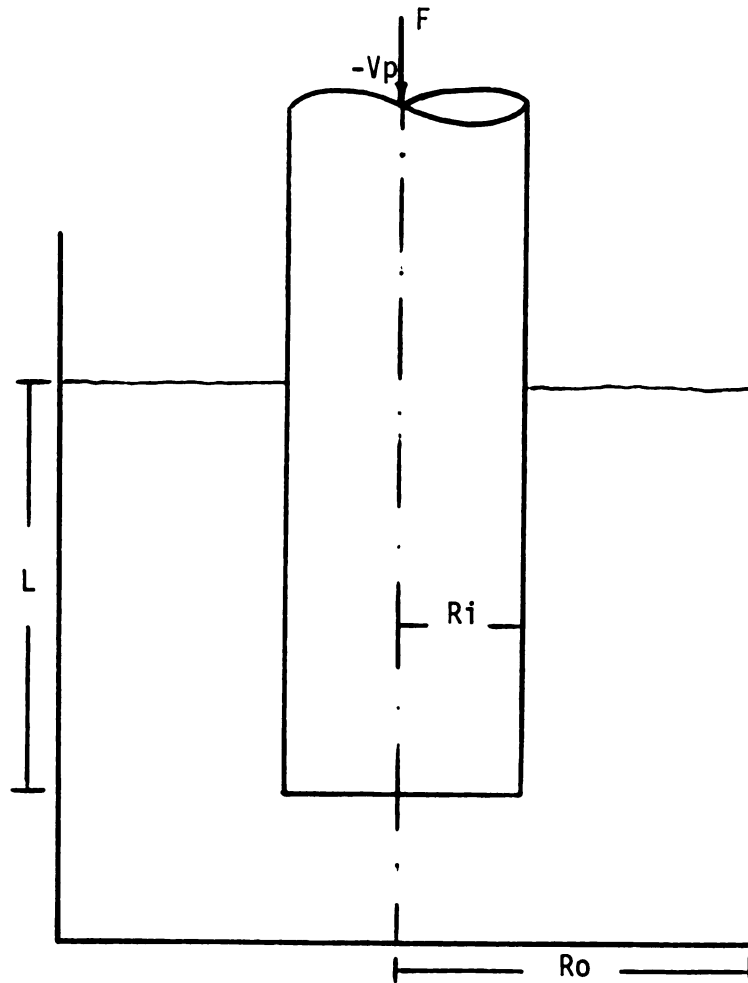


Figure 1. Geometry of the annular back extrusion device.

$$\tau_w = \frac{\alpha F_{pc}}{2 \pi R_i L} \quad (4)$$

where: τ_w = Shear stress on wall of plunger, Pa
 F_{pc} = Total plunger force corrected for buoyancy, N
 R_i = Radius of plunger rod, m
 L = Vertical length of wetted plunger surface, m
 α = Dimensionless geometric coefficient (which depends only on physical geometry of the device for Newtonian flow conditions).

Also

$$\alpha = \frac{1 - K^2}{1 + K^2} \quad (5)$$

where: $K = R_i/R_o$
 R_o = Radius of outside cylinder or container, m

and,

$$\dot{\gamma}_w = \left(\frac{-\alpha}{\ln K + \alpha} \right) \cdot \left(\frac{V_p}{R_i} \right) \quad (6)$$

where: $\dot{\gamma}_w$ = Shear rate at plunger wall, s^{-1}
 V_p = Plunger velocity, m/s

Equations (4) and (6) can be combined to yield an expression for calculating the Newtonian viscosity:

$$\mu = \left[\frac{1}{2 \pi} \right] \left[\frac{F_{pc}}{V_p L} \right] \left[\ln \frac{1}{K} \right] \left[1 + \frac{\alpha}{\ln K} \right] \quad (7)$$

3.1.2 Back Extrusion of Power Law Fluids

Osorio (1985) developed analytical expressions, using the power law fluid model, to describe the fluid behavior in a back extrusion device. The complete theoretical development for the equations presented in this section may be found in Osorio (1985) or Osorio and Steffe (1987).

In the development of the theory for non-Newtonian fluids (both power law and Herschel-Bulkley) the following assumptions were made:

1. The density is constant.
2. The fluid is homogeneous.
3. The fluid has achieved steady state flow.
4. There is no elasticity or time-dependent behavior.
5. The flow is laminar and fully developed.
6. The cylinders are sufficiently long that end effects may be neglected.
7. The temperature is constant.

In addition, the following boundary conditions are assumed for the analysis:

- a. There is no slip at the annulus walls and the velocity at the outer wall (the cup) is zero.
- b. The definition of a Herschel-Bulkley fluid implies a region of "plug flow" where the shear stress must reduce to zero at the boundary and inside the plug.

When a power law fluid is tested in a back extrusion device, at two different plunger velocities, with a plunger radius and outside cylinder combination which are the same in both experiments, the value of s (defined as the inverse of the flow behavior index n) is given by

$$s = \frac{\ln \left[\frac{V_{p2}}{V_{p1}} \right]}{\ln \left[\frac{F_{cb2}}{F_{cb1}} \cdot \frac{L1}{L2} \right]} \quad (8)$$

where: V_p = plunger velocity, m/s

F_{cb} = force corrected for buoyancy, N

L = length of annular region, m

The consistency coefficient can be determined from the following expression:

$$\eta = \frac{P R_o}{2} \left[\frac{\Phi R_o}{V_p K^n} \right]^n \quad (9)$$

where: n = flow behavior index, dimensionless

P = pressure drop per unit of length, Pa/m

R_o = radius of outer cylinder of annulus, m
 K = ratio of radius of plunger to that of outer cylinder, dimensionless
 η = consistency coefficient, Pa sⁿ
 Φ = dimensionless flow rate

Osorio and Steffe (1987) presented a plot of the dimensionless plunger radius (K), the flow behavior index (n) and the dimensionless flow rate (Φ). They also presented a table from which, with the knowledge of the flow behavior index (n) and the dimensionless plunger radius (K), it is possible to obtain the λ value which is the value of the dimensionless radial coordinate for which the shear stress is zero.

The shear stress at the plunger wall is

$$\tau_w = \frac{P R_o T_w}{2} \quad (10)$$

where the dimensionless shear stress at the plunger wall (T_w) is obtained as

$$T_w = \frac{\lambda^2}{K} - K \quad (11)$$

By applying a force balance on the plunger, the following expression was determined:

$$\frac{F_{cb}}{\pi L P R_o R_i} = T_w + K \quad (12)$$

where: F_{cb} = force corrected for buoyancy, N
 L = length of annular region, m
 P = pressure drop per unit of length, Pa/m
 R_o = radius of outer cylinder of annulus, m
 R_i = radius of the plunger, m
 K = R_i/R_o , dimensionless
 T_w = dimensionless shear stress at the plunger wall

The shear rate at the plunger wall is given by

$$\left. \frac{\partial v}{\partial r} \right|_{r=a} = \frac{P R_o}{2 \eta} s \left. \frac{\partial \phi}{\partial \rho} \right|_{\rho=k} \quad (13)$$

where: $\partial v / \partial r$ = shear rate, s^{-1}
 P = pressure drop per unit of length, Pa/m
 R_o = radius of outer cylinder of annulus, m
 n = flow behavior index
 η = consistency coefficient, $Pa \ s^n$
 ρ = dimensionless radial coordinate = r/R_o

and ϕ , the dimensionless velocity, is defined as

$$\phi = \left[\frac{2 \eta}{P R_o^{n+1}} \right]^{1/n} \cdot [V] \quad (14)$$

Also, the dimensionless shear rate at the plunger wall is given by

$$\left. \frac{\delta\phi}{\delta\rho} \right|_{\rho=k} = \left[\frac{\lambda^2}{K} - K \right]^s \quad (15)$$

The buoyancy force is

$$F_b = \zeta g L \pi R_i^2 \quad (16)$$

$$\text{where } L = \frac{\overline{OB}}{1 - K^2} \quad (17)$$

and OB corresponds to the position of the plunger bottom, at the end of the test, measured with respect to the initial level of fluid, in meters.

For a power law fluid, the buoyancy force, F_b , is equal to the recorded force after the plunger is stopped, F_{Te} . With the above equations, and the tables and plots developed by Osorio and Steffe (1987), it is possible to calculate the rheological properties of a power law fluid. In addition, the shear stress and shear rate at which measurements are taken may be determined.

3.1.3 Back Extrusion of Herschel-Bulkley Fluids

For a detailed discussion of the back extrusion theory for Herschel-Bulkley fluids presented in this section, refer to

Osorio (1985) or Osorio and Steffe (1985). The Herschel-Bulkley model is:

$$\tau = \tau_o + \eta_H \dot{\gamma}^n$$

where: τ = shear stress, Pa

τ_o = yield stress, Pa

η_H = consistency coefficient, Pa sⁿ

$\dot{\gamma}$ = shear rate, s⁻¹

n = flow behavior index, dimensionless

The theoretical analysis is conducted using the following dimensionless variables:

$$T = \frac{2 \tau}{P R_o} = \text{dimensionless shear stress} \quad (18)$$

$$T_o = \frac{2 \tau_o}{P R_o} = \text{dimensionless yield stress} \quad (19)$$

$$\phi = \left[\frac{2 \eta}{P R_o^{n+1}} \right]^{1/n} \cdot [V] = \text{dimensionless velocity} \quad (20)$$

where: P = pressure drop per unit of length, Pa/m

R_o = radius of outer cylinder of annulus, m

V = velocity, m/s

Figure 2 shows a schematic representation of the velocity profile of a Herschel-Bulkley fluid in a back extruder. The λ parameter represents the value of the dimensionless radial coordinate (ρ) for which the shear stress is zero. λ_- and λ_+ are the limits of the plunger region in the flow profile. There is a table included in Osorio (1985) which contains values of λ_+ for a value of K (defined as the ratio of the radius of plunger (R_i) to that of the outer cylinder (R_o)) for selected values of To with values of the flow behavior index (n) from 0.1 to 1.0 .

A dimensionless flow rate was obtained:

$$\bar{Q} = \left(\frac{2 \eta}{P R_o} \right)^s \left(\frac{V_p}{R_o} \right) \left(K^s \right) \quad (21)$$

where s is the inverse of the flow behavior index. There are figures in Osorio (1985) and Steffe and Osorio (1987) which give values of \bar{Q} for a selected set of values of K and To when n has values between 0.1 and 1.0.

The dimensionless shear stress at the plunger wall is

$$T_w = \frac{\lambda_+ (\lambda_+ - To)}{K} - K \quad (22)$$

and the dimensionless shear rate at the plunger wall is

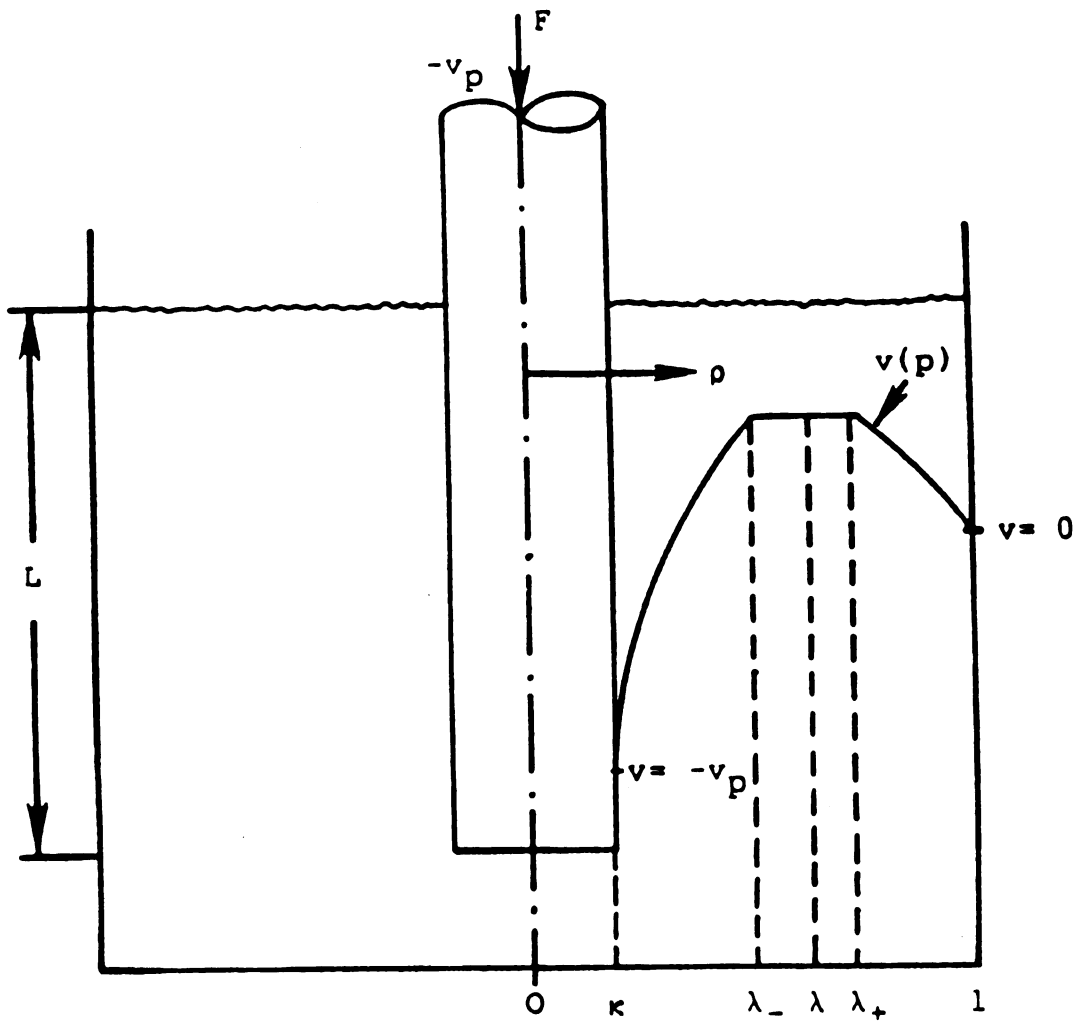


Figure 2. Schematic representation of coordinates describing axial flow in a back extrusion device (Osorio, 1985).

$$\left. \frac{\delta \phi}{\delta \rho} \right|_{\rho=k} = \left[\frac{\lambda_+ (\lambda_+ - T_o)}{K} - K - T_o \right] s \quad (23)$$

By applying a force balance on the plunger, an expression relating the force corrected for buoyancy to the dimensionless shear stress at the wall may be found:

$$\frac{F_{cb}}{\pi L P R_o R_i} = T_w + K \quad (24)$$

where: F_{cb} = force corrected for buoyancy, N

L = length of annular region, m

P = pressure drop per unit of length, Pa/m

R_o = radius of outer cylinder of annulus, m

R_i = radius of the plunger, m

T_w = shear stress at wall, dimensionless

K = ratio of radius of plunger to that of outer cylinder = R_i/R_o , dimensionless

The force corrected for buoyancy is obtained from

$$F_{cb} = F_T - F_b \quad (25)$$

where: F_T = total force applied on the plunger, N

F_b = hydrostatic or buoyancy force, N

and the buoyancy force is calculated from Equation (16):

$$F_b = \zeta g L \pi R_i^2$$

where: ζ = sample density, Kg/m³

g = acceleration due to gravity, m/s²

The length of the annular region, L , is computed using Equation (17),

$$L = \frac{\overline{OB}}{1 - K^2}$$

and OB is the position of the plunger bottom, at the end of the experiment, measured with respect to the initial level of fluid.

The yield stress can be calculated as

$$\tau_o = \frac{F_{Te} - F_b}{2 \pi R_i L} \quad (26)$$

where: F_{Te} = recorded force after the plunger is stopped, N

The shear stress at the plunger wall is obtained with the expression

$$\tau_w = \frac{P R_o T_w}{2} \quad (27)$$

and the shear rate at the plunger wall is calculated from

$$\left. \frac{\delta v}{\delta r} \right|_{r=R_i} = \left[\frac{P R_o}{2 \eta} \right]_s \quad \left. \frac{\delta \phi}{\delta \rho} \right|_{\rho=k} \quad (28)$$

3.1.4 Procedure for the Determination of Rheological Properties of a Herschel-Bulkley Fluid

The rheological properties of a Herschel-Bulkley fluid may be determined from the following steps (Osorio , 1985):

1. For a given plunger velocity V_p , determine the expression $F_{cb}/(\pi L R_i R_o)$, where F_{cb} is obtained from Equation (25). The above quantity may be expressed in terms of P , T_w and K as shown in Equation (24).
2. Assume a value for the flow behavior index n .
3. Assume a value for the dimensionless yield stress T_o .
4. Using Equation (19) determine the pressure drop per unit of length P , with the value of yield stress obtained from Equation (26).
5. With T_o and K use the appropriate graphic from the corresponding figure created by Osorio (1985) to determine the dimensionless flow rate.
6. Determine λ_+ from the corresponding table.
7. Use Equation (22) to determine T_w .
8. Use Equation (21) to determine η .
9. Compute the expression $P(T_w + K)$.
10. Return to step 3, to obtain at least three values of $P(T_w + K)$ and η at a given n .

11. Return to step 2, to plot the necessary curves at different n values that cover the range needed to obtain the correct n value.
12. Plot the values of $P(Tw + K)$ versus η with n as parameter.
13. Draw the line corresponding to the value of $F_{cb}/(\pi L R_i R_o)$ computed in step 1.
14. Use a new plunger velocity V_p and repeat steps 1 to 13 for this new value of V_p .

The rheological properties of the fluid are found when, for a specific flow behavior index n , the consistency coefficient is the same in both curves at two different plunger velocities. With n and η known, the shear stress at the wall may be computed using the values of T_o and λ_+ obtained at either V_{p1} or V_{p2} for the known flow behavior index n .

Equations (23) and (28) are used to calculate the dimensionless shear rate and the actual shear rate, at the plunger wall, respectively; Equations (18) and (22) are used to determine the dimensionless shear stress and the actual shear stress at the plunger wall, respectively.

3.2 Computer Programs For Non-Newtonian Fluids

From all the steps involved in the determination of the rheological properties of a Herschel-Bulkley fluid it is obvious that the application of this theory is very difficult and time consuming. Osorio (1985) created four different programs to

facilitate the calculations. Those programs were adapted for the TI-Professional Computer by Fernando Hirujo and Nelly Marte (1986), and they were recalled and included in Appendix A of this study.

Chapter 4

EXPERIMENTAL PROCEDURES APPLICATIONS

4.1 Equipment, Materials and Methods

All the experimental tests in the laboratory were conducted on a Model 4202 Instron Universal Testing Machine (Instron Inc., Canton MA) located in the food rheology laboratory at Michigan State University, East Lansing, Michigan.

Five plunger rods were made for attachment to the cross head of the Instron. Those plunger rods had different radii corresponding to 1.0, 1.2, 1.36, 1.5 and 1.67 cm respectively. The compression load cell located in the Instron was 50 Newtons.

The automatic control panel adapted to the Instron offered the options of selecting several experimental parameters. In addition, there was a recorder where the force applied in the plunger versus time or versus position is plotted for each experiment.

Graduate cylinders of constant 1.76 cm radius, were used as sample holders. Aqueous solutions of Methocel (Hydroxypropyl-methyl-cellulose) from the Dow Chemical Co., and aqueous solutions of guar gum were used for the experiments with power law fluids. For the experiments with Herschel-Bulkley fluids, aqueous solutions of Kelset (Sodium-calcium alginate) from Kelco Co., at different concentrations were used.

The rheological properties of all fluids were also determined using the Haake RV-12 Viscometer, adapted to a Hewlett-Packard 85 computer and 3497 data acquisition system. The MV I and the MV II concentric cylinder sensors were utilized in the determination of properties. For all tests, the samples were held in the MV cup. The procedure used for the Haake operation and analysis of the data was the same as described in Ford and Steffe (1984).

All test were run at a constant room temperature of $25.0 \pm 1.0^{\circ}\text{C}$.

In the data simulation collection, the RHEO programs described in Appendix A were run in a Texas TI Professional Computer. At this point it is appropriate to note that the original RHEO programs were developed by Osorio (1985) to be run in the CDC Cyber 750 computer at Michigan State University. Since all the computational data analysis and simulation were made in the Dominican Republic, those RHEO programs were adapted to the Texas TI PC that was available. Due to the different capabilities of the Cyber main frame and the Texas TI PC, the TI PC computational period was 30 to 60 times greater than the Cyber computational time. To reduce this time to 5 to 20 minutes the tolerance was reduced to half of the original value, thus resulting in errors of approximately 2% .

4.2 Effect of Plunger Velocity and Plunger Radius

From the study of the mathematical expressions and from experimental conditions, it can be concluded that plunger

velocity (V_p), and plunger radius (R_i), are the most important variables to be controlled when using the back extrusion technique.

To study the effect of V_p and R_i in the determination of rheological properties when using the back extrusion technique, the following procedure is recommended:

1. Select several power law and Herschel-Bulkley fluids, with their flow behavior index value (n) varying from small to large values. In this way the results and conclusions obtained will represent many possible cases of non-Newtonian fluids.
2. Select several plunger velocities, covering the entire range of the Instron 4202. The plunger velocity range for the system was 1.667×10^{-5} to 83.33×10^{-4} m/s.
3. Select different plunger radii (R_i), for a constant cylinder radius (R_o) equal to 1.76 cm, and annular gaps between 0.5 and 0.95.
4. Run the tests in the back extrusion device, under those fixed conditions, for each specific fluid.
5. Collect the data, and determine the experimental rheological properties of those fluids using RHEO programs (Appendix A).
6. At the same time, using the Haake RV-12 Viscometer, determine the rheological properties of all selected fluids.
7. Compare the experimental rheological properties obtained using back extrusion technique to those obtained using

the Haake. Select the 'best' combination of plunger radius and two plunger velocities to get best results in the back extrusion testing of non-Newtonian fluids.

4.3 Newtonian Approximation for Power Law Fluids Based on Simulated Data

According to Morgan (1979) the shear rate at the wall for a Newtonian fluid in a back extruder is given by Equation (6). Therefore, the shear rate at the wall is a constant value affected only by the plunger velocity and the geometry of the equipment K, for any Newtonian fluid.

The values obtained with Equation (6), are considered as 'Newtonian approximations for the shear rate at the wall' when dealing with power law fluids.

The data simulation procedure involves the following steps:

1. Consider five different standard power law fluids, with known rheological properties, and with flow behavior indices varying from 0.15 up to 1.0, where the fluid is considered Newtonian.
2. Select five different plunger velocities, as in step 2 in Section 4.2.
3. Select five different plunger radii, with the same considerations as in step 3 in Section 4.2.
4. For each one of the five power law fluids and for each gap, vary the plunger velocities from V_{p1} to V_{p5} .

With the input data: n , η , R_i , R_o , V_p , RHEO-3 will

compute the shear stress and the shear rate at the wall:

$\tau_{w\ pl}$, $\dot{\gamma}_{w\ pl}$ respectively.

5. Compare the shear rates at the wall, for all the power law fluids at each condition of V_p and R_i , with the shear rates at the wall for Newtonian fluids, obtained using Equation (6) under the same conditions of V_p and R_i .

From this comparison, some conclusion will be drawn about using Newtonian approximation for calculating shear rate at the wall for power law fluids. This comparison will be made in terms of the percentage difference of the two shear rates, expressed as:

$$\Delta \dot{\gamma}_{w_1} = \frac{\dot{\gamma}_{w\ New} - \dot{\gamma}_{w\ PL}}{\dot{\gamma}_{w\ PL}} \quad (100) \quad (29)$$

where: $\dot{\gamma}_{w\ New}$ = shear rate at the wall according to Equation (6): Newtonian Approximation

$\dot{\gamma}_{w\ PL}$ = real shear rate at the wall for the power law fluid, obtained from RHEO-3

6. Analysis of the data will be made to check how the Newtonian approximation for the shear rate at the wall works when dealing with power law fluids. The effect of V_p and R_i will also be considered.

Figure 3 shows a flow chart of this procedure for the Newtonian shear rate approximation of power law fluids based on simulated data.

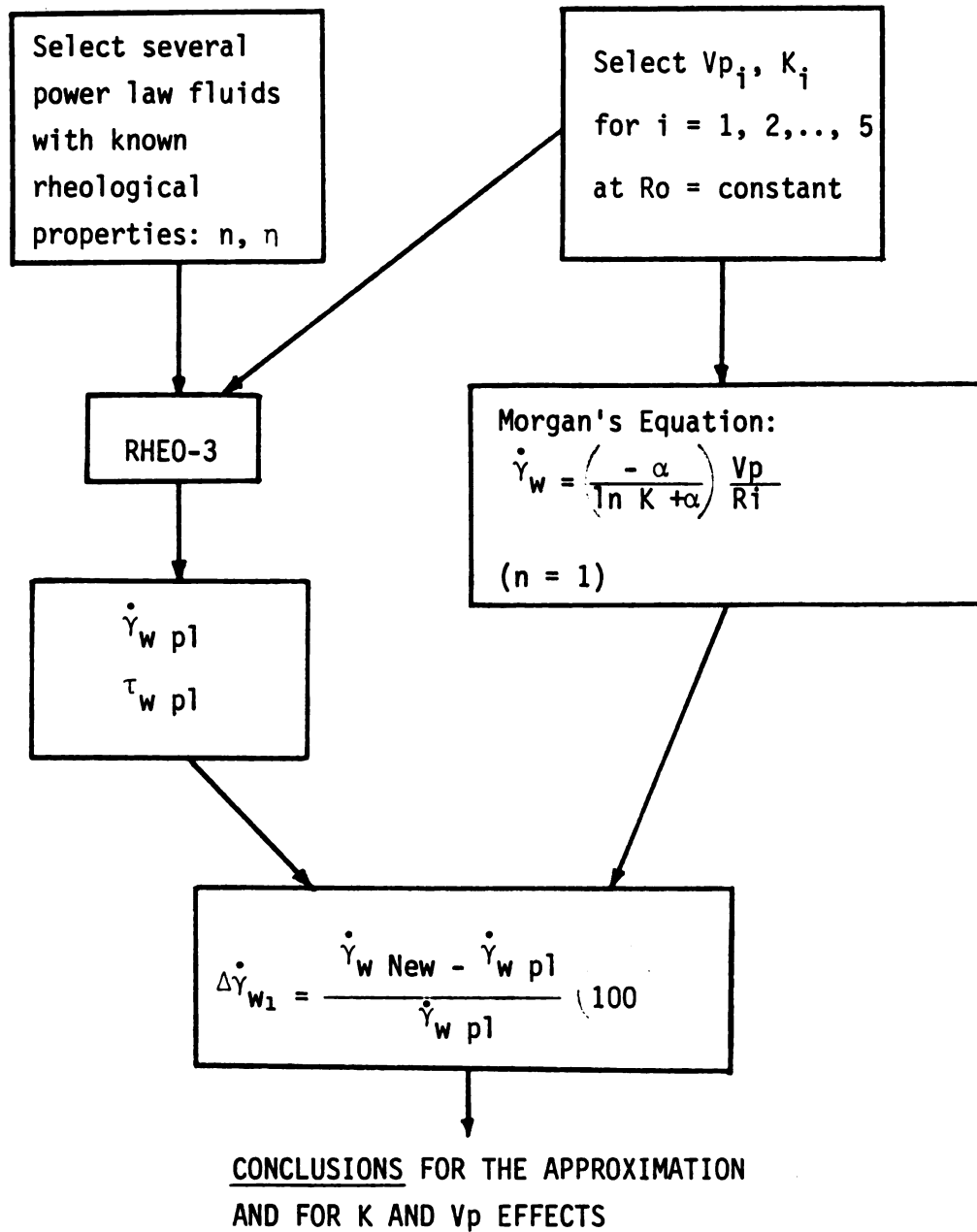


Figure 3. Newtonian shear rate approximation of power law fluids based on simulated data.

The rheological properties of the standard power law fluids used in the Newtonian approximation are shown in Table 1. They were taken from Osorio (1985) and Steffe and Ford (1985).

4.4. Power Law Approximation for Herschel-Bulkley Fluids Based on Simulated Data

In this case, the power law fluid model equation $\tau_1 = \eta_1 \dot{\gamma}^{n_1}$ is used as an approximation for the Herschel-Bulkley (H-B) fluid model equation $\tau_2 = \tau_0 + \eta_2 \dot{\gamma}^{n_2}$.

Since the yield stress is affected by the consistency coefficient (η_2) and the flow behavior index (n_2) it will be necessary to generate η_1 and n_1 (different than η_2 and n_2 respectively) from the Herschel-Bulkley data. η_1 and n_1 (power law parameters) are obtained from the H-B model, and they account for the effect of τ_0 (which is not present in τ_1). Then, τ_1 and τ_2 will be approximated considering the effect of η and n at the same time.

The procedure for this option, as shown in Figure 4, will be as follows:

1. Use several Herschel-Bulkley fluids, with known rheological properties, varying the yield stress range.
2. Repeat steps 2 and 3 as in Section 4.2.
3. For each of the H-B fluids, with known rheological properties, take five different V_p , and for each annular gap (K) vary V_p from V_{p1} to V_{p5} . With the input data in RHEO-3: n , τ_0 , η , R_i , R_o , and V_p , compute the shear rate at the wall ($\dot{\gamma}_w^{HB}$), the shear stress at the wall

Table 1. Rheological properties and experimental conditions for power law fluids used in the Newtonian approximation based on simulated data

<u>Fluid</u>	<u>Rheological Equation</u>
1.5% Guar Gum	$\tau = 31.315 \dot{\gamma}^{0.158}$
1.0% Guar Gum	$\tau = 7.916 \dot{\gamma}^{0.259}$
2.5% Methocel	$\tau = 16.155 \dot{\gamma}^{0.513}$
2.0% Methocel	$\tau = 3.056 \dot{\gamma}^{0.690}$
1.5% Methocel	$\tau = 1.33 \dot{\gamma}^{0.750}$
Corn Syrup	$\tau = 2.67 \dot{\gamma}^{1.000}$

Experimental Conditions:

j	Plunger Velocity ($V_{pj} \times 10^4$ m/s)	Plunger radius ($R_{ij} \times 10^2$ m)	Annular Gap K_j
1	1.667	1.670	0.950
2	16.67	1.500	0.852
3	45.00	1.360	0.773
4	62.00	1.200	0.682
5	83.33	1.000	0.568

For $Ro = 1.76 \times 10^{-2}$ m.

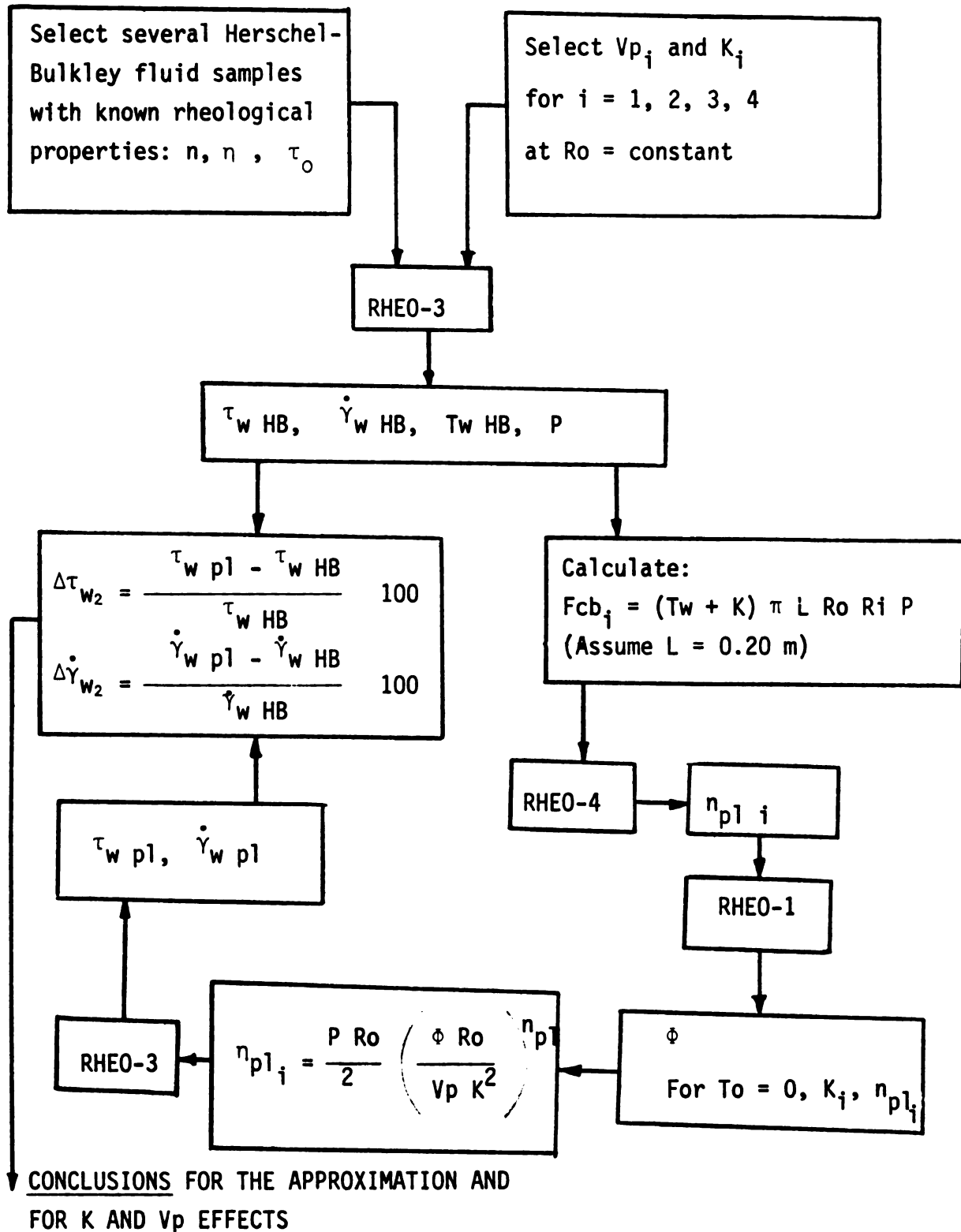


Figure 4. Power law shear rate approximation of Herschel-Bulkley fluids based on simulated data.

- (τ_w HB), the dimensionless shear stress at the wall (T_w), and the pressure drop per unit of length (P) corresponding to each combination of conditions. The $\dot{\gamma}_w$ HB and τ_w HB are called the real shear rate and shear stress at the wall respectively, for the H-B fluids used.
4. For each of the H-B fluids considered in step 1, calculate the force corrected for buoyancy (F_{cb}) from equation (24) knowing plunger radius, outside cylinder radius, annulus gap, pressure drop per unit of length, and the dimensionless shear stress at the wall T_w (obtained with RHEO-3). In all cases, for the calculation of the F_{cb} the value of L , the length of annular region, is assumed to be 0.20 m. With this value it is ensured that the flow is laminar, fully developed, and at steady state.
 5. The F_{cb} obtained for the H-B standard fluids at different plunger velocities, for each annular gap considered, are used to obtain the flow behavior index, (n) given by Equation (8), using RHEO-4. In this way, the original H-B fluids are approximated by power law models. The new n value will correspond to the approximated power law model, for two different plunger velocities.
To get better results for the data simulation section, n is obtained as the inverse of the slope when plotting Equation (8) using the five different plunger velocities, for a specific fluid at a constant annular gap K .
 6. Obtain the dimensionless flow rate defined by Equation (21) using RHEO-1, knowing K , $T_o=0$ (approximated to power law) and n .

7. With n (from power law) and the dimensionless flow rate (from power law), calculate the consistency coefficient using Equation (9), for all the H-B fluids considered, at each plunger velocity, for the different K values.
8. Obtain the shear rate and the shear stress at the wall for the H-B fluids now approximated by power law, ($\dot{\gamma}_w$ pl, τ_w pl), using RHEO-3 and the n , η , K , V_p values, with $\tau_0 = 0$.
9. Compare the shear rate and the shear stress at the wall using power law approximations with the real shear rate and shear stress at the wall for the H-B fluids (from step 3), at each conditions of V_p and R_i , with the following rates of difference:

$$\Delta \dot{\gamma}_{w_2} = \frac{\dot{\gamma}_w \text{ PL} - \dot{\gamma}_w \text{ HB}}{\dot{\gamma}_w \text{ HB}} \quad (100 \%) \quad (30)$$

$$\Delta \tau_{w_2} = \frac{\tau_w \text{ PL} - \tau_w \text{ HB}}{\tau_w \text{ HB}} \quad (100 \%) \quad (31)$$

10. From those comparisons, conclusions will be made about how the power law approximation works for Herschel-Bulkley fluids and about K and V_p effects.

For the power law approximation of H-B fluids, three different concentrations of Kelset solutions, were used as

'standards'. These standards were obtained from data collected by Osorio (1985) and others using the back extruder.

Table 2 summarizes the total set of data used in the power law shear rate approximation of Herschel-Bulkley fluids.

Appendix B encloses an example of the calculations of the shear rates at the wall as an approximation for Herschel-Bulkley fluids.

It was found from experimental tests that when using an annular gap of 0.95 the results from the back extrusion device were affected by the presence of small air bubbles inside the fluid samples which produced wrong readings. Also there were problems with the alignment between the outside cylinder and the plunger rod. For very viscous fluids too much pressure is involved and the glass containers could be broken, causing injuries to the operator or damages to the equipment. At the same time, it was found that when working at $V_p = 1.667 \times 10^{-4}$ m/s, the information obtained in the chart recorder was not reliable because of the shape of the force versus distance curve. For the above reasons, the conditions $R_i = 0.0167$ m and $V_p = 1.667 \times 10^{-4}$ m/s were not considered in the theoretical or experimental procedures.

4.5 Newtonian Approximation for Power Law Fluids Based on Experimental Data

The back extrusion device was used to determine rheological properties of several aqueous solutions, with the following procedure, as shown in Figure 5:

Table 2. Rheological properties and experimental conditions for Herschel-Bulkley fluids used in the power law approximation based on simulated data.

<u>Fluid</u>	<u>Rheological Equation</u>
2.0 % Kelset	$\tau = 8.8 + 27.0 \dot{\gamma}^{0.5}$
1.5 % Kelset	$\tau = 9.746 + 9.1 \dot{\gamma}^{0.6}$
1.0 % Kelset	$\tau = 2.409 + 5.2 \dot{\gamma}^{0.4}$

Experimental Conditions

<u>j</u>	<u>Plunger Velocity</u> ($V_{pj} \times 10^4$ m/s)	<u>Plunger Radius</u> ($R_{ij} \times 10^2$ m)	<u>Annular Gap</u> K_j
1	16.67	1.500	0.852
2	45.00	1.360	0.773
3	62.00	1.200	0.682
4	83.33	1.000	0.568

For $Ro = 1.760 \times 10^{-2}$ m.

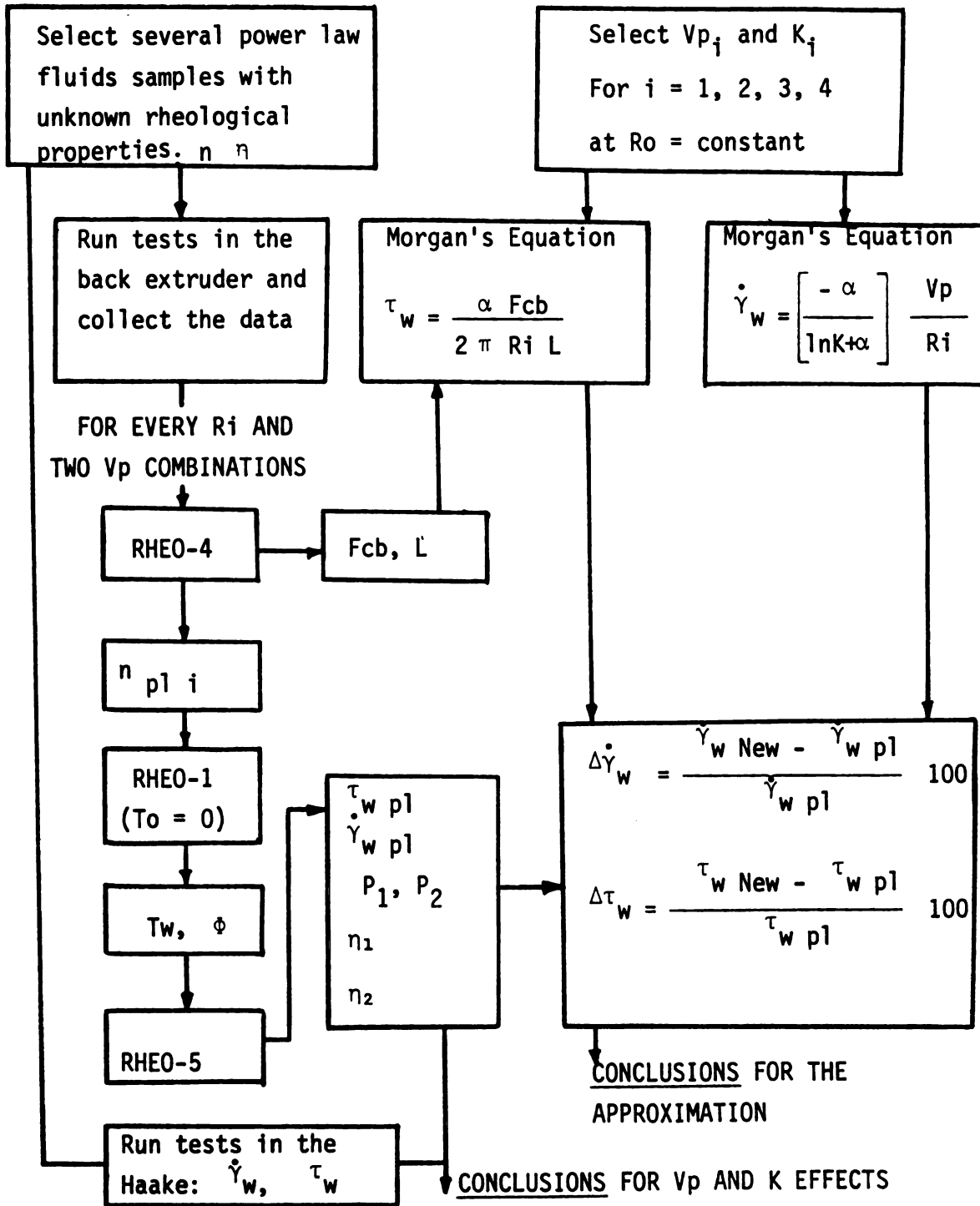


Figure 5. Newtonian shear rate approximation of power law fluids based on experimental data.

1. Five different power law model fluids were selected to be used in the back extrusion device: 1.0 % Methocel, 1.0 % guar gum, 1.5 % Methocel, 1.5 % guar gum and 2.0 % Methocel.

The solutions were prepared at the laboratory.

2. An additional fluid, high sucrose corn syrup, was also used to check the Newtonian behavior.

3. The plunger velocities and the plunger radii selected were the same as in Section 4.4.

4. The sample fluids were placed in glass cylinders ($R_o = 0.0176$ m) and allowed to sit until the air bubbles were out of the fluid.

5. The Instron compression cell capacity was 50 Newtons. For each fluid, at each one of the four different plunger radii, the experiments were run for the four different plunger velocities, and the data was collected.

In the chart recorder, as shown in Figure 6, the force recorded while the plunger is traveling down (F_T) and the force recorded after the plunger is stopped (F_{Te}), are functions of the specific fluid tested, of the plunger velocity and of the geometry of the system.

6. The set of collected data from the charts and from the specific conditions for each experiment were

F_T , F_{Te} , V_p , R_o , R_i , and fluid density.

7. The values of n were obtained with Equation (8) using RHEO-4 for every possible velocity combination. In this way, the effect of V_p and R_i in the general results in the back extrusion are considered.

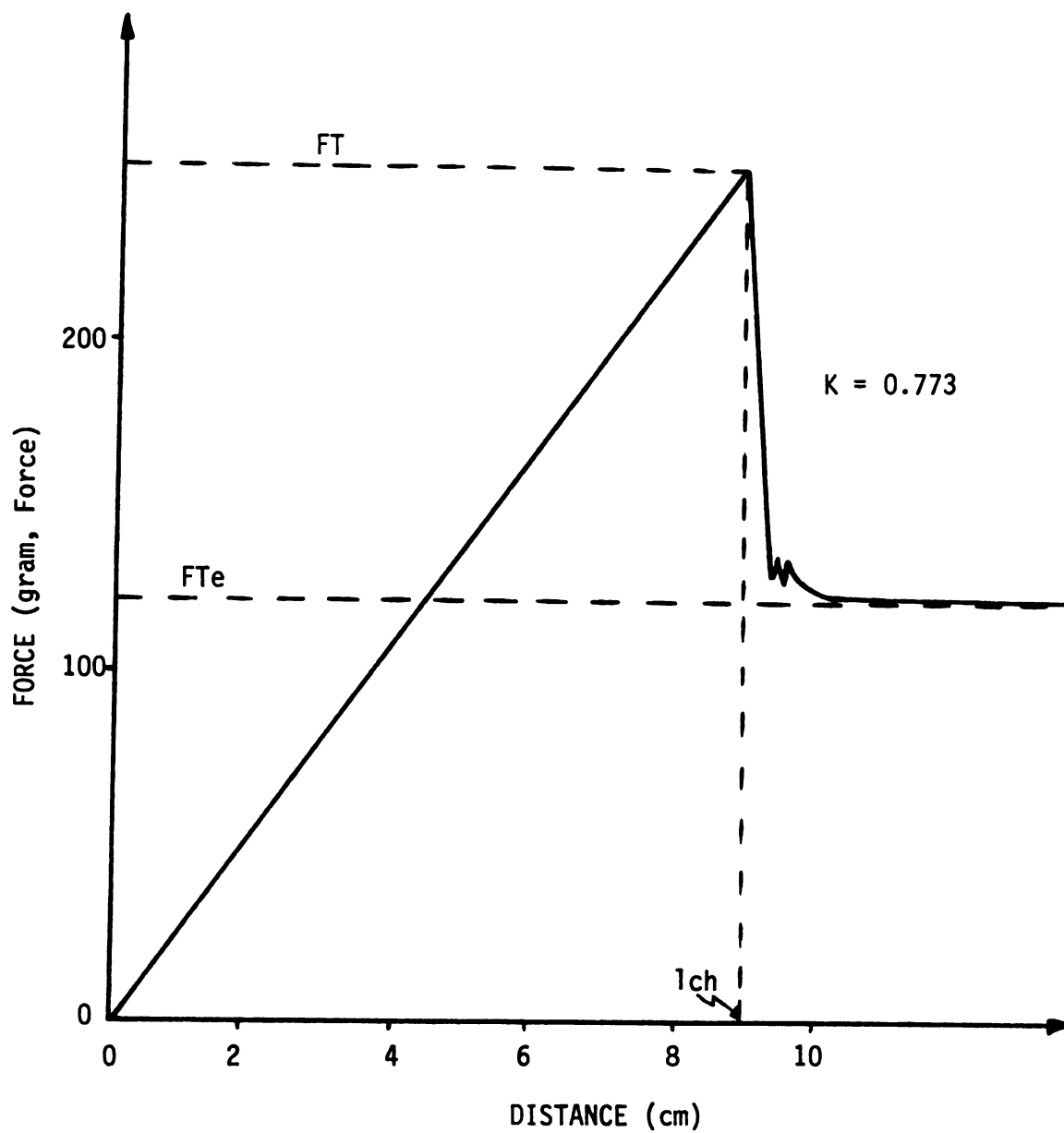


Figure 6. Diagram of force versus distance obtained from the Instron to recorder, for 1.5 % Methocel with plunger velocity of 8.33×10^{-3} m/s and a chart speed of 5.0×10^{-4} m/s (Osorio, 1985).

8. Using RHEO-1, knowing K , n and $T_o = 0$ for every fluid at different two V_p combinations, values of T_w and Φ were obtained.

9. Using RHEO-5, with n , F_{cb} , K , T_w , Φ and L , for every set of data corresponding to two velocities, the following parameters were determined: P_1 , P_2 , η_1 , η_2 , $\tau_w pl$ and $\dot{\gamma}_w pl$.

10. The values of $\tau_w pl$ and $\dot{\gamma}_w pl$ were compared with $\tau_w New$ and $\dot{\gamma}_w New$ respectively, obtained from Equations (4) and (6).

11. Using data from the Haake, the rheological properties of each fluid were determined and the results were compared to those obtained using the back extrusion.

12. After the analysis of the data, some conclusions will be made to evaluate the effect of V_p and R_i in the determination of the rheological properties, and about the Newtonian approximation of the power law fluids.

13. Shear rate ranges were established from all the collected data.

An example calculation of the total procedure used in the determination of the rheological properties of a power law fluid using the back extrusion device is given in Appendix C.

4.6 Power Law Approximation for Herschel-Bulkley Fluids

Based on Experimental Data

1. Three different kelset solution concentrations were prepared for the experiments: 1.25 % Kelset, 1.50 % Kelset and 2.00 % Kelset.

2. The plunger velocities and the plunger radii used were the same as in the Newtonian approximation procedure.

3. Steps 4 to 6 from the Newtonian approximation for power law fluids procedure were repeated.

4. Using RHEO-2, with the collected data, the values for $P(T_w + K)$ versus η were generated for each fluid at different annular gaps. τ_o , n and η were obtained from those plots.

5. With the τ_o , n and η values, using RHEO-3, the shear rate at the wall and the shear stress at the wall ($\dot{\gamma}_w$ HB and τ_w HB) were calculated at different velocity and annulus combinations.

6. Proceed to calculate the power law approximation for the H-B fluids: $\dot{\gamma}_w$ PL and τ_w PL.

In this case, as was explained in Chapter 3, with the F_{cb} obtained at different plunger velocities, for each constant K , the flow behavior index will be calculated using RHEO-2. The new n (pl) value correspond to the flow behavior index of the H-B fluid approximated to the power law model, for two different V_p values.

7. Using RHEO-1, Knowing K , $T_o = 0$ and $n(pl)$, the values of Φ and T_w were obtained.

8. For all fluids, with $n(PL)$ and Φ , the consistency coefficient (η_{pl}) was calculated according with Equation (9) for different plunger velocity and K values.

9. Using RHEO-3, with $n(pl)$, η_{pl} , $\tau_o = 0$, K and V_p values, the $\dot{\gamma}_w$ pl and the τ_w pl were obtained and compared to $\dot{\gamma}_w$ HB and τ_w HB respectively, to check the effect of V_p and R_i

on the results and to check for the power law approximation of H-B fluids.

10. The rheological properties of the three Kelset solutions were also determined using the Haake viscometer, and were used as reference in the evaluation of back extrusion results.

11. Shear rate ranges were established.

The experimental procedure for the power law shear rate approximation for Herschel-Bulkley fluids is summarized in Figure 7.

Appendix C shows an example of the calculations involved in the estimation of the real H-B values and the power law approximation values for the shear rate and the shear stress.

4.7 End Effects

To evaluate the end effect during the determination of the rheological properties using a back extrusion device, the procedure, as shown in Figure 8, is:

1. Select a power law fluid.

2. Fill several containers with the sample at different levels. Let them set to remove the air bubbles from the fluid samples.

3. Select a specific plunger radius to be used during the experiments so that the annular gap is constant.

4. Select a specific plunger velocity to use during the experiments.

5. Run tests for each different fluid level in the containers. Allow the plunger to travel the same distance inside

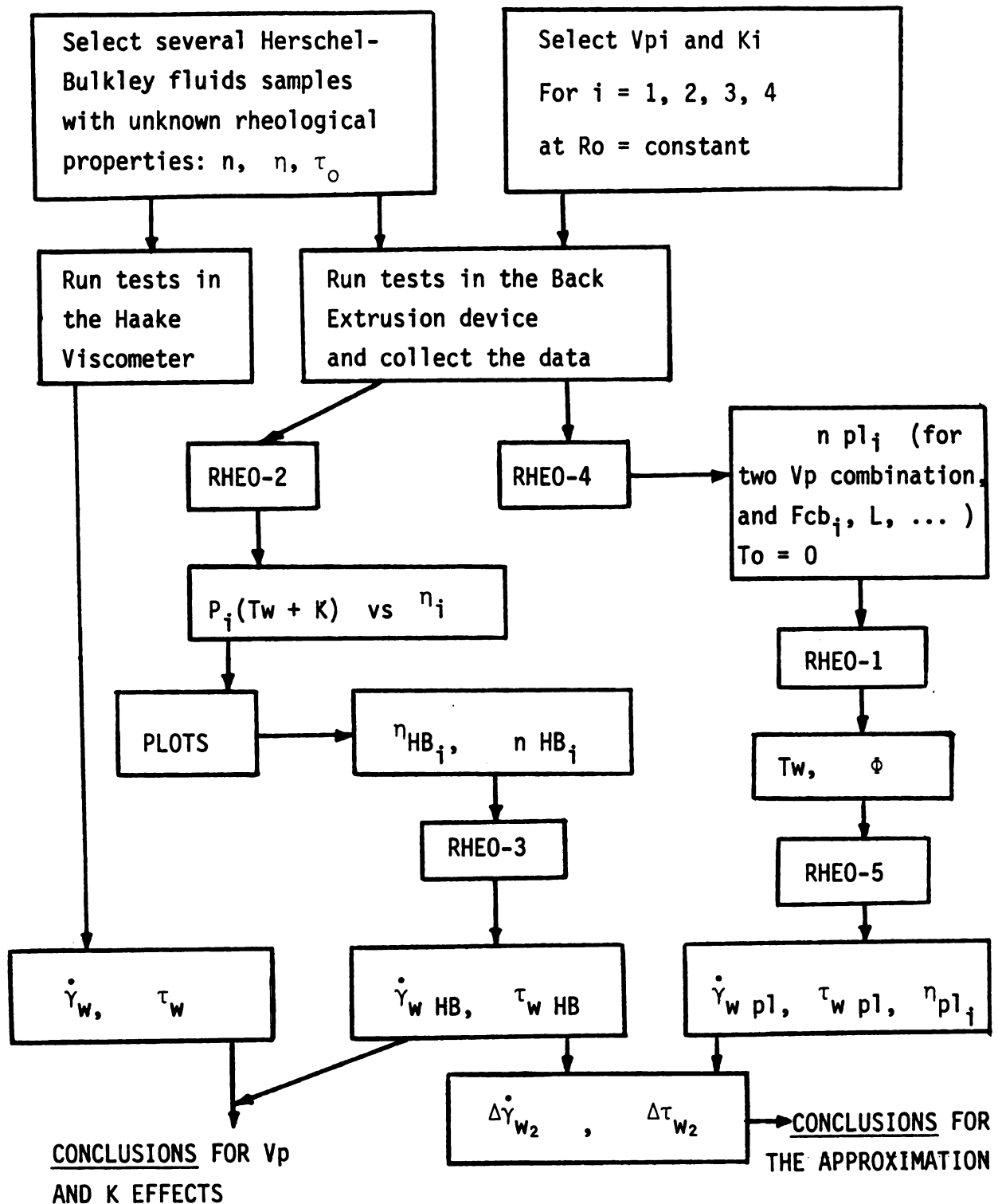


Figure 7. Power law shear rate approximation of Herschel-Bulkley fluids based on experimental data.

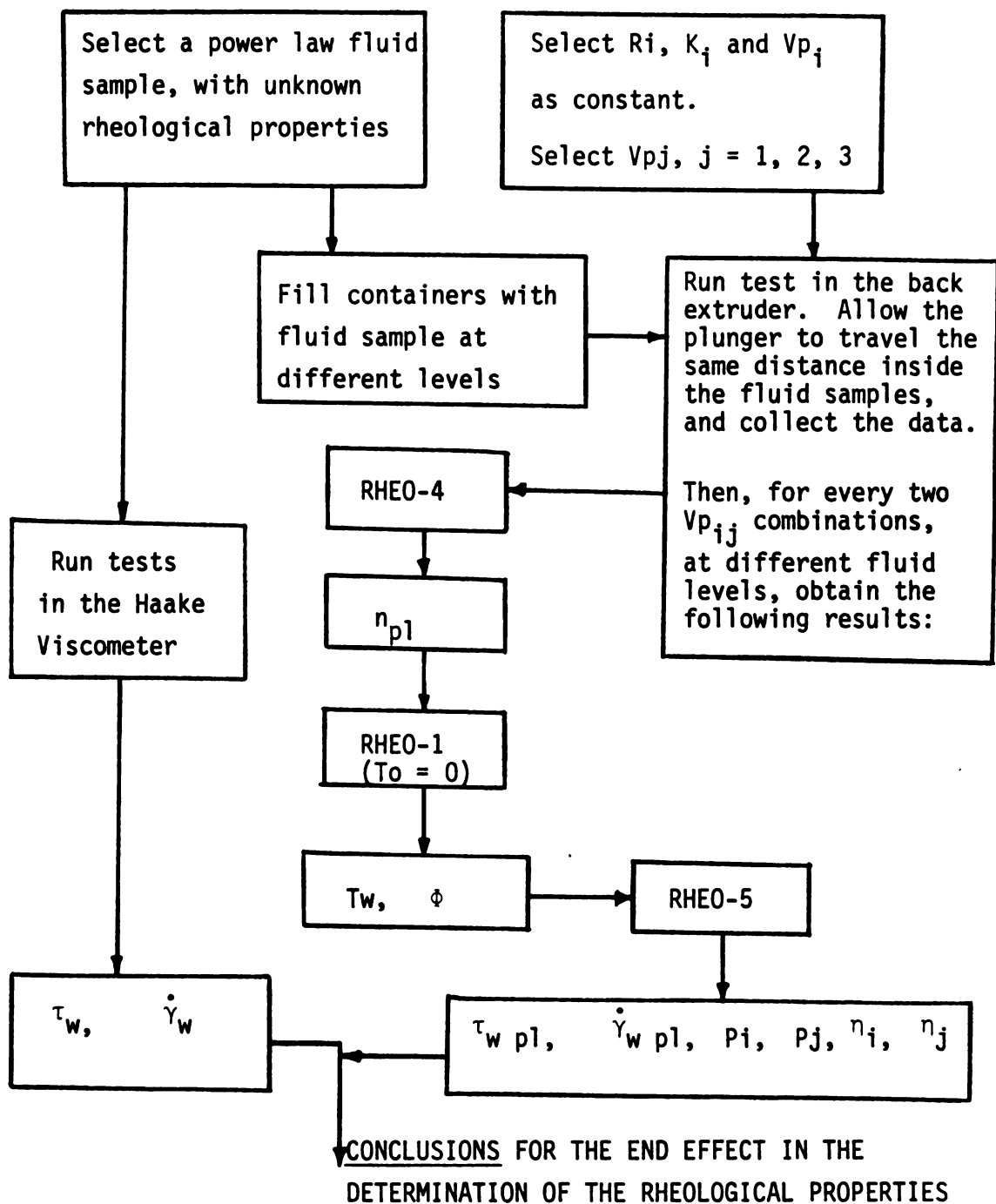


Figure 8. End Effect Evaluation .

the fluid samples, so that while the plunger is closer and closer to the cylinder (container) bottom, the end effect is taken into account for the same fluid, at different levels.

6. Collect the data, and determine if the rheological properties change when the plunger bottom approaches the container base (end effect).

The power law fluid selected was: 1.0 % Methocel solution. The plunger velocity selected was 45.00×10^{-4} m/s and the plunger radius was $R_i = 0.012$ m. The time axis was set to 1.0 min, and the scale range was 5.0 % (2.5 N).

Data were collected for the different test runs at eight different lengths of fluid in the container cylinders, for a constant plunger traveling distance. The smaller the length of fluid, the closer is the plunger rod end to the container bottom, (End Effect).

Since the theory of the power law fluid considered the use of two plunger velocities to determine the rheological properties, experimental data was also collected for the 1.0 % methocel solution at two other plunger velocities.

For the eight different fluid lengths, the n value was calculated using RHEO-2, for the three possible V_p combinations: 45.00 and 16.67, 45.00 and 62.00 and 45.00 and 83.33 ($\times 10^{-4}$ m/s). With RHEO-5 and the collected data, the η , P , $\dot{\gamma}_w$ and τ_w values were obtained for the different fluid lengths (0), and the different V_p combinations.

Chapter 5

RESULTS AND DISCUSSION

5.1 Shear Rate Approximations Based on Theoretical Data

The shear rate at the wall for Newtonian fluids, calculated using Equation (8) is shown in Table 3. The velocities of the plunger, and the plunger radii selected were the same as described in Table 1.

At the same time, Figure 9 shows the same values included in Table 3 but with the advantage that for other different conditions of V_p and R_i , the shear rate at the wall values for Newtonian fluids can be interpolated.

5.1.1 Newtonian Approximation for Power Law Fluids

Using RHEO-3, as explained in Chapter 4, the data included in Tables D1 to D5 of the Appendix D were generated. These tables summarize the shear rate at the wall (Equation (13)), shear stress at the wall (Equation (10)), and the difference between the shear rate at the wall for the five power law fluids (obtained using RHEO-3) with the shear rate at the wall approximated by Newtonian approximations (Equation (30)), at the five different plunger velocities and plunger radii selected.

Table 3. Shear rate at the wall for Newtonian fluids from Morgan's equation .

K V _p x10 ⁴ (m/s)	0.9500	0.8523	0.7727	0.6818	0.5682
	$\dot{\gamma}_w$ (s ⁻¹)	$\dot{\gamma}_w$ (s ⁻¹)	$\dot{\gamma}_w$ (s ⁻¹)	$\dot{\gamma}_w$ (s ⁻¹)	$\dot{\gamma}_w$ (s ⁻¹)
1.67	10.871	1.307	0.556	0.287	0.160
16.67	108.709	13.070	5.556	2.869	1.598
45.00	293.454	35.283	14.998	7.744	4.313
62.00	404.315	48.612	20.665	10.670	5.943
83.33	543.412	65.336	27.774	14.341	7.988

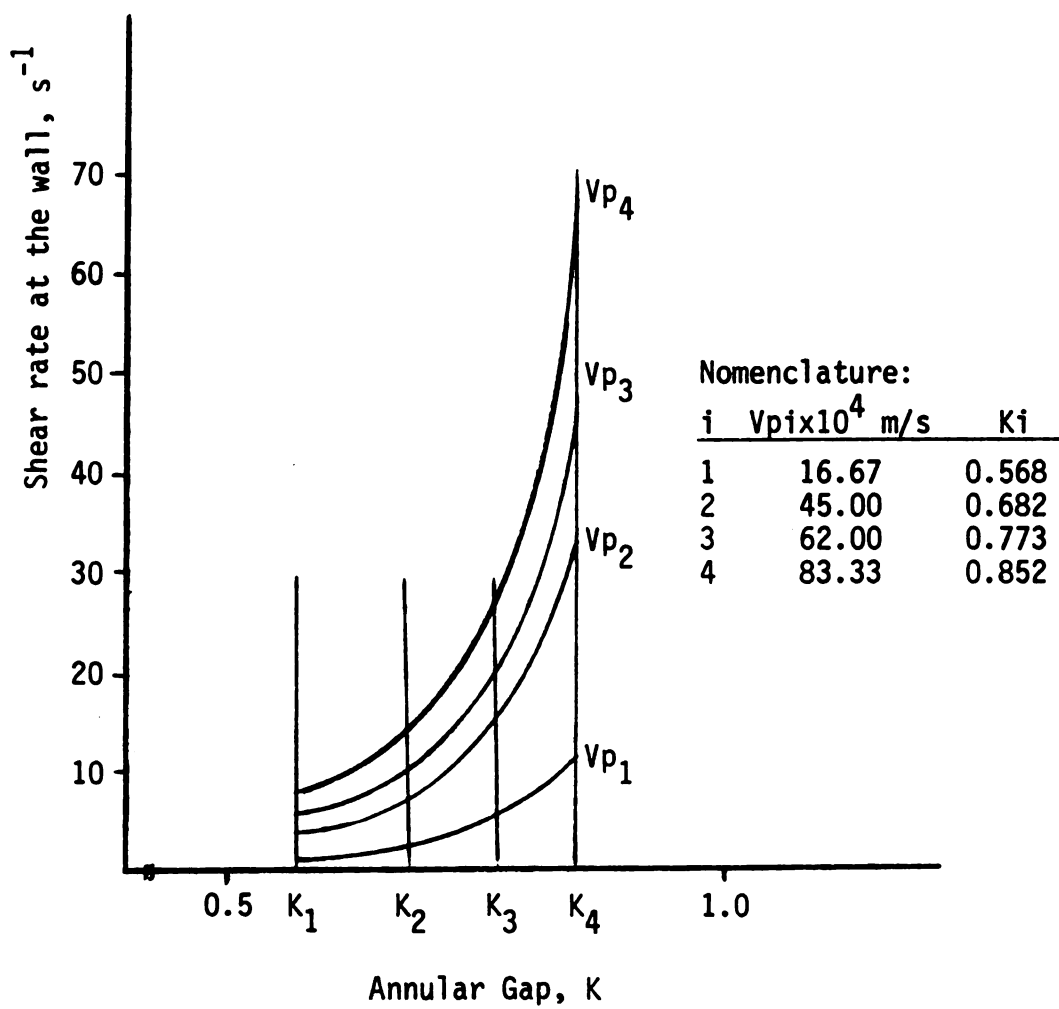


Figure 9. Shear rate at the wall for Newtonian fluids, based on Morgan's equation (Equation 6).

From Tables D1 to D5 it can be observed that:

1. At a constant annular gap ($K = R_i/R_o$), the $\Delta \dot{\gamma}_{w_1}$ is a constant for different plunger velocities (V_p).
2. For a specific power law fluid, at a constant V_p , if the annular gap decrease, so does the $\Delta \dot{\gamma}_{w_1}$ value. In other words, the greater the plunger radius value, the smaller the difference between the real value of $\dot{\gamma}_{w_{pl}}$ and the $\dot{\gamma}_{w_{New}}$. Then, a smaller error in $\Delta \dot{\gamma}_{w_1}$ corresponds to a smaller annular gap (or a greater K value).
3. As expected, the closer the flow behavior index (n) to the Newtonian case ($n=1$) the smaller the difference between the $\dot{\gamma}_{w_{PL}}$ and the $\dot{\gamma}_{w_{New}}$, which is desired, at a constant V_p .
4. In all cases, the difference range is small when n tends to 1 (Newtonian case). For a constant n and K values, $\Delta \dot{\gamma}_{w_1}$ varies less than 10 % when plunger velocity varies from V_{p1} (1.667×10^{-4} m/s) to V_{p5} (83.33×10^{-4} m/s). This result indicates that a relationship could exist between this velocity range and the n value or between the $\Delta \dot{\gamma}_{w_1}$ and the n value. The idea is supported by the fact that the same five plunger radii were used with all fluids, and V_p was found to have little influence on $\Delta \dot{\gamma}_{w_1}$ values obtained in the data simulation.

Table D6 summarize the shear rate at the wall and the shear stress at the wall for corn syrup at five different K and at two V_p . In this Table, the back extrusion equations developed by Osorio (1985) for Newtonian fluids and the equations developed by Morgan (1979) also for Newtonian fluids in a back extruder are compared. It can be seen that in all cases the difference

between the two shear rates at the wall was zero, which means that it is correct to consider the Morgan equation for the shear rate at the wall for Newtonian fluids as the approximation when dealing with power law fluids.

Table 4 shows the $\dot{\Delta\gamma}_{w_1}$ ranges corresponding to each specific n value for annular gaps ranging from 0.568 to 0.950, and for the plunger velocity ranging from 1.667×10^{-4} to 83.33×10^{-4} m/s. On the other hand, from the data included in Tables D1 to D6 the differences in shear rates at the wall ($\dot{\Delta\gamma}_{w_1}$) were plotted as function of the annular gaps (K), for different plunger velocities. Figures 10, 11, 12 and 13 show some examples of those plots for 1.5% guar gum, 2.0% Methocel, 1.5% Methocel and corn syrup.

From those figures, for the theoretical data simulation for power law fluids, the same observations established from Tables D1 to D6 were confirmed. In addition, it was noted that the Newtonian approximation will work independently of the V_p used, but will work better at the highest possible K value which corresponds to the smaller annular gap.

Therefore, plunger velocity does not affect the results, and there exists an optimum plunger radius to get a smaller difference between the shear rate at the wall for the power law fluids and the shear rate at the wall for Newtonian approximation. Finally, it can be observed that the n and the η values also affect the results: the closer the rheological properties of the power law fluids to the Newtonian case, the smaller is the difference between the shear rate at the wall of both.

Table 4. Shear rate at the wall ranges
for different flow behavior
indices corresponding to
different power law fluids

n	$\dot{\gamma}_w$ Range (s ⁻¹)
1.000	0.000 - 0.000
0.750	0.105 - 0.140
0.690	0.136 - 0.184
0.513	0.250 - 0.325
0.259	0.501 - 0.599
0.159	0.651 - 0.739

K range : 0.950 - 0.568

Vp range : 1.67×10^{-4} - 83.33×10^{-4} m/s

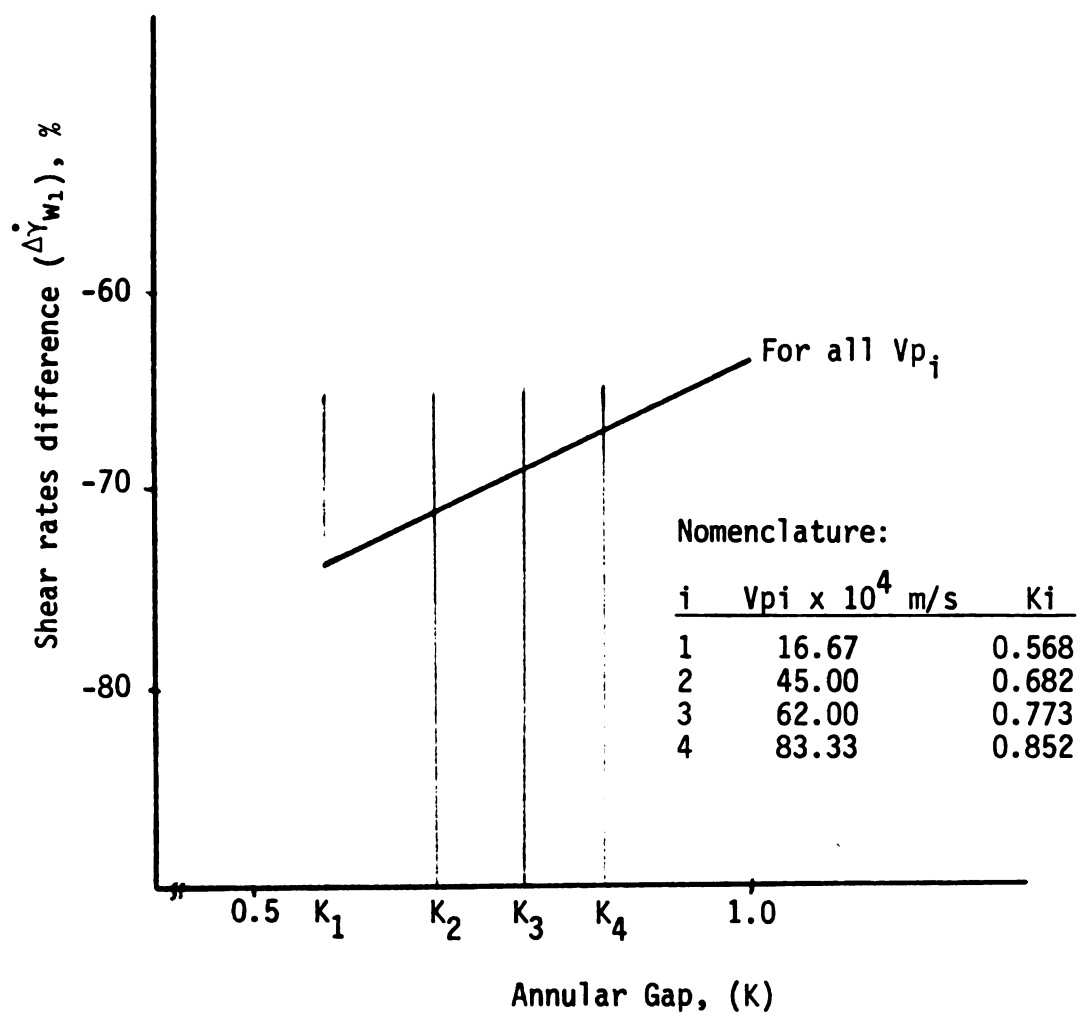


Figure 10. Shear rates difference versus annular gap, at different plunger velocities, for 1.5 % guar gum.

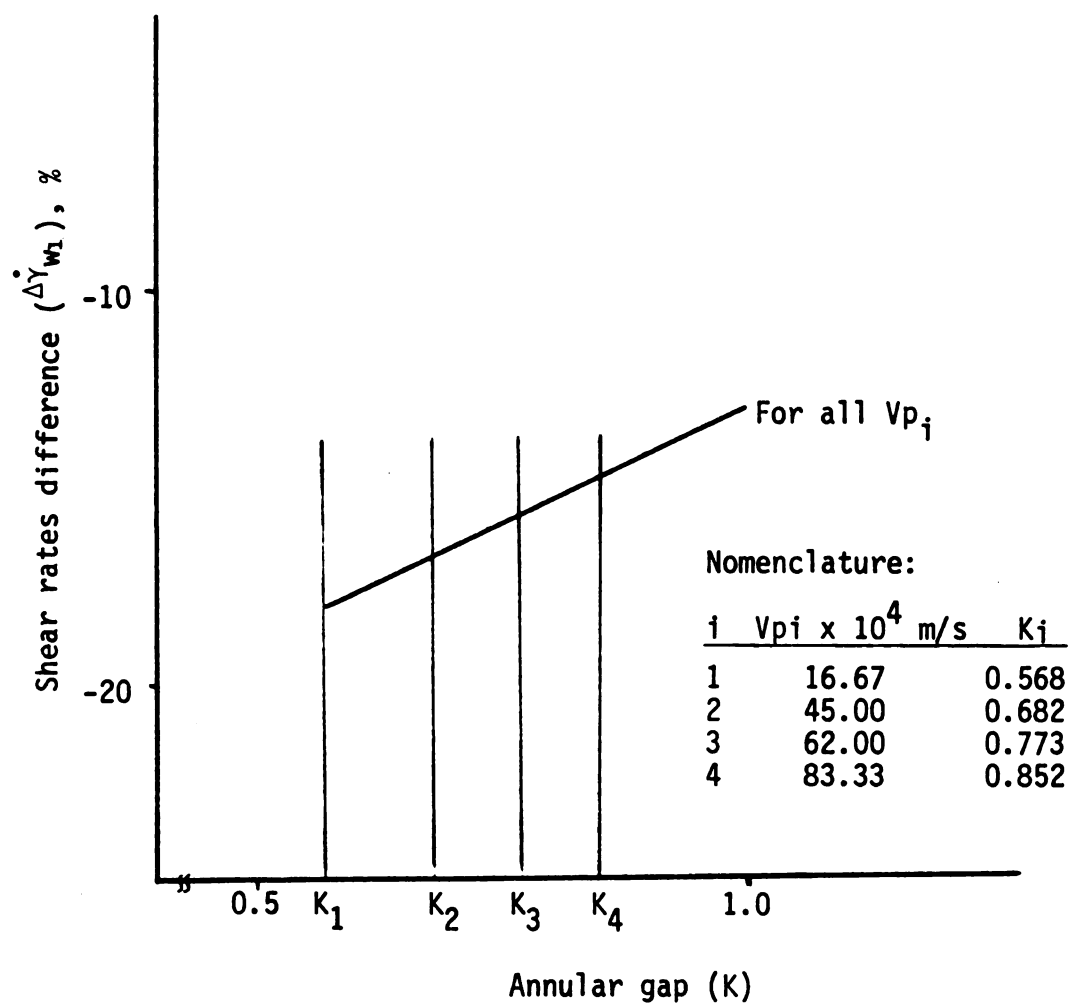


Figure 11. Shear rates difference versus annular gap, at different plunger velocities, for 2.0 % Methocel.

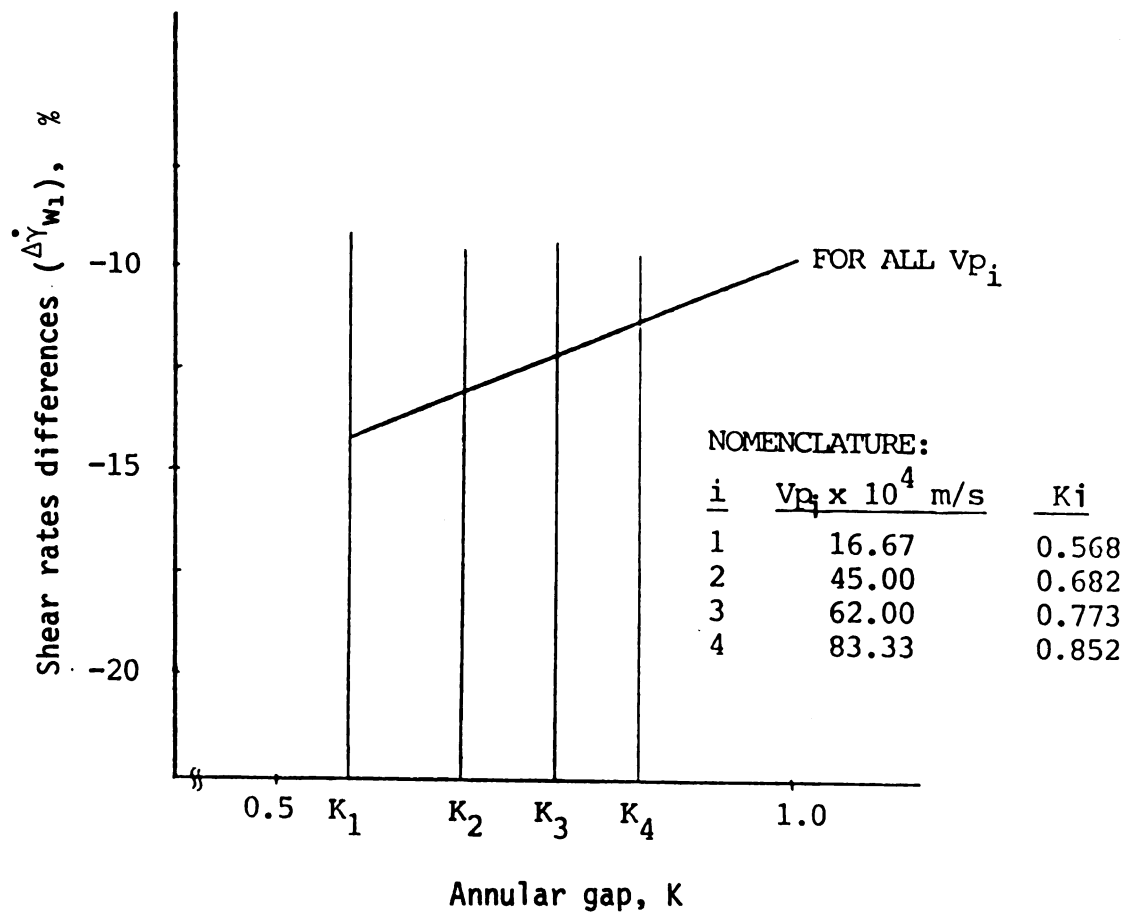


Figure 12. Shear rates differences versus annular gap, at different plunger velocities, for 1.5 % Methocel.

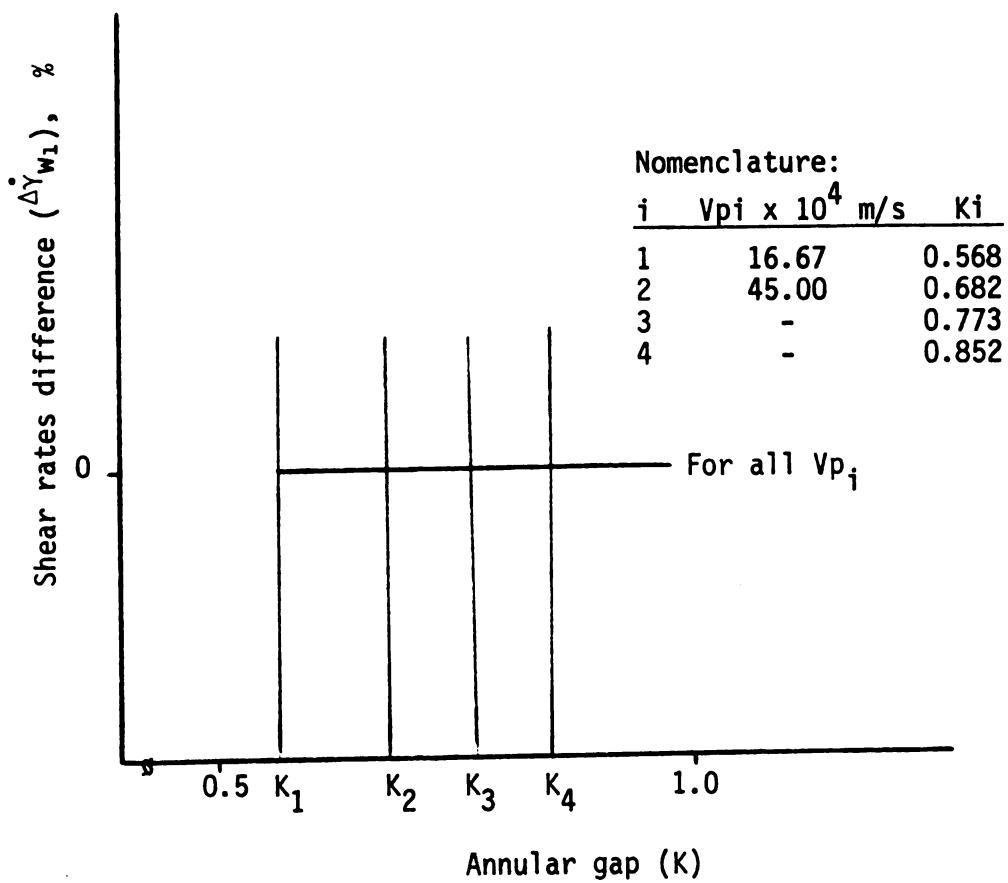


Figure 13. Shear rates difference versus annular gap, at different plunger velocities, for corn syrup.

At the same time, the data included in Tables D1 to D6 were plotted as shown in Figure 14 for 1.5 % guar gum and in Figure 15 for 2.0 % Methocel, where the shear rate at the wall of the power law fluids was plotted as a function of the annular gap at different plunger velocities. From those figures, it was noted that the plunger velocity and the plunger radius affect the shear rate at the wall range as was expected: the higher V_p and higher K (smaller annular gap), the higher shear rate at the wall value for the same fluid.

5.1.2 Power Law Approximation for Herschel-Bulkley Fluids

As explained in Chapter 4, the following sets of data were generated:

Tables D7 to D9 (Appendix D) summarize the shear rate at the wall ($\dot{\gamma}_w \text{ HB}$) for the three H-B fluids obtained from RHEO-3, with their rheological properties known, at five different V_p and at four different K values. Also included are the shear rate at the wall approximated to power law ($\dot{\gamma}_w \text{ pl}$), for the same fluids, under the same conditions, as explained in Chapter 4, and their difference (Equation (31)) $\Delta\dot{\gamma}_w$.

From Tables D7 to D9 it can be observed that:

1. For all velocities, except $V_p = 1.667 \times 10^{-4} \text{ m/s}$, the $\dot{\gamma}_w \text{ pl}$ calculated as the approximation is higher than $\dot{\gamma}_w \text{ HB}$, which implies a positive value for $\Delta\dot{\gamma}_w$. For $V_p = 1.667 \times 10^{-4} \text{ m/s}$ the $\dot{\gamma}_w \text{ pl}$ is smaller than $\dot{\gamma}_w \text{ HB}$, giving a negative value for $\Delta\dot{\gamma}_w$.

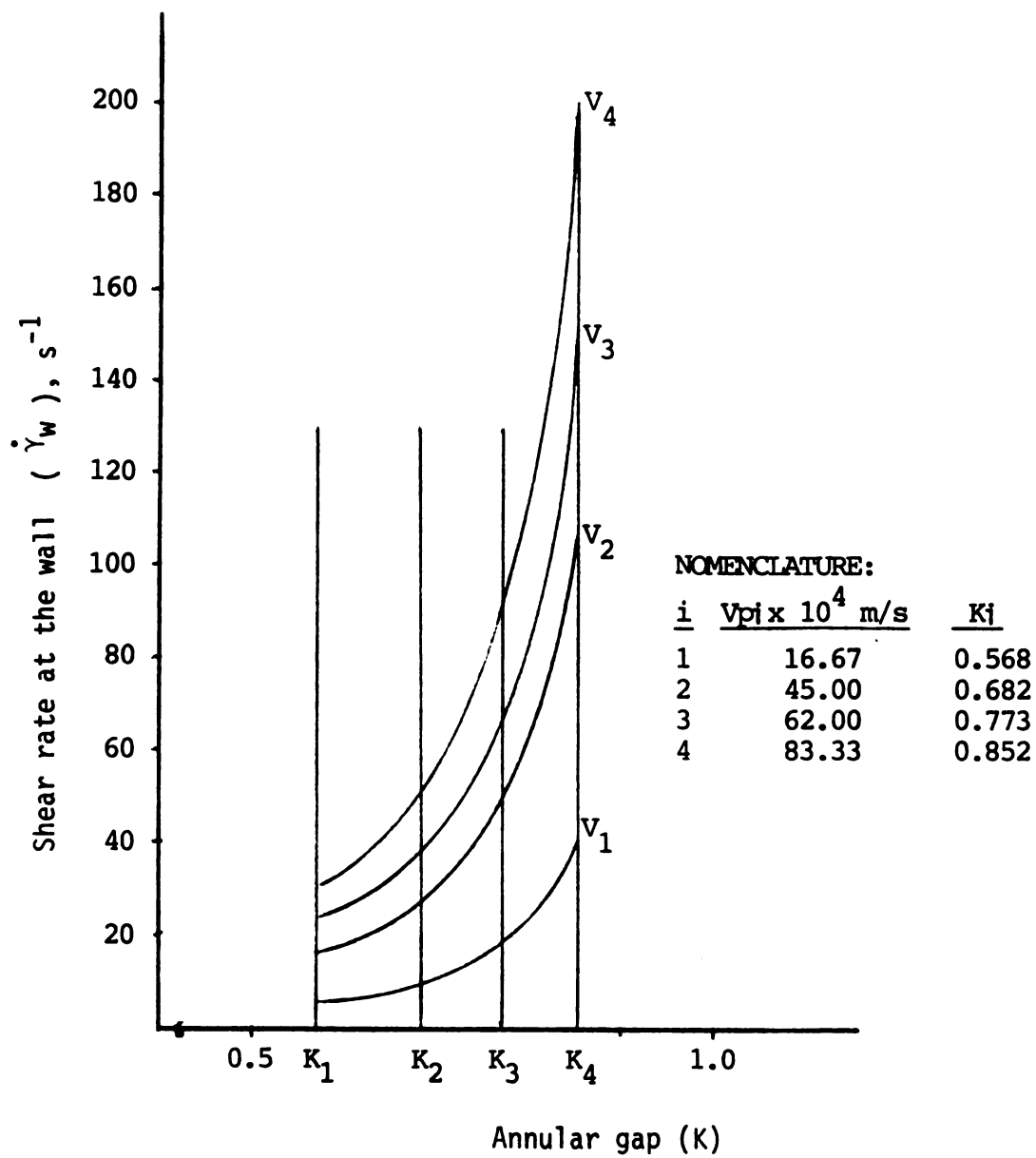


Figure 14. Shear rate at the wall versus annular gap, at different plunger velocities, for 1.5 % guar gum.

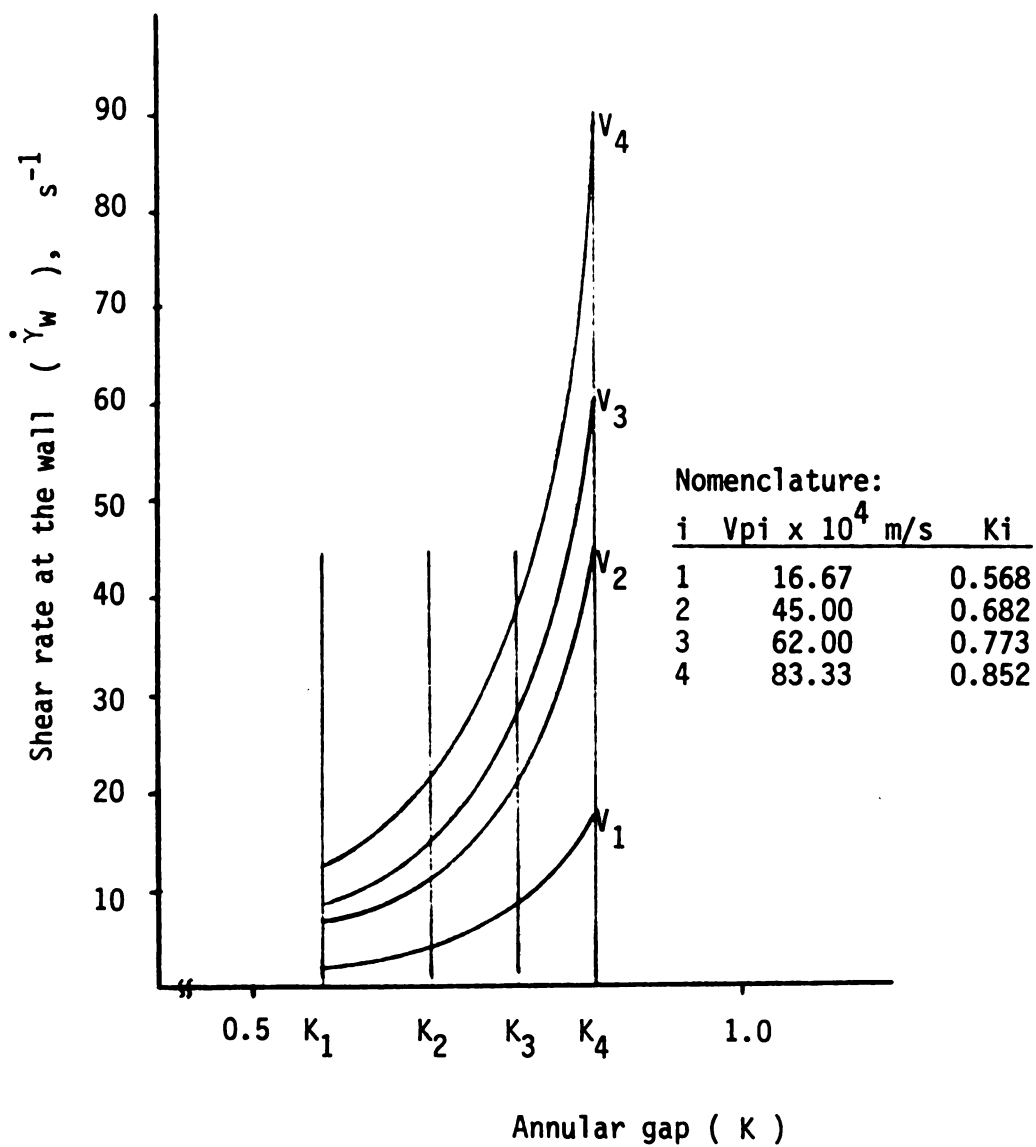


Figure 15. Shear rate at the wall versus annular gap, at different plunger velocities, for 2.0 % Methocel.

2. $\dot{\Delta\gamma}_{w_2}$ decreases when K increases (Ri increases); and $\dot{\Delta\gamma}_{w_2}$ increases when Vp increases from 16.67×10^{-4} to 83.33×10^{-4} m/s.
3. As a result, the best combination to obtain a smaller $\dot{\Delta\gamma}_{w_2}$ value as desired is when the plunger velocity is 16.67×10^{-4} m/s and the plunger radius is 0.015 m, which correspond to $K = 0.85$ for $R_o = 0.0176$ m.
4. A higher $\dot{\Delta\gamma}_{w_2}$ corresponds to a higher yield stress present in the H-B fluid. Working under the best conditions of K and Vp ($V_p = 16.67 \times 10^{-4}$ m/s and $K = 0.85$), when the yield stress has values from 1 to 5 Pa, the $\dot{\Delta\gamma}_{w_2}$ range is not higher than 10 %; when the yield stress has values from 5 to 10 Pa, the $\dot{\Delta\gamma}_{w_2}$ range is not higher than 20 %.

The data included in Tables D7 to D9 were plotted for all Herschel-Bulkley fluids as shown in Figure 16 for 1.0 % Kelset and in Figure 17 for 1.5 % Kelset, where the real difference of the shear rates at the wall ($\dot{\Delta\gamma}_{w_2}$) was plotted as a function of the annular gap (K), at different plunger velocities (Vp).

From these figures it can be observed again that there exists an optimum plunger radius (for $K = 0.85$) which gives smaller values for the difference $\dot{\Delta\gamma}_{w_2}$, and there exists an optimum plunger velocity ($V_p = 16.67 \times 10^{-4}$ m/s) which also gives smaller values for $\dot{\Delta\gamma}_{w_2}$. At the same time, the rheological properties (n , η , τ_o) are also affecting the results: the closer to the power law case ($\tau_o = 0$), the smaller the difference $\dot{\Delta\gamma}_{w_2}$.

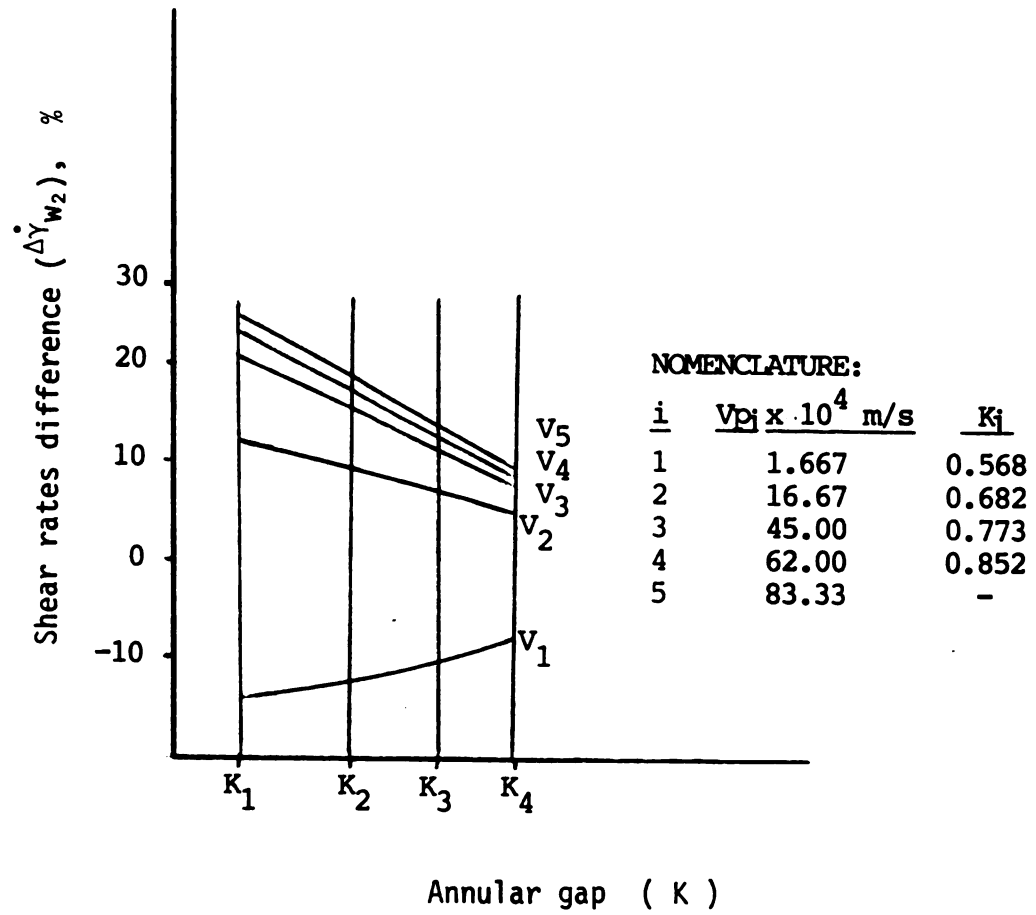


Figure 16. Shear rates difference versus annular gap, at different plunger velocities, for 1.0 % Kelset.

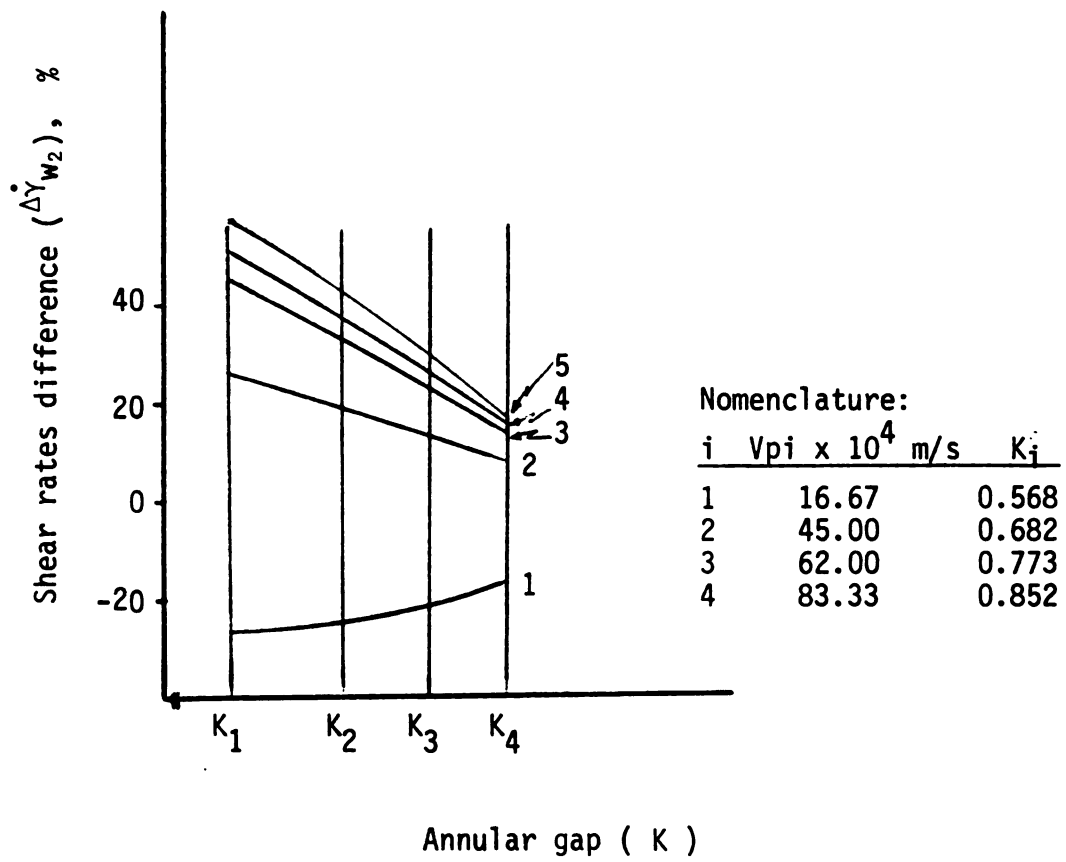


Figure 17. Shear rates difference versus annular gap, at different plunger velocities, for 1.5 % Kelset.

Tables D10 to D12 (Appendix D) summarize the shear stress at the wall for the three Kelset solutions used as H-B samples, obtained using RHEO-3 at the five plunger velocities and the four plunger radii selected. Also included are the shear stress values at the wall approximated by power law equation ($\tau_w pl$) for the same fluids under the same conditions of V_p and K , as was explained in Chapter 4, and their difference expressed by Equation (32).

From Tables D10 to D12 very good observations can be made:

1. The τ_w is affected by both V_p and R_i . However, for a constant R_i , the $\Delta\tau_{w_2}$ is almost constant for different V_p , which means that the plunger velocities do not affect the overall results.
2. At a constant V_p , the $\Delta\tau_{w_2}$ decreases with the increasing of R_i .
3. In a small range (lower than 3 %), at a constant K , the $\Delta\tau_{w_2}$ decreases with decreasing V_p .
4. For all V_p and K used, the $\tau_w HB$ is higher than the $\tau_w pl$, which implies a negative value in the $\Delta\tau_{w_2}$.
5. In general, the $\Delta\tau_{w_2}$ are higher than the $\Delta\dot{\gamma}_{w_2}$. This fact suggests that, under the same conditions of V_p and R_i , τ_0 affects the results.
6. The best combinations to obtain smaller values in $\Delta\tau_{w_2}$, which is desired, are when the V_p is 1.667×10^{-4} or 16.67×10^{-4} m/s and $K = 0.85$.

In addition, from Figures 18 and 19, where the $\Delta\tau_{w_2}$ was plotted as function of K , for different V_p , for 1.0 % and 1.5 %

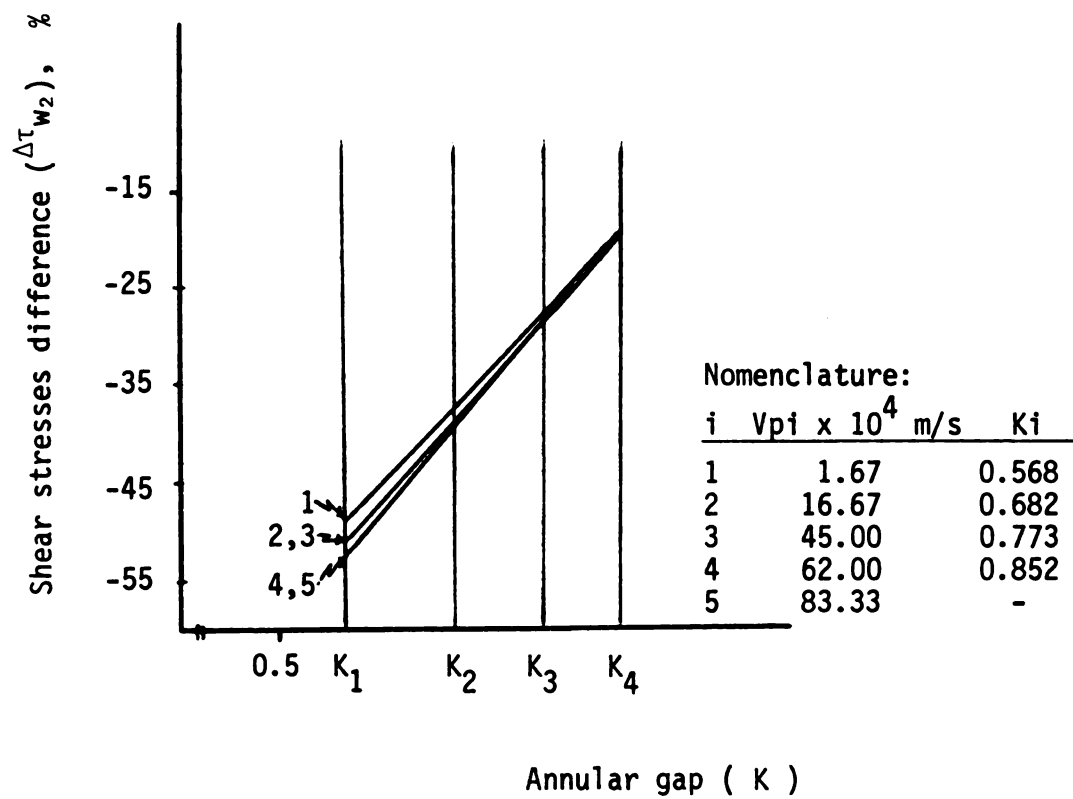


Figure 18. Shear stresses difference versus annular gap, at different plunger velocities, for 1.0 % Kelset.

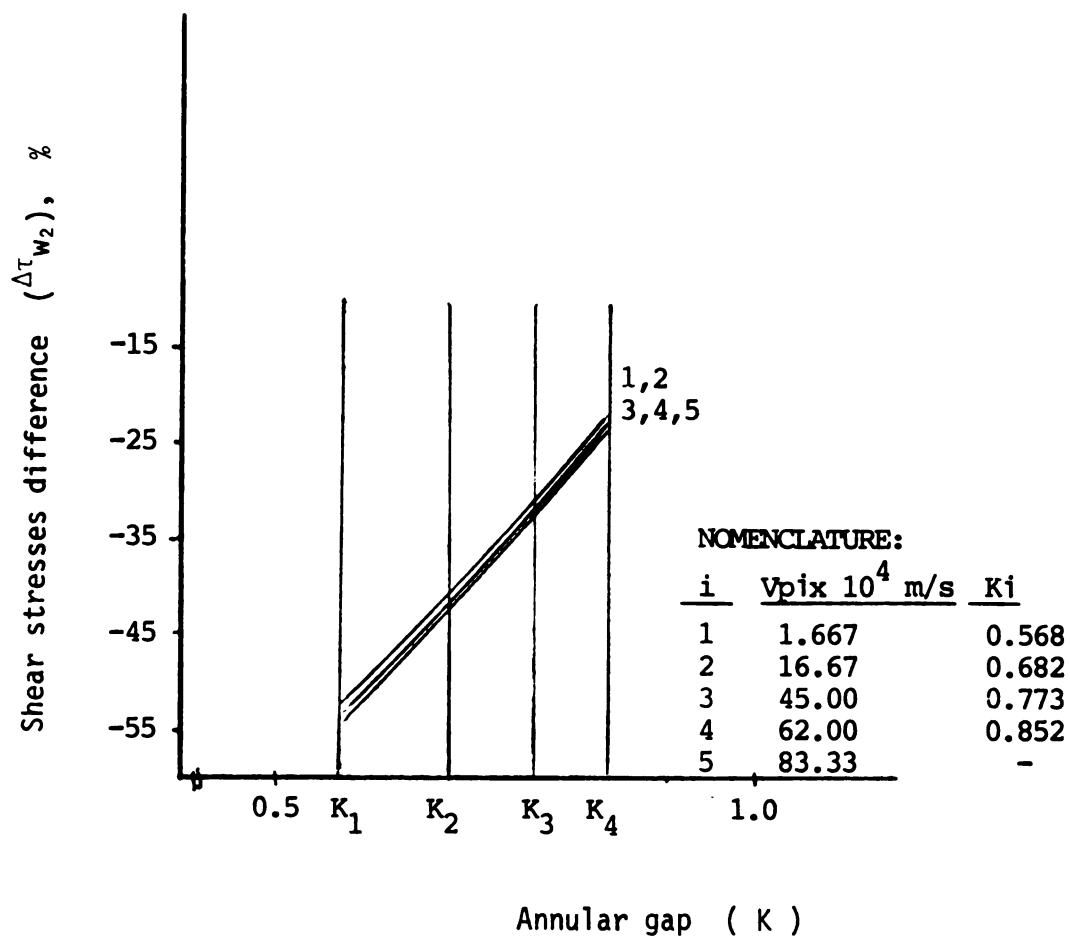


Figure 19. Shear stresses difference versus annular gap, at different plunger velocities, for 2.0 % Kelset.

Kelset solutions respectively, it can be observed that:

a)- Since the τ_w HB is approximated by τ_w pl, the $\Delta\tau_{w_2}$ plots reflects that the smaller $\Delta\tau_{w_2}$ will exist when the smaller annular gap (larger K value) is used.

b)- For all different plunger velocities, the slopes are almost the same for each H-B fluid meaning that the plunger velocity does not strongly affect the approximation results.

Finally, consider Figure 20 for 2.0 % Kelset solution, as an example, where the shear rates at the wall for the Herschel-Bulkley fluids were plotted as function of the annular gaps for different plunger velocities. The data show that the plunger velocity affects the shear rate ranges in the same way that the annular gap does: the higher V_p , the higher shear rate at the wall value at constant K, and the higher K value (smaller annular gap), the higher shear rate at the wall value at constant V_p .

The theoretical rheograms developed for the H-B fluids and their power law approximation were also plotted. Figure 21, 22 and 23 are some examples of those rheograms for 2.0 % and 1.5 % Kelset solutions. Once again, it can be observed that:

1- From Figure 21, the smaller V_p , the closer the power law approximation for the Herschel-Bulkley fluids, but the shear rate at the wall range is smaller. Therefore, the rheograms of the power law approximation are affected by the plunger velocity. The H-B rheogram is not affected by V_p .

2- From Figures 22 and 23, the smaller annular gap (bigger K value), the higher shear rate at the wall range and closer the power law approximation rheogram to the H-B rheogram, which

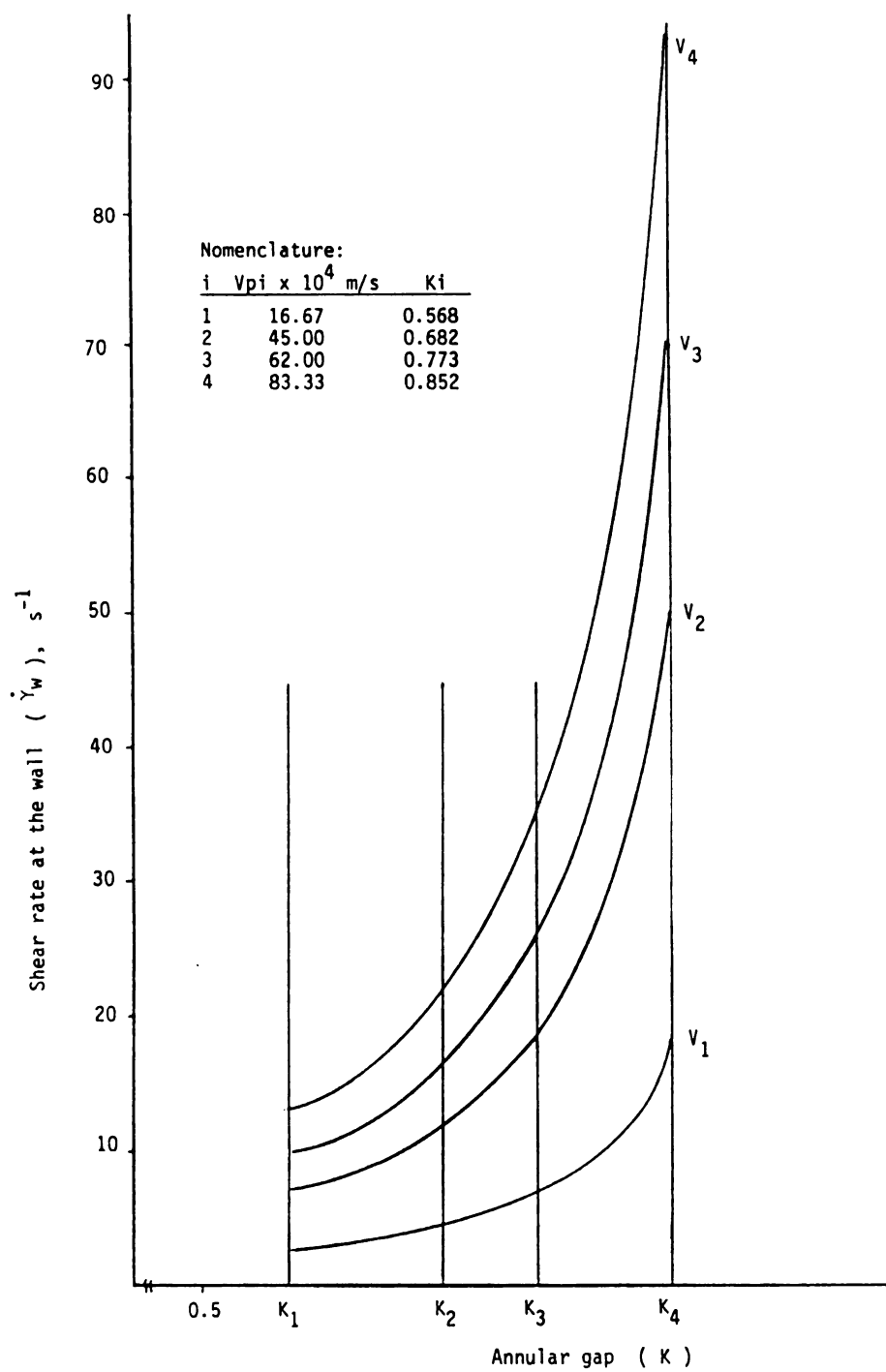


Figure 20. Shear rate at the wall versus annular gap, at different plunger velocities, for 2.0 % Kelset.

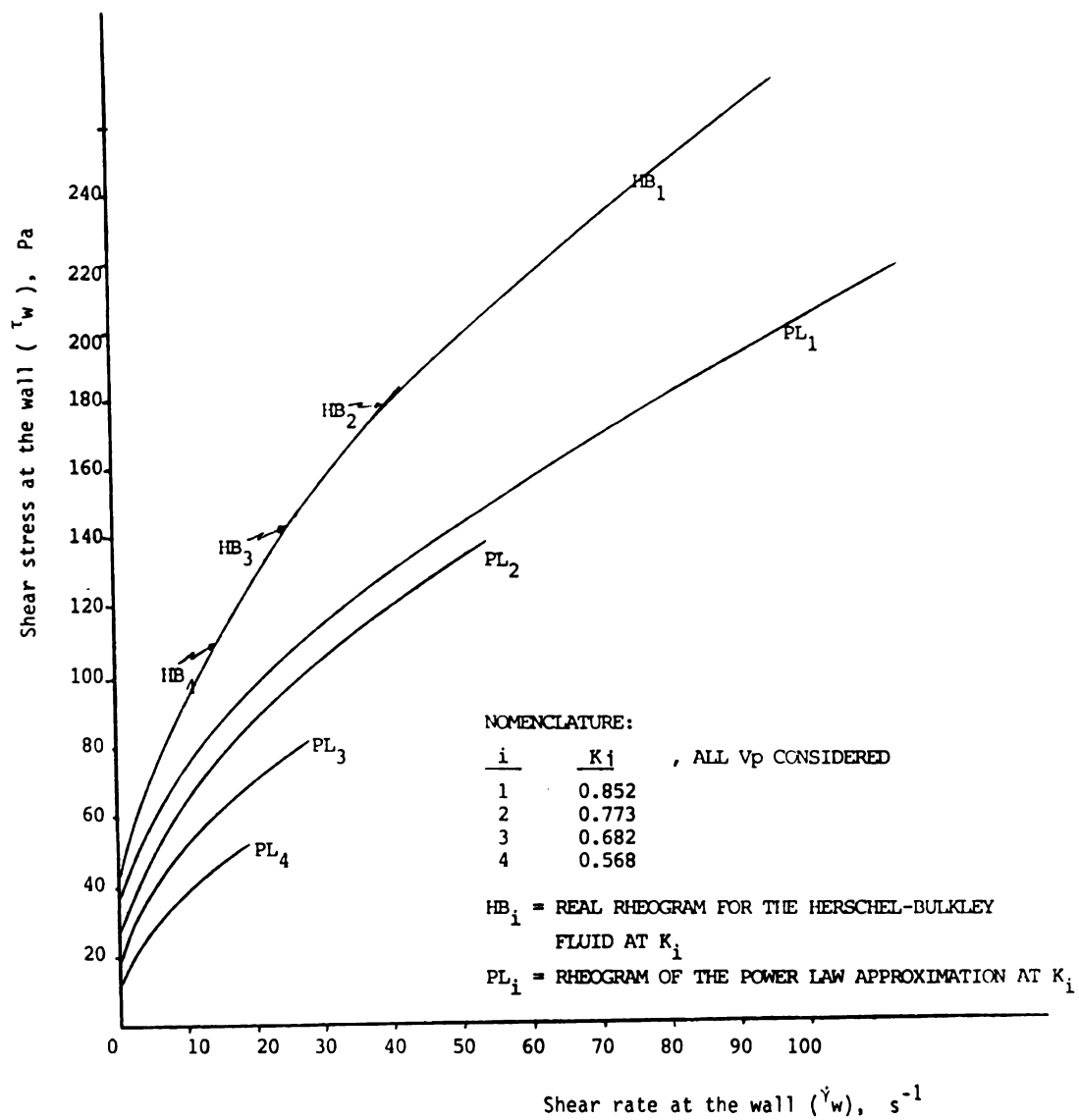


Figure 21. Effect of the dimensionless annular gap (K) on the power law approximation of a Herschel-Bulkley fluid (2.0 % Kelset).

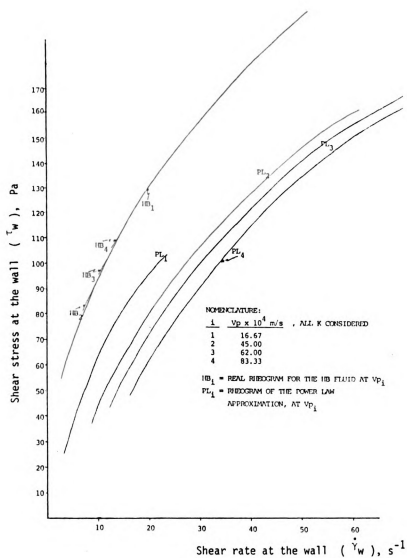


Figure 22. Effect of the plunger velocity (V_p) on the power law approximation of a Herschel-Bulkley fluid (2.0 % Kelset).

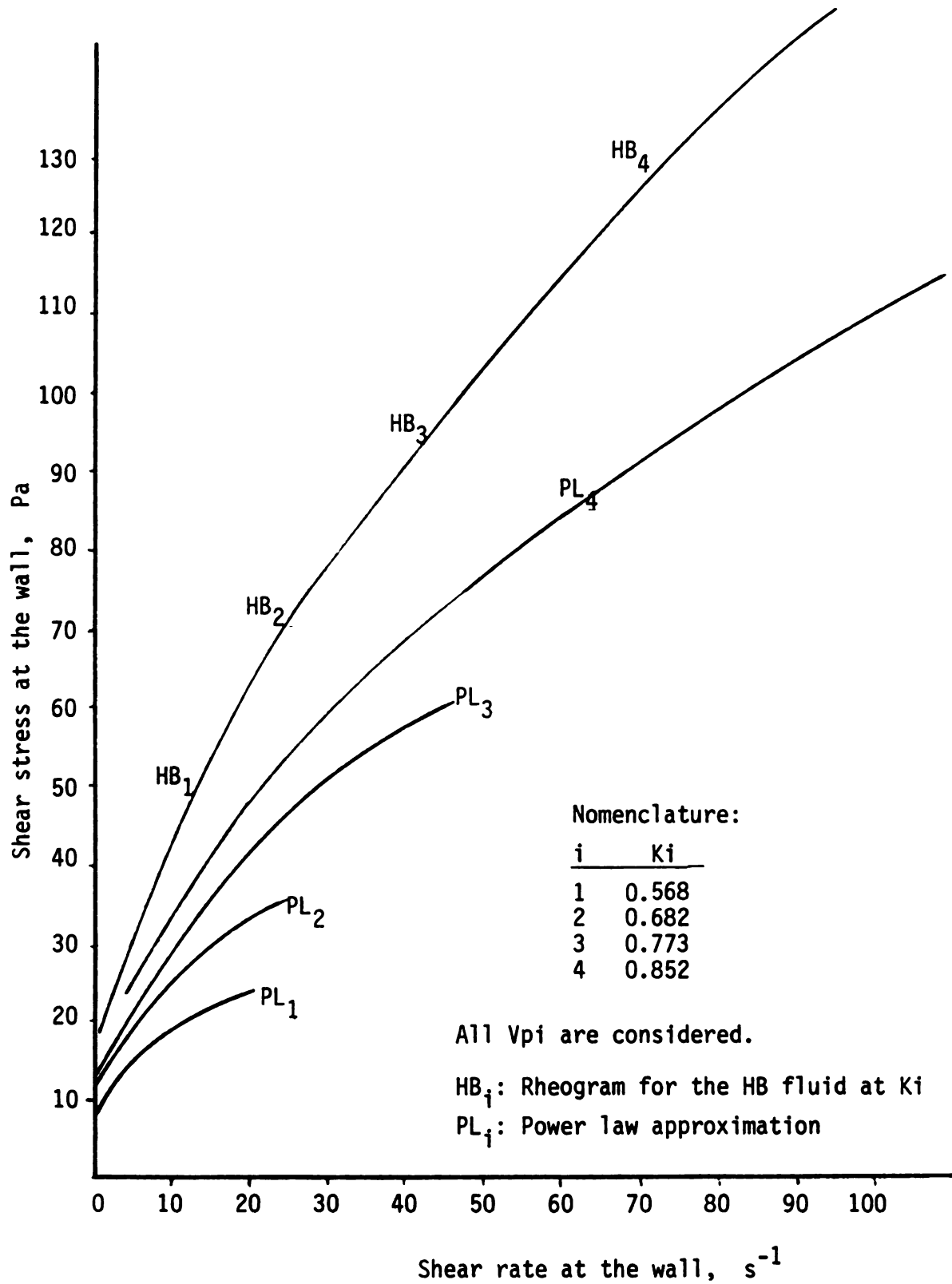


Figure 23. Effect of the dimensionless annular gap (K) on the power law approximation of a Herschel-Bulkley fluid. (1.5 % Kelset).

means lower error in the approximation.

Therefore, the rheogram of the power law approximation is affected by the annular gap. The H-B rheogram is not affected by K.

3- The higher the shear rate value, the larger the difference between the H-B and the power law rheograms.

5.2 Shear Rate Approximation Based on Experimental Data

5.2.1 Newtonian Approximation for Power Law Fluids

Experimental results of Newtonian approximation of power law fluids, using the back extrusion technique, are shown in the following tables (Appendix D):

Tables D13 to D16 summarize the results for 1.0 % Methocel solution at different Ri and Vp.

Tables D17 to D20 summarize the results for 2.0 % Methocel solution at different Vp and Ri.

Tables D21 to D24 summarize the results for 1.0 % guar gum solution at different Vp and Ri.

Tables D25 to D28 summarize the results for 1.5 % guar gum solution at different Vp and Ri.

Tables D29 to D32 summarize the results for 1.5 % Methocel solution at different Vp and Ri.

Tables D33 to D36 summarize the results for high sucrose corn syrup, at different Vp and Ri.

All tables include the difference $\Delta \dot{\gamma}_{w_1}$. In addition, at the bottom of all tables, from D13 to D36, the best two Vp

combinations, according to the smaller $\dot{\Delta\gamma} w_1$ values, were established.

Rheological properties, determined with Haake data, for the different power law fluids are included in Table 5. The values of shear stress versus shear rate obtained from the Haake are included in Tables 6, 7, 8, 9, and 10, for 1.0 % Methocel, 2.0 % Methocel, 1.0 % guar gum, 1.5 % guar gum, and for high sucrose corn syrup respectively.

For all different power law fluids, the rheograms obtained from the back extrusion data were plotted along with the rheograms obtained from the Haake Viscometer, and with the rheograms of the Newtonian approximation.

Figures 24 to 27 are examples for 1.0 % Methocel, high sucrose corn syrup, 1.5 % guar gum and 1.0 % guar gum, of the rheograms obtained from Tables D13 to D36, for different power law fluids. From all those figures it can be observed that:

1- For all power law fluids considered, only when the plunger radius used is bigger than 1.36 cm ($K = 0.77$ or $K = 0.85$), is the back extrusion data in good agreement with the Haake viscometer values.

2- In general the best V_p combinations are

$$V_{p1} = 83.33 \times 10^{-4} \text{ m/s and } V_{p2} = 16.67 \times 10^{-4} \text{ m/s or}$$

$$V_{p1} = 62.00 \times 10^{-4} \text{ m/s and } V_{p2} = 16.67 \times 10^{-4} \text{ m/s}$$

which means that the best V_p combinations to work with are when a high velocity is used with a lower one, considering that $V_p = 1.667 \times 10^{-4} \text{ m/s}$ can not be used experimentally with confidence, as was explained in Chapter 4.

Table 5. Rheological Properties of power law fluids determined using the Haake viscometer data over the shear rate range of 10 - 100 s⁻¹.

Fluid Samples	Equation	R ²
1.5% Guar Gum	$\tau = 14.195 \dot{\gamma}^{0.226}$	0.993
1.0% Guar Gum	$\tau = 4.880 \dot{\gamma}^{0.319}$	0.998
2.0% Methocel	$\tau = 5.379 \dot{\gamma}^{0.503}$	0.996
1.0% Methocel	$\tau = 1.218 \dot{\gamma}^{0.673}$	0.998

Table 6. Shear stress and shear rate values for 1.0% Methocel obtained using the Haake viscometer.

Shear Rate (s ⁻¹)	Shear Stress (Pa)
1.81	1.41
4.77	3.07
6.93	4.16
9.16	5.18
11.54	6.22
16.33	8.02
23.57	10.54
30.82	12.66
35.62	13.94
47.72	17.01
52.85	18.09
57.84	19.06
62.66	19.98
67.46	20.89
72.44	21.76
77.17	22.60
84.91	23.87
91.95	24.94
96.50	25.67
109.00	27.43

Table 7. Shear stress and shear rate values for 2.0% Methocel obtained using the Haake viscometer.

Shear Rate (s^{-1})	Shear Stress (Pa)
2.18	9.64
4.82	17.57
7.06	23.33
11.66	34.34
23.83	54.39
36.26	69.50
49.07	80.93
74.06	98.50
99.34	111.20

Table 8. Shear stress and shear rate values for 1.0% guar gum obtained using the Haake Viscometer.

Shear Rate (s^{-1})	Shear Stress (Pa)
2.10	3.10
4.79	6.71
7.19	8.12
9.47	9.39
12.07	10.50
19.83	12.82
27.87	14.37
38.66	15.87
52.26	17.28
65.35	18.39
77.64	19.41
104.00	21.23

Table 9. Shear stress and shear rate values for 1.5% guar gum obtained using the Haake Viscometer.

Shear Rate (s^{-1})	Shear Stress (Pa)
3.11	13.27
4.94	18.69
7.72	20.61
12.60	24.55
25.86	29.91
40.25	33.81
56.94	35.59
70.80	37.13
87.69	38.32
98.17	39.29

Table 10. Shear stress and shear rate values for high sucrose corn syrup obtained using the Haake viscometer.

Shear Rate (s^{-1})	Shear Stress (Pa)
2.45	0.22
4.71	0.48
6.87	0.68
9.10	0.92
11.49	1.13
16.10	1.60
23.17	2.41
35.00	3.54
46.66	4.71
58.34	5.93
70.28	7.20
82.10	8.31
92.97	9.47
104.90	10.71

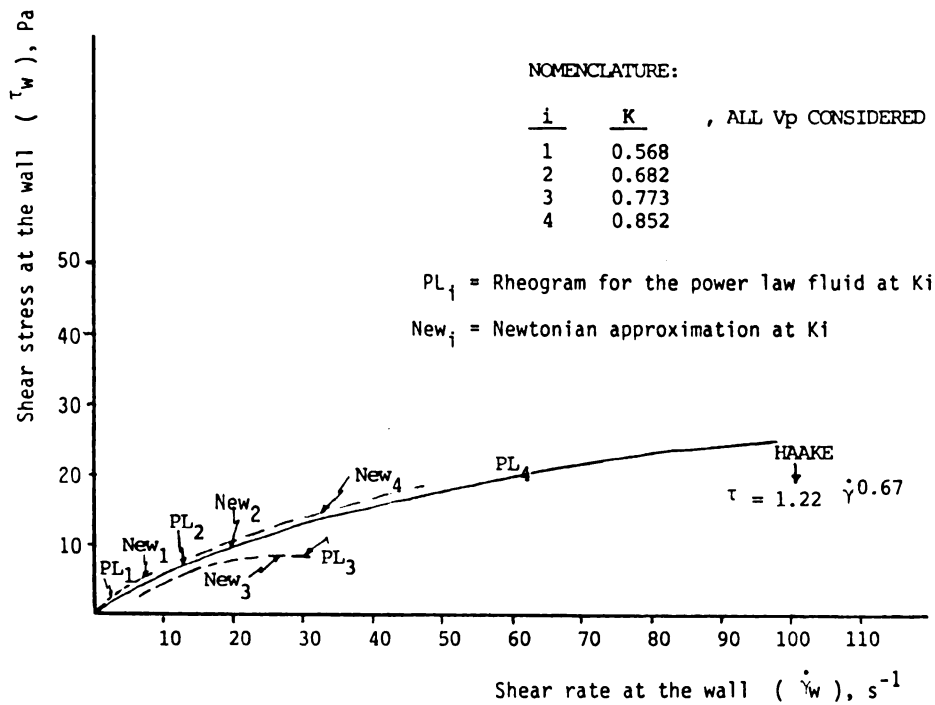


Figure 24. Rheograms for 1.0 % Methocel, considering the power law data from the back extruder, the Newtonian approximation of the power law fluid, and Haake viscometer data.

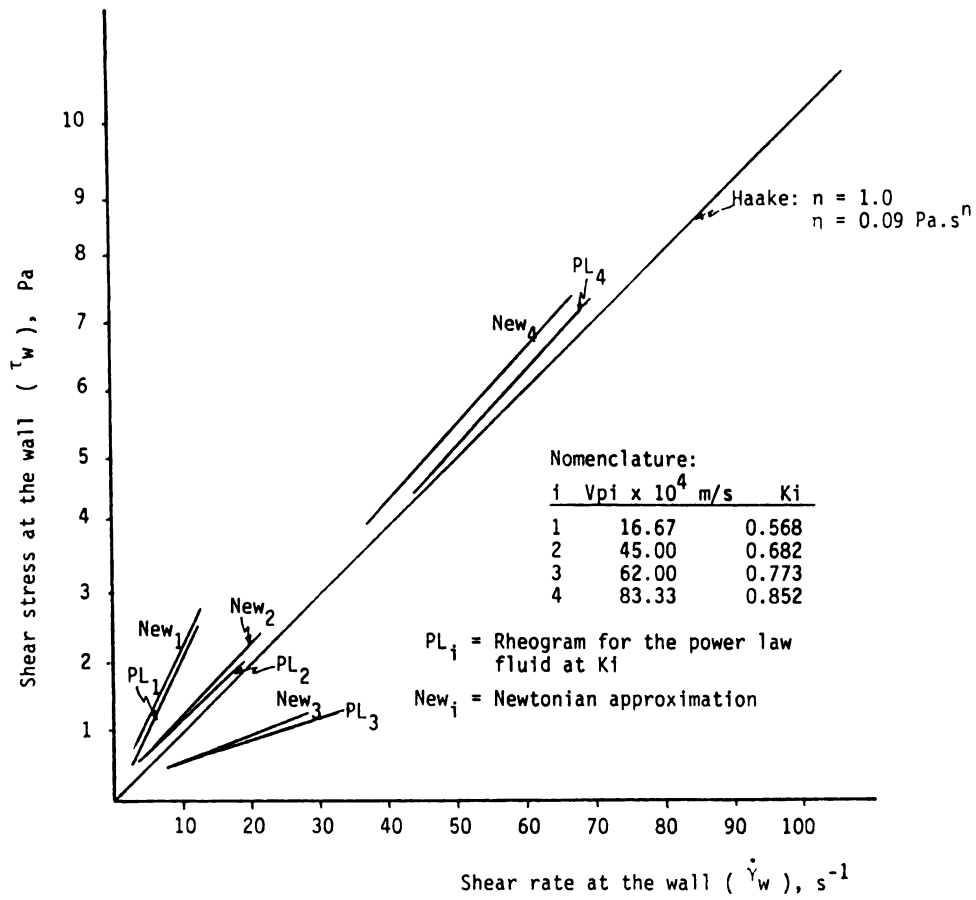


Figure 25. Rheograms for high sucrose corn syrup, considering the power law data from the back extruder, the Newtonian approximation of the power law fluid, and Haake viscometer data.

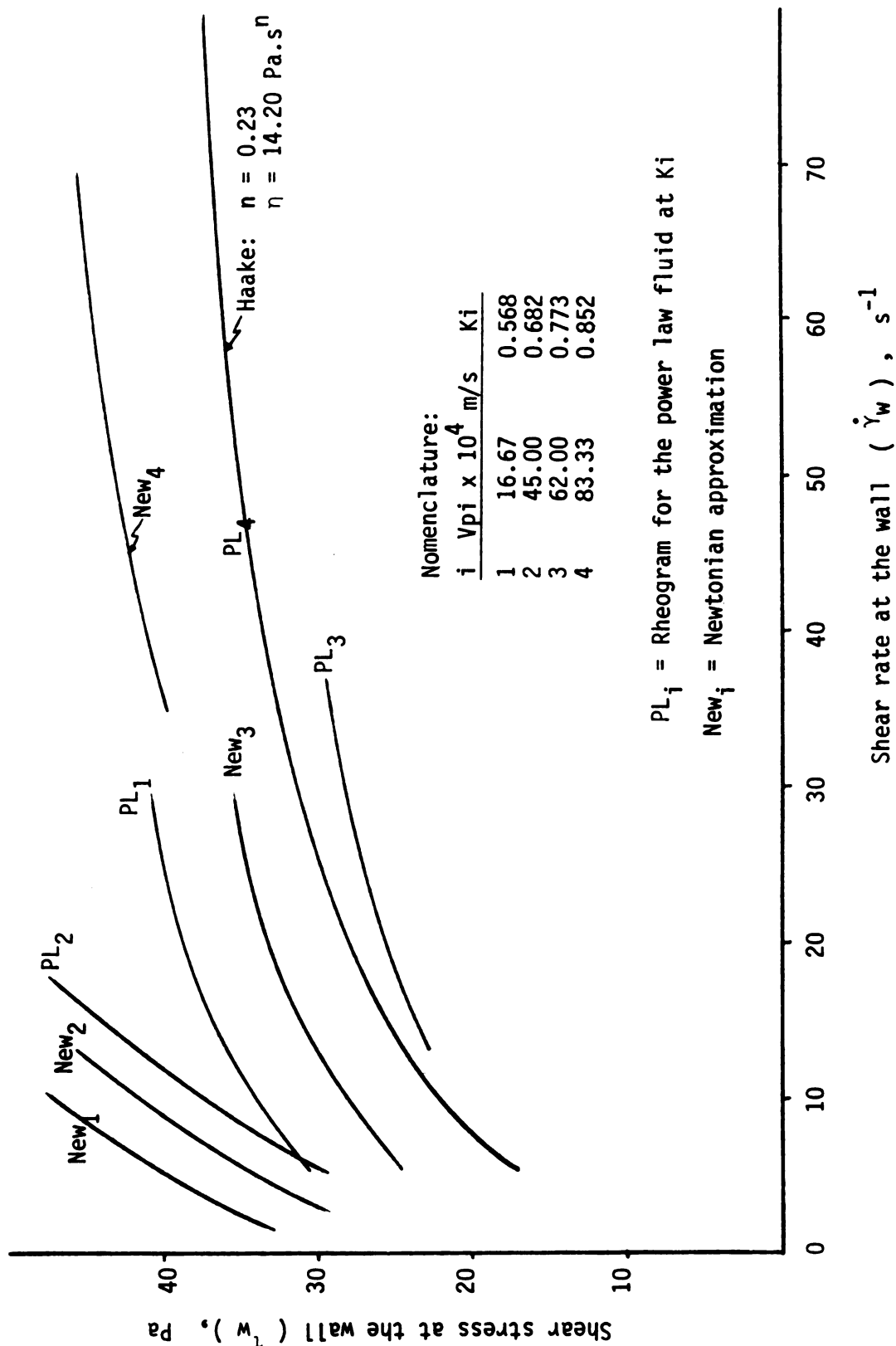


Figure 26. Rheograms for 1.5 % guar gum, considering the power law data from the back extruder, the Newtonian approximation of the power law fluid, and Haake viscometer data.

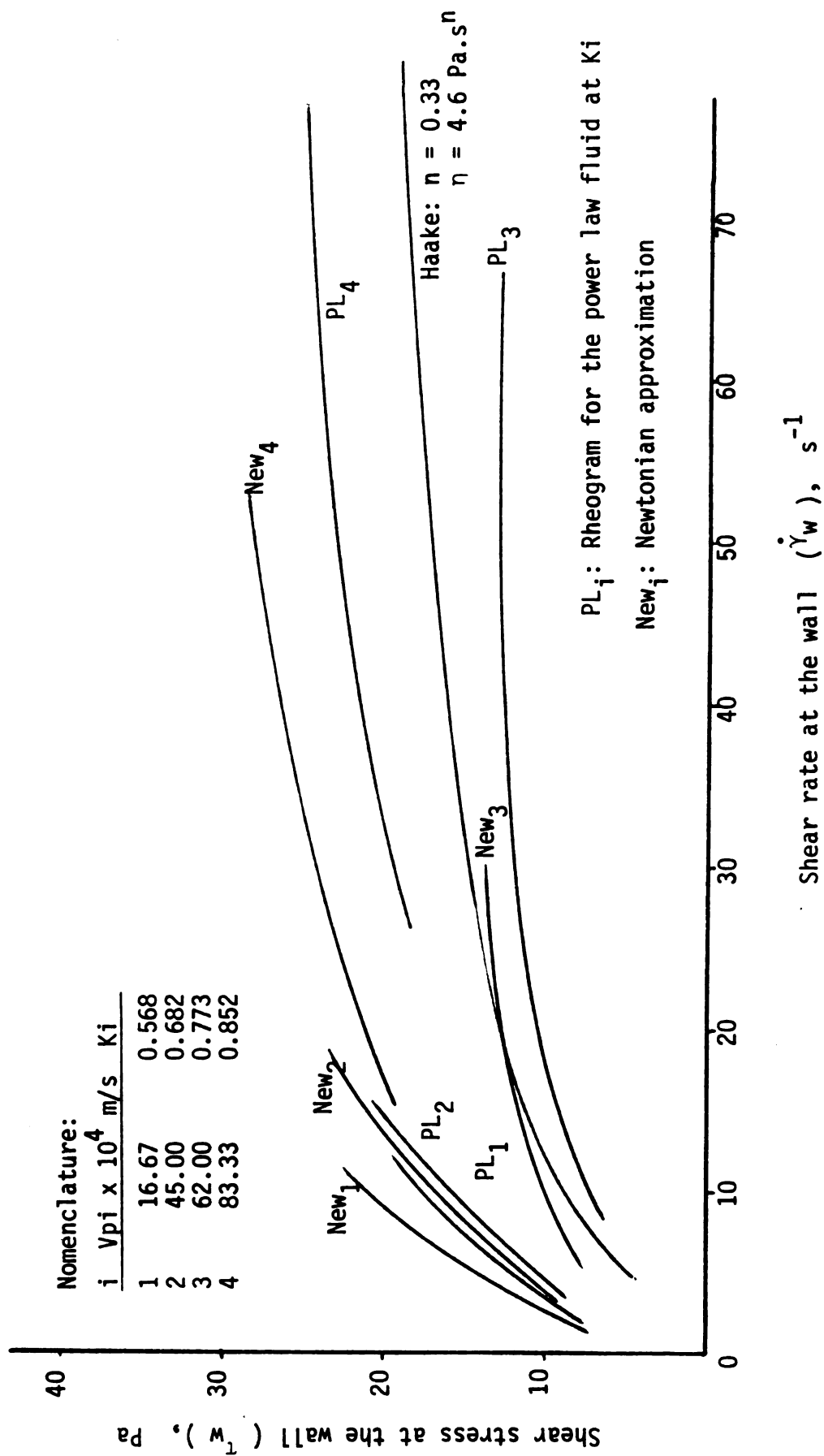


Figure 27. Rheograms for 1.0 % guar gum, considering the power law data from the back extruder, the Newtonian approximation of the power law fluid, and Haake viscometer data.

3- The Newtonian approximation of power law fluids does work. However, further work needs to be done to determine the relationship between the real power law rheograms and the approximation to Newtonian. In general, in all figures the real rheograms (power law) and the rheograms approximated to Newtonian have the same shape; however for the same shear rate at the wall value, the Newtonian approximation gives higher shear stress at the wall values, and the difference is almost constant for all shear rates. This difference between the two rheograms could be a function of the rheological properties of the power law fluids because it is smaller when the rheological properties are closer to the Newtonian case ($n = 1$), and it works better when $K = 0.77$ or $K = 0.85$ and V_p combinations are 83.33 with 16.67 or 62.00 with 16.67 ($\times 10^{-4}$ m/s).

4- The shear rate ranges are affected in the same way by the plunger velocity and by the plunger radius: the higher V_p is, and the higher K values are, the higher shear rates at the wall can be achieved for the same fluid.

5- In general the shear rate ranges for all velocities, and for all K , vary from 10 to 100 sec^{-1} , which are the same as those achieved with the Haake.

6- When the plunger rod used was $R_i = 1.36$ cm, for all experiments run at the laboratory for both power law and Herschel-Bulkley fluids, the back extrusion data was affected by an error that could be explained as a function of the slip present at the wall of this plunger which was made of a different material. Future works will include the use of several plunger rods made of the same material to avoid this problem.

5.2.2 Power Law Approximation for Herschel-Bulkley Fluids

Following the procedures described in Chapter 4, the experimental parameters obtained in the back extrusion device for the three Kelset solutions (1.25 %, 1.5 %, 2.0 %), are included in Table 11.

Tables D37 to D39 (Appendix D) summarize the shear rate at the wall and the real shear stress at the wall for the H-B fluids ($\dot{\gamma}_w \text{ HB}$, $\tau_w \text{ HB}$); the shear rate and the shear stress at the wall for the H-B fluids approximated to power law ($\dot{\gamma}_w \text{ pl}$, $\tau_w \text{ pl}$), and the difference $\Delta \dot{\gamma}_{w_2}$ for 1.25 % Kelset. Tables D40 to D43 and Tables D44 to D47 summarize the same results for 1.5 % and 2.0 % Kelset, respectively. Tables 12 to 14 include the Haake values for the shear stress and the shear rate corresponding to the three Kelset solutions.

Figures 28 and 29 show examples of the rheograms for all Herschel-Bulkley fluids according with the data obtained from: 1) the Haake, 2) the back extrusion data, 3) the approximated to power law data.

From those figures, it may be observed that:

1- The plunger velocity V_p and the plunger radius R_i affect the results of the rheograms and the approximation. The best combination is when $K = 0.85$ or $K=0.77$ and the V_p are 83.33 with 16.67 or 62.00 with 16.67 ($\times 10^{-4}$ m/s). Under those conditions the rheological properties of the Herschel-Bulkley fluids obtained from the Haake are in good agreement with those obtained from the back extrusion device.

Table 11. Values of the experimental parameters for 1.25%, 1.5% and 2.0% Kelset samples using the back extruder.

R1 (cm)	Vp Used x 10 ⁴ m/s	% Kelset Solution	n _{HE}	η _{HE} (Pa.s ⁿ)	τ ₀ (Pa)
1.00	62.00 & 16.67	1.25	0.50	15.95	3.91
1.20	45.00 & 16.67	1.25	0.60	10.75	2.07
1.36	-	1.25	0.52	-	0.00
1.50	62.00 & 16.67	1.25	0.40	7.25	4.96
1.00	62.00 & 16.67	1.50	0.60	12.33	4.70
1.20	62.00 & 45.00	1.50	0.60	9.20	3.74
1.36	62.00 & 45.00	1.50	0.60	5.05	0.51
1.50	62.00 & 45.00	1.50	0.40	9.15	6.40
1.00	62.00 & 16.67	2.00	0.60	2.10	7.18
1.20	62.00 & 16.67	2.00	0.60	23.10	6.81
1.36	83.33 & 45.00	2.00	0.60	9.20	1.68
1.50	62.00 & 16.67	2.00	0.40	22.45	7.99

Table 12. Shear stress and shear rate values for 1.25% Kelset obtained using the Haake viscometer.

Shear Rate (s^{-1})	Shear Stress (Pa)
10.01	13.92
12.39	14.98
17.12	17.21
24.54	20.41
32.23	22.78
36.96	24.16
49.24	27.70
54.63	28.90
59.50	29.98
64.10	31.09
68.68	32.19
73.15	32.92
73.64	33.34
78.60	34.34
86.16	35.94
91.31	36.86
95.42	37.70
97.66	38.11
103.00	38.94

Table 13. Shear stress and shear rate values for 1.5% Kelset obtained using the Haake viscometer.

Shear Rate (s^{-1})	Shear Stress (Pa)
3.57	7.62
4.64	13.22
7.20	16.88
9.83	19.02
12.24	20.28
16.68	24.21
24.16	30.45
37.04	35.88
48.89	41.05
60.86	46.14
73.85	50.86
86.29	54.21
99.29	57.95
112.10	60.37

Table 14. Shear stress and shear rate values for 2.0% Kelset obtained using Haake viscometer.

Shear Rate (s^{-1})	Shear Stress (Pa)
3.96	17.17
4.64	23.44
7.28	29.09
10.03	32.25
11.98	34.17
16.82	43.90
24.81	49.33
34.91	55.87
39.90	55.88
50.46	64.62
56.01	66.07
59.80	68.72
64.14	70.75
69.68	73.56
75.14	75.29
79.36	77.57
92.32	80.48
100.20	81.32
105.60	85.17

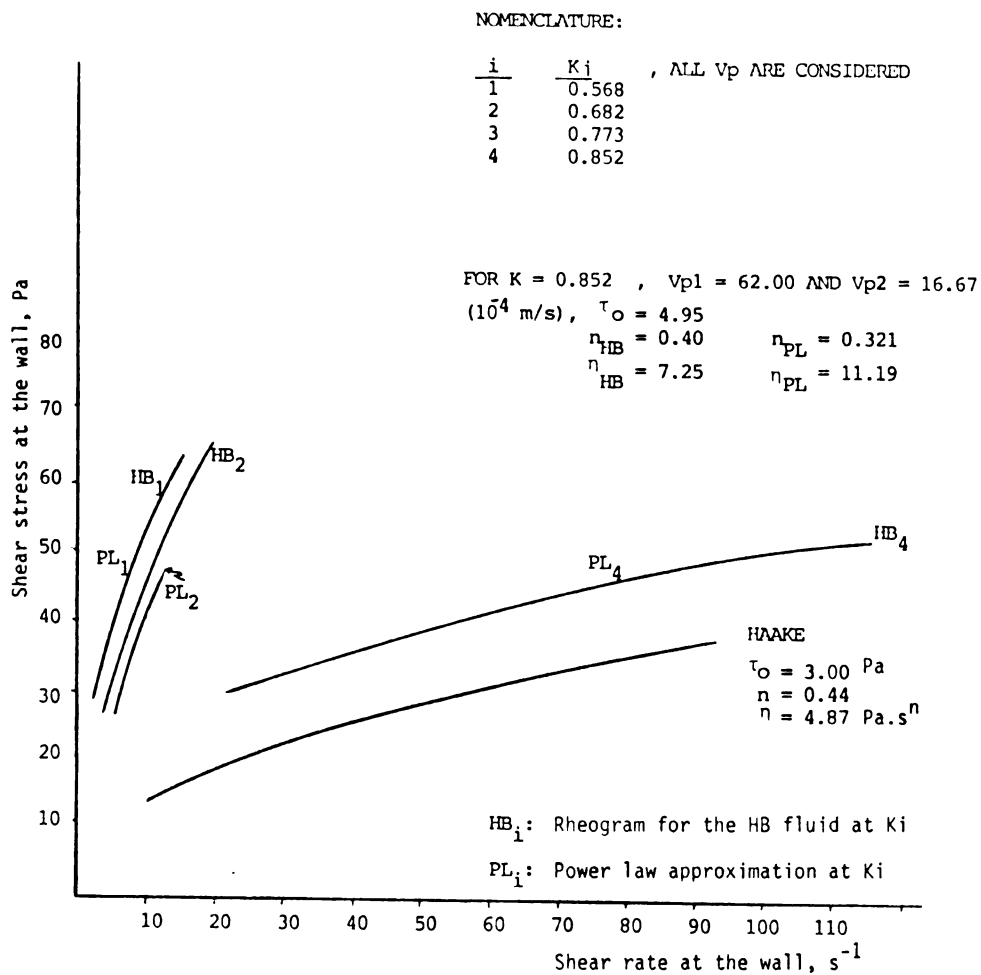


Figure 28. Rheograms for 1.25 % Kelset, considering data obtained from the Haake viscometer, the back extruder, and the power law approximation.

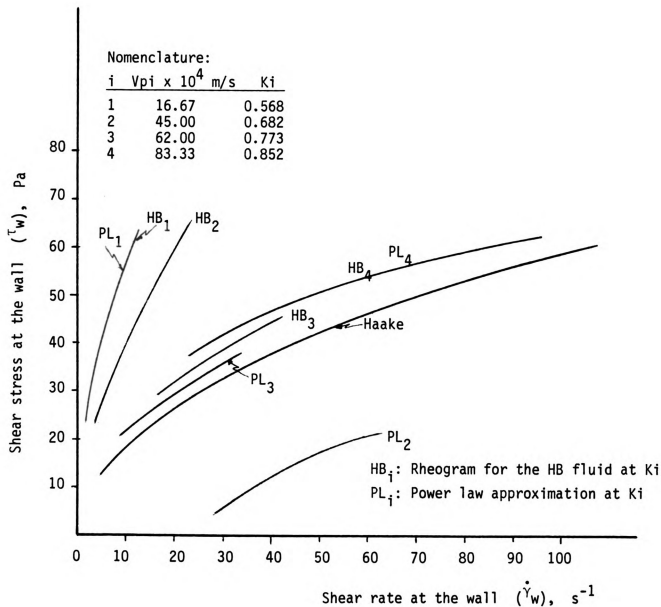


Figure 29. Rheograms for 1.5 % Kelset, considering data obtained from the Haake viscometer, the back extruder, and the power law approximation.

- 2- For $K = 0.85$ the power law approximation curve is the same as the real Herschel-Bulkley curve, which means that under those conditions ($K = 0.85$ and $V_p = 62.00$ and 16.67×10^{-4} m/s), the approximation works well.
- 3- Since the yield stresses of the fluids range from 4 to 10 Pa, further studies need to be done in order to check for the effect of high yield stress values in the approximation.
- 4- In general the shear rate ranges for all different velocities, but not for $V_p = 1.667 \times 10^{-4}$ m/s, and for all K , go from 10 to 100 sec^{-1} , which are the same as those achieved with the Haake.

5.3 End Effect Evaluation

Table 15 shows the experimental data collected from the back extrusion device, for the different test runs, at different fluid lengths in the container cylinder, for a constant plunger traveling distance, as explained in Section 4.7. Because the theory of power law fluids in a back extruder considers the use of two different plunger velocities, Table 16 shows the experimental data collected for the 1.0% Methocel solution at three different V_p .

Tables 17 to 19 illustrate all the experimental values of consistency coefficient, shear rate at the wall and shear stress at the wall, for 1.0 % Methocel solution, at different fluid lengths (0), and at different V_p combinations.

From Tables 15 to 19 the following observations can be made:

- 1- At a constant plunger radius ($R_i = 1.2$ cm) ($K = 0.68$), for a power law fluid sample, the end effect is present.

Table 15. Experimental data, collected from the back extrusion device for 1.0% Methocel, used in the end effect evaluation.

length of fluid "O" (cm)	F_T (N)	F_{Tm} (N)	L (m)	l_{cm} (cm)
17.00	0.90	0.71	0.18	12.92
16.00	0.88	0.71	0.18	13.06
15.00	0.88	0.71	0.18	13.06
14.00	0.95	0.73	0.16	12.19
13.00	0.96	0.73	0.16	12.08
12.00	0.92	0.73	0.16	12.22
11.00	0.90	0.73	0.16	12.22
10.00	0.92	0.71	0.16	12.08

$V_{p1} = 45.00 \times 10^{-4} \text{ m/s}$ Scale range = 5.0% (2.5 N)

Time set=1.00 min $R_1 = 1.20 \text{ cm}$

Table 16. Experimental data Collected from the back extrusion for 1.0% Methocel at four plunger velocities.

$V_p \times 10^4$ (m/s)	Time Set (min)	F_T (N)	F_{T_e} (N)	l_{cm} (cms)
83.33	0.50	1.04	0.72	14.23
62.00	0.80	0.95	0.72	12.06
45.00	1.00	0.90	0.73	13.34
16.67	1.50	0.81	0.75	22.00

($R_1 = 1.20$ cm)

Table 17. Experimental rheological parameters
for 1.0% $V_{p1} = 45.00 \times 10^{-4}$ m/s,
 $V_{p2} = 16.67 \times 10^{-4}$ m/s and $R_1 = 1.2$ cm.

n	"O" (cm)	P _i , P _j (Pa/m)	η_i, η_j (Pa.s ⁿ)	τ_w (Pa)	$\dot{\gamma}_w$ (s ⁻¹)
0.43	17.00	1560.79	1.73	5.07	12.50
		1788.98	1.73	5.82	17.23
0.76	16.00	1381.69	0.90	4.69	8.85
		1762.13	0.90	5.98	12.19
0.84	15.00	1343.15	0.77	4.59	8.43
		1757.98	0.77	6.00	11.61
0.19	12.00	1714.51	2.88	5.27	22.72
		1824.18	1.33	5.60	31.30
0.56	11.00	1821.92	2.88	6.04	10.53
		1776.29	1.33	5.89	14.51

Table 18. Experimental rheological parameter for 1.0% Methocel for $V_{p1} = 45.00 \times 10^{-4}$ m/s, $V_{p2} = 16.67 \times 10^{-4}$ m/s and $R_i = 1.2$ cm.

n	"O" (cm)	P _i , P _j (Pa/m)	η_i, η_j (Pa.s ⁿ)	τ_w (Pa)	$\dot{\gamma}_w$ (s ⁻¹)
0.97	17.00	1528.48	0.71	5.27	7.87
		584.17	0.71	2.01	2.91
0.86	16.00	1343.15	0.76	4.71	8.30
		585.76	0.76	2.00	3.08
0.86	15.00	1343.15	0.72	4.58	8.43
		586.19	0.74	2.03	3.12
1.15	14.00	1828.66	0.64	6.37	7.28
		581.85	0.65	2.03	2.70
1.22	13.00	1950.78	0.63	6.82	7.11
		581.12	0.62	2.03	2.64
1.04	12.00	1643.64	0.69	5.69	7.59
		583.12	0.69	2.02	2.81
0.93	11.00	1467.74	0.73	5.05	8.01
		584.70	0.73	2.00	2.97
1.13	10.00	1790.48	0.65	6.23	7.34
		582.06	0.65	2.03	2.72

Table 19. Experimental rheological parameter for
1.0% Methocel for $V_{p1} = 45.00 \times 10^{-4} \text{ m/s}$
 $V_{p2} = 83.33 \times 10^{-4} \text{ m/s}$ and $R_1 = 1.2 \text{ cm}$.

n	"O" (cm)	P _i , P _j (Pa/m)	η_i, η_j (Pa.s ⁿ)	τ_w (Pa)	$\dot{\gamma}_w$ (s ⁻¹)
0.79	17.00	1535.97	0.95	5.22	8.68
		2499.47	0.95	8.50	16.07
0.96	16.00	1373.70	0.65	4.73	7.87
		2487.27	0.65	8.57	14.57
1.01	15.00	1337.33	0.59	4.62	7.73
		2485.02	0.59	8.59	14.31
0.49	14.00	1867.79	1.85	6.14	11.37
		2530.13	1.85	8.31	21.06
0.38	13.00	2007.63	2.38	6.48	13.36
		2546.37	2.38	8.22	24.74
0.67	12.00	1661.62	1.24	5.58	9.48
		2509.93	1.24	1.24	17.55
0.86	11.00	1470.40	0.82	5.03	8.30
		2494.04	0.82	8.53	15.37
0.53	10.00	1824.60	1.71	6.03	10.89
		2525.52	1.71	8.34	20.17

2- For every specific Vp combinations, the height of fluid (O) inside the cylinder container affects the rheological properties.

3- For the three different Vp combinations used the one which gives better results in the determination of the rheological properties was 45.00 with 83.33×10^{-4} m/s, from the comparison of the back extrusion data with those values obtained using the Haake.

4- When $Vp1 = 45.00 \times 10^{-4}$ m/s and $Vp2 = 83.33 \times 10^{-4}$ m/s, for a fluid length (O = 12.0 cm), the flow behavior index (n) and the consistency coefficient values are approximately the same as the values obtained from the Haake:

From back extruder: $\tau = 1.2179 \dot{\gamma}^{0.6733}$

From Haake viscometer: $\tau = 1.2370 \dot{\gamma}^{0.6699}$

Then, in this case the best position is when the plunger bottom is separated from the container bottom at the end of the experiment by at least 2.0 cm.

To express this result in dimensionless terms, knowing that the ratio of this distance (2.0 cm) to the outside cylinder container radius (1.76 cm) is approximately equals to 1.0, the best position of the plunger at the end of the experiment is when it is separated from the container bottom a minimum distance equivalent to the container radius (Ro). Thus, to be conservative, a distance equivalent to the cup diameter is recommended for practical applications.

Chapter 6

CONCLUSIONS

From the theoretical data simulation procedure the conclusions are:

1. The Newtonian approximation for power law fluids and the power law approximation for Herschel-Bulkley (H-B) fluids work independently of the plunger velocity (V_p) used, but work better at the experimentally highest possible K value which corresponds to the smaller annular gap, $K = 0.85$.
2. The rheological properties of the power law fluids (n, η) affect the Newtonian approximation results: the closer the rheological properties to the Newtonian case ($n = 1$), the smaller the difference between the shear rate at the wall for the power law fluid and the shear rate at the wall for the Newtonian approximation.
3. The rheological properties of the H-B fluids (τ_0, n and η) affect the power law approximation results: the closer the rheological properties are to the power law model ($\tau_0 = 0$), the smaller the difference between the shear rate at the wall of the H-B fluid and the shear rate at the wall for the power law approximation.

From the experimental data procedure the conclusions are:

1. For all power law and H-B fluids used, only when the plunger radius used was bigger than 1.36 cm ($K = 0.77$ or $K = 0.85$) was the back extrusion data for the rheograms in good agreement with the values determined from the Haake viscometer data.
2. The best V_p combinations to work with are when $V_{p1}/V_{p2} = 4$ to 5. Those combinations are:
 $V_{p1} = 83.33 \times 10^{-4}$ m/s with $V_{p2} = 16.67 \times 10^{-4}$ m/s or
 $V_{p1} = 62.00 \times 10^{-4}$ m/s with $V_{p2} = 16.67 \times 10^{-4}$ m/s.
3. For $K = 0.85$, the power law approximation rheogram is the same as the real H-B curve which means that under the best operational conditions ($K = 0.85$ and $V_p = 62.00$ and 16.67×10^{-4} m/s) the approximation working is in excellent agreement with actual values.
4. Under the best operational conditions ($K = 0.85$ and $V_p = 62.00$ and 16.67×10^{-4} m/s) the Newtonian approximation of power law fluids works but may vary with the rheological properties.
5. At a constant plunger radius for a power law fluid sample, the end effect is present.
6. To avoid end effects in back extrusion testing, the plunger bottom should be separated from the container bottom a minimum distance equivalent to the inner container diameter at the end of the experiment.

Chapter 7

PRACTICAL GUIDELINES FOR CONDUCTING BACK EXTRUSION TESTS

1. Prepare the samples and place them in the cylindrical container. Avoid the presence of air bubbles in the fluid, and keep sample at constant temperature.
2. Select an annular gap (K) between 0.77 and 0.85.
3. Select a plunger velocity combination in the ratio of $V_{p1}/V_{p2} = 4$ to 5.
4. Allow the plunger to travel enough distance inside the fluid to ensure that the flow is laminar, fully developed, and at steady state. Experimentally was found that the ratio of this distance (L_i) to the container diameter (D_o) should be in the range of $(L_i/D_o) = 10$ to 15.
5. To avoid end effects in back extrusion testing, the plunger bottom should be separated from the container bottom a minimum distance equivalent to the inner container diameter at the end of the experiment.
6. Use the power law approximation when dealing with Herschel-Bulkley fluids to reduce the calculation time. Under the best operational conditions ($K = 0.85$, $V_{p1} = 82.00 \times 10^{-4}$ m/s and $V_{p2} = 16.67 \times 10^{-4}$ m/s) this approximation is in excellent agreement with actual values.

Chapter 8

SUGGESTIONS FOR FUTURE RESEARCH

1. From this study it was found that the Newtonian approximation for the shear rate of power law fluids does not work as well as the power law approximation for Herschel-Bulkley fluids. For all power law fluids considered the real rheograms (power law) and the rheograms approximated by Newtonian equation have the same shape; however, for the same shear rate at the wall value, the Newtonian approximation gives a higher shear stress at the wall and the difference between the two shear rates is almost constant for all shear rates. This difference could be a function of the rheological properties of the fluids (flow behavior index (n) and consistency coefficient) and it works better when the optimal experimental conditions for back extrusion testing are maintained. As a result, further work needs to be done to determine the relationship between the power law rheogram and the Newtonian approximation as a function of the rheological properties.

2. In the power law approximation of H-B fluids, the different Kelset solutions used have yield stress values ranging from 4 to 10 Pa. To check for the larger effect of the yield stress in the approximation, high yield stress samples (above 10 Pa) should be used in future experiments.

3. End effects were found for a power law fluid (1.0 % Methocel) using a plunger radius (R_i) of 1.2 cm, at three plunger velocity (V_p) combinations. However, future experiments need to be run for different non-Newtonian fluids to determine if the rheological properties affect the results. On the other hand, different plunger velocity combinations and optimum plunger radius could be used to evaluate the influence of those experimental parameters on the end effect. Finally, the same fluid height inside the container could be used for each velocity of the two V_p combinations to guarantee more reliable conclusions from the experiments.

4. Statistical analysis of the data should be conducted to obtain more specific results for the shear rate approximations of non-Newtonian fluids and for the effect of the experimental conditions in back extrusion testing.

Chapter 9

REFERENCES

- Chee, K.K., and Rudin, A. 1970. A study of low shear viscosity of polymer melts. The Canadian Journal of Chemical Engineering 48 (8):362.
- Chee, K.K., and Rudin, A. 1976. Flow analysis and end corrections in falling coaxial cylinder viscometry. The Canadian Journal of Chemical Engineering 54 (6):129.
- Darby, R. 1976. Viscoelastic fluids. Marcel Dekker, Inc. New York.
- Ellis, T.M.R. 1982 A Structural Approach to Fortran 77 Programming. Addison-Wesley Publishing Company. London, Massachusetts, California.
- Ferry, J.D. 1970. Viscoelastic Properties of Polymers. John Wiley and Sons, Inc. New York, New York.
- Fredrickson, A.G. 1959. Flow of non-Newtonian fluids in annuli. Ph.D. Thesis, University of Wisconsin.
- Geankoplis, C.J. 1983. Transport Processes and Unit Operations. Allyn and Bacon, Inc. Boston, London, Toronto.
- Hanks, R.W. 1979. The axial laminar flow of yield-pseudoplastic fluids in concentric annuli. Ind. Eng. Chem. Fundam. 19(1):33.
- Hirujo, F. and Marte, N. 1987. Adaptation of RHEO programs for non-Newtonian fluids in a back extruder. INTEC, Dominican Republic.
- Morgan, R.G., Suter, D.A., and Sweat, V.E. 1979. Mathematical analysis of a simple back-extrusion device. Paper No. 79-6001. American Society of Agricultural Engineers. St. Joseph, MI.
- Osorio-Lira, F.A. 1985. Back extrusion of power law, Bingham plastic and Herschel-Bulkley fluids. M.S. Thesis, Department of Food Science and Human Nutrition, Michigan State University. East Lansing, MI
- Osorio, F.A., and Steffe, J.F. 1985. Back extrusion of Herschel-Bulkley fluids -Example problem. Paper No. 85-6004. American Society of Agricultural Engineers. St. Joseph, MI.

- Osorio, F.A., and Steffe, J.F. 1985. Back extrusion of power law fluids .-Example problem. Paper No. 85-6003. American Society of Agricultural Engineers. St. Joseph, MI.
- Osorio, F.A., and Steffe, J.F. 1987. Back extrusion of power law fluids. Journal of Texture Studies 18(1987):43-63.
- Prentice, J.H. 1984. Measurements in the Rheology of Foodstuffs. Elsevier Applied Science Publishers. London and New York.
- Rao, M.A., and Rizvi, S.S.H. 1986. Engineering Properties of Food. Marcell Dekker, Inc. New York.
- Schummer, P., and Worthoff, R.H. 1978. An elementary method for the evaluation of a flow curve. Chemical Engineering Science 33(3):759-763.
- Skelland, A.H.P. 1967. Non-Newtonian Flow and Heat Transfer. John Wiley and Sons, Inc, New York.
- Steffe, J.F., and Ford, E.W. 1985. Rheological techniques to evaluate the shelf-stability of starch-thickened, strained apricots. Journal of Texture Studies 16(1985):179-192.
- Steffe, J.F., and Osorio, F.A. 1987. Back extrusion of non-Newtonian fluids. Food Technology 41(3):72-77.
- Steffe, J.F., and Morgan, R.G. 1986. Pipeline design and pump selection for non-Newtonian fluid foods. Food Technology 40(12):78-85.
- Tiu, C., and Bhattacharyya, S. 1974. Developing and fully developed velocity profiles for inelastic power law fluids in an annulus. AIChE Journal 20(6):1140.
- Walters, K. 1975. Rheometry. Halsted Press. John Wiley and Sons, Inc. New York.
- Worlow, R.W. 1980. Rheological Techniques. Halsted Press. John Wiley and Sons, Inc. New York.

APPENDICES

Appendix A
RHEO - PROGRAMS

RHEO - 1

This option computes the dimensionless shear stress at the wall (T_w), and the dimensionless flow rate \bar{Q} defined in Equation (22) for different values of n , T_0 and K .

T_w and \bar{Q} will be used in the calculation of the consistency coefficient for power law and Herschel-Bulkley fluids according with the Equation (9).

Input variables are:

Tolerance

Max

Initial value of n , T_0 and K

Final value of n , T_0 and K

Increment rate of n , T_0 and K

Output variables are:

For each corresponding combinations of n , T_0 and K it will gives
PL = pressure in excess of hydrostatic pressure at the plunger
base

T_w = dimensionless shear stress at the plunger wall

\bar{Q} = dimensionless flow rate defined in Equation (22)

\bar{v} = dimensionless velocity defined in Equation (21)

RHEO - 2

This option computes the rheological properties of Herschel-Bulkley and power law fluids, knowing the experimental conditions and the collected data from the back extrusion device.

Input variables are:

Number of experiments

Plunger radius, R_i

Outside cylinder radius, R_o

Fluid density, ζ

For each experiment:

Plunger velocity, V_p

Chart Speed, C_{sp}

Chart Length, l_{ch}

Recorded force after the plunger is stopped, F_{Te}

Recorded force while plunger is traveling down, F_T

Output variables are:

Average yield stress for all experiments, $\tau_o \text{ ave}$

For each experiment:

Force corrected for buoyancy, F_{cb}

Buoyancy force, F_b

Yield stress, τ_o

Guess for the dimensionless yield stress, $To \text{ guess}$

The ratio $F_{cb}/(\pi L R_o R_i)$

Then, for each experiment, at a specific plunger velocity, for selected n and $To \text{ guess}$ intervals, this program will generate

data of $P(T_w + K)$ versus η which will be plotted in order to obtain the n and η values according with the procedure explained in Chapter 4.

If the fluid is power law, $\tau_0 = 0$, this program will gives immediately the n value without asking for the n and T_0 guess intervals.

RHEO - 3

This option computes the shear stress at the wall τ_w , and the shear rate at the wall $\dot{\gamma}_w$ for power law or Herschel-Bulkley fluids when their rheological properties are known.

Input variables are:

Tolerance

Max

Flow behavior index, n

Yield stress, τ_0

Plunger radius, R_i

Outside cylinder radius, R_o

Plunger velocity, V_p

Consistency coefficient, η

Lower limit of pressure drop interval guess

Upper limit of pressure drop interval guess

Output variables are:

Pressure in excess of hydrostatic pressure at the plunger base,

PL

Pressure drop per unit of length, P

Shear stress at the wall, τ_w

Shear rate at the wall, $\dot{\gamma}_w$

Dimensionless shear stress at the wall, T_w

Dimensionless flow rate, \bar{Q}

Dimensionless velocity, \bar{v}

Dimensionless yield stress, T_0

RHEO - 4

This option is only used when dealing with power law fluids.

With this program, Knowing the experimental conditions of the equipment, the flow behavior index n can be obtained according with Equation (8).

RHEO - 4 also calculates the yield stress τ_0 which can be used as reference when the Herschel-Bulkley fluids are being approximated to power law models.

Input variables are:

Cell capacity

Annulus gap, $K = R_i/R_o$

Fluid density, ζ

Plunger radius, R_i

Outside cylinder radius, R_o

Number of experiments

For each experiment:

Scale range

Plunger velocity, V_p

Recorded force while plunger is traveling down, F_T (cm)

Recorded force after the plunger is stopped, F_{Te} (cm)

Time set axis

Chart length, obtained from the recorder, lch

Output variables are:

Yield stress, τ_0

Force corrected for buoyancy, Fcb

Length of annular region, L

$$\ln \left[\frac{F_{cbj}}{F_{cbi}} \cdot \frac{L_i}{L_j} \right], \quad \text{called } \ln(F)$$

$$\ln \frac{V_{pj}}{V_{pi}}, \quad \text{called } \ln(V)$$

$$\text{Flow behavior index, } n = \frac{\ln(F)}{\ln(V)}$$

RHEO - 5

This option was created as an alternative to reduce the calculation time when dealing with power law fluids. After determining the flow behavior index n with the experimental data in RHEO - 4, and T_w and $\dot{\gamma}$ with RHEO - 1, the values of the consistency coefficient η , the shear rate at the wall $\dot{\gamma}_w$, the shear stress at the wall τ_w , and the pressure drop per unit of length P , can be obtained for two different plunger velocities according with Equations (9), (10), (12) and (13).

Input variables are:

Flow behavior index, n

Plunger radius, R_i

Outside cylinder radius, R_o

Plunger velocity, V_p

Length of annular region, L

Force corrected for buoyancy, F_{cb}

Dimensionless shear stress at the plunger wall, T_w

Dimensionless flow rate, \bar{Q}

Output variables are:

Pressure drop per unit of length, P

Consistency coefficient, η

Shear rate at the wall, $\dot{\gamma}_w$

Shear stress at the wall, τ_w

Appendix B

CALCULATION EXAMPLE FOR THE POWER LAW SHEAR RATE AT THE WALL AS AN APPROXIMATION TO THE SHEAR RATE AT THE WALL FOR HERSCHEL-BULKLEY FLUIDS, BASED ON SIMULATED DATA

Sample solution: 2.0 % Kelset

Rheological equation: $\tau = 8.8 + 27.0 \dot{\gamma}^{0.5}$

1. Using RHEO-3, the following set of data was generated, using the known rheological properties and at different conditions of plunger velocity (V_p) and plunger radius (R_i):

$$K = (0.010 \text{ m} / 0.0178 \text{ m}) = 0.568$$

P (Pa/m)	$V_p \times 10^4$ (m/s)	τ_w (Pa)	$\dot{\gamma}_w$ (s^{-1})	T_w	F_{cb} (N)
22182.99	83.33	106.552	13.108	0.5458	2.7328
19542.69	62.00	93.649	9.876	0.5445	2.4047
17087.91	45.00	81.650	7.280	0.5430	2.0997
11550.83	16.67	54.560	2.872	0.5368	1.4114
5596.09	1.667	25.307	0.374	0.5139	0.6696

In all cases, to calculate F_{cb} (Equation 12) the value $L = 0.20$ was assumed. With this value it is ensured that the plunger is traveling enough distance inside the fluid so that the flow is laminar, fully developed and at steady state.

For the other plunger radii ($R_i = 1.2, 1.36$ and 1.5 cm) the same sets of data were generated, as shown in the following tables.

$K = 0.682$

P (Pa/m)	$V_{px}10^4$ (m/s)	τ_w (Pa)	$\dot{\gamma}_w$ (s^{-1})	Tw	Fcb (N)
41593.23	83.33	135.773	22.115	0.3709	5.8107
36439.60	62.00	118.812	16.602	0.3705	5.0886
31649.10	45.00	103.045	12.184	0.3700	4.4174
20851.08	16.67	67.495	4.726	0.3678	2.9044
9289.19	1.667	29.361	0.580	0.3592	1.2832

$K = 0.773$

P (Pa/m)	$V_{px}10^4$ (m/s)	τ_w (Pa)	$\dot{\gamma}_w$ (s^{-1})	Tw	Fcb (N)
82059.62	83.33	181.555	40.938	0.2514	12.6393
71576.93	62.00	158.275	30.648	0.2513	11.0232
61834.16	45.00	136.637	22.417	0.2511	9.5211
39883.35	16.67	87.881	8.579	0.2504	6.1369
16452.20	1.67	35.800	1.000	0.2473	2.5238

$K = 0.852$

P (Pa/m)	$V_{px}10^4$ (m/s)	τ_w (Pa)	$\dot{\gamma}_w$ (s^{-1})	Tw	Fcb (N)
194512.11	83.33	268.913	92.811	0.1571	32.5674
169010.82	62.00	233.606	69.325	0.1571	28.2967
145311.47	45.00	200.793	50.564	0.1570	24.3278
91931.08	16.67	126.883	19.127	0.1568	15.3881
35070.08	1.67	48.136	2.123	0.1560	5.8653

2. In the power law approximation of Herschel-Bulkley fluids, the flow behavior index (n pl) was calculated for each specific plunger radius and for all possible two plunger velocity combinations according with the following equation:

$$\ln \left[\frac{F_{cbj}}{F_{cbi}} \cdot \frac{L_i}{L_j} \right] = n \left[\ln \frac{V_{pj}}{V_{pi}} \right]$$

Then, n (pl) is obtained, from the linear regression, as the slope of the curve corresponding to all Vp combinations and Ri used.

For example: Ri = 1.36 cm

<u>(Vp) i,j</u>	<u>ln(Fcbj/Fcbi)</u>	<u>ln(Vpj/Vpi)</u>
1,2	0.8888	2.3026
1,3	1.3277	3.2958
1,4	1.4742	3.6161
1,5	1.6110	3.9118
2,3	0.4392	0.9931
2,4	0.5857	1.3135
2,5	0.7225	1.6092
3,4	0.1465	0.3205
4,5	0.1368	0.2957

From the linear regression of the data,

$$\text{slope} = n \text{ (pl)} = 0.3977$$

$$r^2 = 0.9985$$

3. Using RHEO-1, with the annular gap ($K = 0.773$), $To = 0.0$ (approximated to power law), and $n = 0.3977$, the following values were generated:

$$Tw = 0.2495 \text{ and } \Phi = 190.159 \times 10^{-6}$$

Therefore, with Φ , P , Ri , Vp , K and n known, the consistency coefficient was calculated from Equation (9). At this point, the approximated to power law rheological properties (η_{pl} and n_{pl}) have been obtained.

4. In the calculation of the shear stress and the shear rate at the wall approximated to power law for the Herschel-Bulkley fluids, RHEO-3 is used. Those values were compared to the original shear stress and shear rate at the wall corresponding to the Herschel-Bulkley fluids calculated in Step 1 of this procedure. The differences (Equations 30 and 31) reflect how the power law approximation works for Herschel-Bulkley fluids.

For example: $K = 0.772$ and $n(pl) = 0.3977$ for 2.0 % Kelset

$Vp \times 10^4$ (m/s)	η_{pl} (Pa s)	P (Pa/m)	$\tau_{w pl}$ (Pa)	$\dot{\gamma}_{w pl}$ (s ⁻¹)	$\Delta\tau_{w_2}$ %	$\Delta\dot{\gamma}_{w_2}$ %
83.33	27.576	57251.33	125.686	45.334	-30.77	10.74
62.00	27.054	49937.77	109.630	33.730	-30.73	10.06
45.00	26.549	43140.49	94.707	24.481	-30.69	9.21
16.67	26.417	27825.72	61.087	9.069	-30.49	5.71
1.67	26.197	11459.11	25.157	0.903	-29.73	-9.70

Conclusions about the power law approximation for Herschel-Bulkley fluids are presented in Chapters 4 and 5 of this study, at different V_p and R_i conditions for 2.0%, 1.5 % and 1.0 % Kelset solutions used as standards in the data simulation procedure. All tables of results are included in Appendix D.

Appendix C

1. CALCULATION EXAMPLE FOR THE DETERMINATION OF RHEOLOGICAL PROPERTIES OF A POWER LAW FLUID USING THE BACK EXTRUSION DEVICE

Sample solution: 1.0 % Methocel

Plunger radii used: $R_i = 1.0, 1.2, 1.36, \text{ and } 1.5 \text{ cm}$

Plunger velocities used: $V_p = 83.33, 62.00, 45.00 \text{ and } 16.67$
($\times 10^{-4} \text{ m/s}$)

Cell capacity: 50 Newtons (compression)

Outside cylinder radius: $R_o = 1.76 \text{ cm}$

RHEO-Programs used: RHEO-4 to determine n with the experimental data collected.

RHEO-1 to determine T_w and $\dot{\gamma}$.

RHEO-5 to determine $P, \eta, \tau_w \text{ pl}$
and $\dot{\gamma}_w \text{ pl}$.

The following table shows an example of the data collected from the Instron for 1.0 % Methocel sample:

Data collected from the Instron for 1.0 % Methocel.

Ri (cm)	Vp (cm/min)	Time set (min)	FT (N)	F _{Te} (N)	lch (cm)
1.0	500.0	0.5	0.4081	0.3215	11.250
	372.0	0.8	0.4738	0.4030	11.844
	270.0	1.0	0.5074	0.4220	12.371
	100.0	1.5	0.4389	0.4150	24.000
1.2	500.0	0.5	1.0390	0.7235	14.295
	372.0	0.8	0.9476	0.7245	12.058
	270.0	1.0	0.8980	0.7250	13.344
	100.0	1.5	0.8134	0.7450	22.000
1.36	500.0	0.5	1.4670	0.9300	11.350
	372.0	0.8	1.4510	0.9500	9.544
	270.0	1.0	1.3180	0.9400	10.640
	100.0	1.5	1.1010	0.9350	18.996
1.50	500.0	0.5	4.8540	1.5235	8.700
	372.0	0.8	3.9150	1.4580	7.308
	270.0	1.0	3.0580	1.5000	8.340
	100.0	1.5	2.3540	1.4000	13.250

With the collected data , for Ri = 1.36 cm as an example, using RHEO-4, RHEO-1 and RHEO-5, the following set of data was generated:

Values of the experimental parameters for 1.0 % Methocel.

Ri (cm)	n	Vpi, Vpj $\times 10^4$ m/s	Li, Lj (m)	Fcb (i,j) (N)	Tw	ϕ $\times 10^6$	Pi, Pj (Pa/m)	η_i, η_j (Pa.s ⁿ)	τ_w pl (Pa)	$\dot{\gamma}_w$ pl (s ⁻¹)
1.36	0.5899	83.33 45.00	0.1878 0.1901	0.537 0.378	0.2544	773.866	3702.191 2573.94	1.003 1.003	8.2877 5.7620	35.8811 19.3766
	0.7320	83.33 16.67	0.1878 0.1886	0.537 0.166	0.2571	1379.740	3692.571 1136.623	0.660 0.660	8.3531 2.5712	32.0320 6.4079
	0.9147	62.00 45.00	0.1880 0.1901	0.501 0.378	0.2597	2246.940	3432.427 2561.127	0.4752 0.4754	7.8456 5.8540	21.4430 15.5635
	0.8433	62.00 16.67	0.1880 0.1886	0.501 0.166	0.2588	1908.94	3435.401 1134.655	0.5732 0.5732	7.8254 2.5846	22.1880 5.9657
	0.8203	45.00 16.67	0.1901 0.1886	0.378 0.166	0.2585	1794.30	2564.299 1135.077	0.5894 0.5891	5.8325 2.5817	16.3507 6.0570

2. CALCULATION EXAMPLE FOR SHEAR STRESS AND SHEAR RATE
AT THE WALL OF HERSCHEL-BULKLEY FLUID AND
APPROXIMATED TO POWER LAW VALUES

Fluid sample: 2.0 % Kelset

The Kelset solution was prepared at the laboratory, at a constant room temperature of 25 ± 1 °C. The back extrusion device was balanced, calibrated, and prepared to be used. The fluid sample was placed in glass containers of constant radius ($R_o = 1.76$ cm) and tests were run at different plunger velocities (V_p) and plunger radius (R_i) and all data were collected.

With the collected data, using RHEO-4, the following set of parameters was obtained from the $P(Tw + K)$ versus η graphs generated as explained in Chapter 3.

For 2.0 % Kelset,

R_i (cm)	V_{pi}, V_{pj} (10^4 m/s)	n	η (Pa s ⁿ)	τ_o (Pa)
1.0	62.00, 16.67	0.6	29.1	7.180
1.2	62.00, 16.67	0.6	23.1	6.810
1.36	83.33, 16.67	0.6	9.2	1.678
1.5	62.00, 16.67	0.4	22.45	7.994

Then, with the rheological properties obtained above, for different Ri values, the shear rates and the shear stresses at the wall for the Herschel-Bulkley fluids were calculated using RHEO-3 at different plunger velocities.

For example, for 2.0 % Kelset solution at $Ri = 1.0$ cm, $n = 0.6$, $\eta = 29.1 \text{ Pa s}^n$, and $\tau_o = 7.18 \text{ Pa}$,

$V_p \cdot 10^4$ (m/s)	P (Pa/m)	τ_w (Pa)	$\dot{\gamma}_w$ (s ⁻¹)	Tw	$\Phi \times 10^6$
16.67	11704.89	56.790	2.433	0.5513	3719.437
45.00	19214.48	94.256	6.214	0.5574	4395.568
62.00	22757.72	111.923	8.454	0.5589	4567.135
83.33	26688.51	131.516	11.251	0.5599	4706.958

or at $Ri = 1.2$ cm, $n = 0.6$, $\eta = 23.1 \text{ Pa s}^n$ and $\tau_o = 6.8 \text{ Pa}$,

$V_p \cdot 10^4$ (m/s)	P (Pa/m)	τ_w (Pa)	$\dot{\gamma}_w$ (s ⁻¹)	Tw	$\Phi \times 10^6$
16.67	18533.32	60.928	4.133	0.3736	1694.815
45.00	30984.18	102.475	10.681	0.3785	1942.221
62.00	36860.69	122.076	14.572	0.3763	2003.675
83.33	43380.71	143.823	19.436	0.3767	2052.806

Therefore, τ_w and $\dot{\gamma}_w$ correspond to the Herschel-Bulkley (H-B) shear stress and shear rate at the wall values: τ_w HB and $\dot{\gamma}_w$ HB, respectively. Then, the procedure to obtain the

approximated to power law values was:

- a) With the same data collected from the back extrusion device for the H-B fluids, run RHEO-2 to generate the flow behavior index as power law (n_{pl}), at every two possible plunger velocity combinations, as explained in Chapter 4.
- b) With the (n_{pl}) values generated, $T_o = 0$ (power law), and K value known, the T_w and $\dot{\gamma}_w$ values were obtained using RHEO-1.
- c) Using the data obtained for $\dot{\gamma}_w$, T_w , V_p , R_i , L , F_{cb} , etc., the consistency coefficient, the shear rate at the wall, and the shear stress at the wall, approximated to power law, were calculated using RHEO-5.

For example, for 2.0 % Kelset, at $R_i = 1.0$ cm,

n	$V_p(i,j)$ 10 m/s	L m	F_{cb} N	P Pa/m	η Pa.s ^{n}	τ_w pl Pa	$\dot{\gamma}_w$ pl s ⁻¹
0.572	62.00	0.131	1.787	21568.319	28.678	108.604	7.454
	45.00	0.112	1.235	17441.118	28.679	87.822	5.410
0.519	62.00	0.134	1.787	21858.320	34.782	107.154	8.733
	16.67	0.136	0.934	11046.256	34.764	54.151	2.348
0.473	45.00	0.112	1.235	17766.574	34.927	86.195	6.757
	16.67	0.136	0.934	11103.091	34.907	53.867	2.503

Finally, the $\dot{\gamma}_w$ pl and the τ_w pl are compared to the $\dot{\gamma}_w$ HB and the τ_w HB according with their differences (Equations 30 and 31). From those differences, the effect of V_p and R_i in the determination of the rheological properties of a H-B fluid in back extrusion testing are considered, as well as the power law approximation for H-B fluids. All results are presented in Appendix D, and discussion and conclusions about them are included in Chapter 5.

Appendix D
TABLE OF RESULTS

Table D1. Power law shear stress and shear rate at the wall and the difference between the shear rate at the wall as power law fluid and the shear rate at the wall approximated to Newtonian fluid, for 1.5 % guar gum: $\eta = 31.315$ and $n = 0.1585$.

K $\nu_p \times 10^4$ (m/s)	0.950		0.852		0.773		0.682		0.568	
	τ_w p1	$\dot{\gamma}_w$ p1	τ_w p1	$\dot{\gamma}_w$ p1	τ_w p1	$\dot{\gamma}_w$ p1	τ_w p1	$\dot{\gamma}_w$ p1	τ_w p1	$\dot{\gamma}_w$ p1
		$\Delta \dot{\gamma}_w$		$\Delta \dot{\gamma}_w$		$\Delta \dot{\gamma}_w$		$\Delta \dot{\gamma}_w$		$\Delta \dot{\gamma}_w$
1.667	54.002	31.125	39.004	3.996	34.371	1.799	31.300	0.997	28.971	0.612
		-65.07		-67.29		-69.09		-71.21		-73.86
16.67	77.787	311.247	56.184	39.961	49.509	17.993	45.086	9.969	41.732	6.122
		-65.07		-67.29		-69.12		-71.22		-73.90
45.00	91.047	840.199	65.761	107.874	57.949	48.572	52.771	26.911	48.846	16.525
		-65.07		-67.29		-69.12		-71.22		-73.90
62.00	95.791	-	69.188	148.626	60.968	66.921	55.521	37.078	51.391	22.768
		-		-67.29		-69.12		-71.22		-73.90
83.33	100.388	-	72.507	199.759	63.894	89.944	58.185	49.834	53.857	30.601
		-		-67.29		-69.12		-71.22		-73.90

Table D2. Power law shear stress and shear rate at the wall and the difference between the shear rate at the wall as power law fluid and the shear rate at the wall approximated to Newtonian, for 1.0 % guar gum: $\eta = 7.916$ and $n = 0.2588$.

K $\nu_p \times 10^4$ (m/s)	0.950		0.852		0.773		0.682		0.568	
	τ_w pl	$\dot{\gamma}_w$ pl	τ_w pl	$\dot{\gamma}_w$ pl	τ_w pl	$\dot{\gamma}_w$ pl	τ_w pl	$\dot{\gamma}_w$ pl	τ_w pl	$\dot{\gamma}_w$ pl
		$\Delta \dot{\gamma}_w$		$\Delta \dot{\gamma}_w$		$\Delta \dot{\gamma}_w$		$\Delta \dot{\gamma}_w$		$\Delta \dot{\gamma}_w$
1.667	17.574	21.794	10.289	2.754	8.339	1.223	7.125	0.666	6.241	0.399
		-50.12		-52.54		-54.54		-56.91		-59.90
16.67	31.891	217.937	18.672	27.544	15.133	12.229	12.930	6.658	11.325	3.990
		-50.12		-52.55		-54.57		-56.91		-59.95
45.00	41.236	588.313	24.143	74.353	19.568	33.012	16.719	17.974	14.644	10.771
		-50.12		-52.55		-54.57		-56.91		-59.95
62.00	44.802	810.564	26.231	102.442	21.260	45.483	18.165	24.765	15.910	14.841
		-50.12		-52.55		-54.57		-56.91		-59.95
83.33	48.365	-	28.317	137.685	22.950	61.131	19.609	33.284	17.176	19.946
		-		-52.55		-54.57		-56.91		-59.95

Table D3. Power law shear rate and shear stress at the wall and the difference between the shear rate at the wall as power law fluid and the shear rate at the wall approximated to Newtonian, for 2.5 % Methocel: $\eta = 16.155$ and $n = 0.5128$.

K	0.950		0.852		0.773		0.682		0.568	
	τ_w pl	$\dot{\gamma}_w$ pl	τ_w pl	$\dot{\gamma}_w$ pl	τ_w pl	$\dot{\gamma}_w$ pl	τ_w pl	$\dot{\gamma}_w$ pl	τ_w pl	$\dot{\gamma}_w$ pl
		$\Delta\dot{\gamma}_w$		$\Delta\dot{\gamma}_w$		$\Delta\dot{\gamma}_w$		$\Delta\dot{\gamma}_w$		$\Delta\dot{\gamma}_w$
1.667	63.642	14.493 -24.99	21.747	1.785 -26.78	14.176	0.775 -28.26	10.233	0.410 -30.00	7.715	0.231 -32.49
16.67	207.274	144.927 -24.99	70.826	17.854 -26.79	46.169	7.750 -28.31	33.326	4.105 -30.11	25.128	2.367 -32.49
45.00	344.908	391.224 -24.99	117.856	48.195 -26.79	76.826	20.922 -28.31	55.456	11.080 -30.11	41.814	6.389 -32.49
62.00	406.513	539.020 -24.99	138.907	66.403 -26.79	90.549	28.826 -28.31	65.361	15.266 -30.11	49.282	8.802 -32.48
83.33	473.067	724.461 -24.99	161.649	89.247 -26.79	105.373	38.743 -28.31	76.062	20.518 -30.11	57.351	11.830 -32.48

Table D4. Power law shear stress and shear rate at the wall and the difference between the shear rate at the wall as power law and the shear rate at the wall approximated to Newtonian, for 2.0 % Methocel: $\eta = 3.056$ and $n = 0.6897$.

K	0.950		0.852		0.773		0.682		0.568	
	$\tau_{w\ pl}$	$\dot{\gamma}_{w\ pl}$	$\tau_{w\ pl}$	$\dot{\gamma}_{w\ pl}$	$\tau_{w\ pl}$	$\dot{\gamma}_{w\ pl}$	$\tau_{w\ pl}$	$\dot{\gamma}_{w\ pl}$	$\tau_{w\ pl}$	$\dot{\gamma}_{w\ pl}$
		$\Delta\dot{\gamma}_{w1}$		$\Delta\dot{\gamma}_{w1}$		$\Delta\dot{\gamma}_{w1}$		$\Delta\dot{\gamma}_{w1}$		$\Delta\dot{\gamma}_{w1}$
1.667	17.528	12.586	4.104	1.533	2.292	0.659	1.467	0.345	0.992	0.196
		-13.63		-14.74		-15.63		-16.81		-18.37
16.67	85.790	125.856	20.084	15.332	11.220	6.591	7.179	3.450	4.856	1.957
		-13.62		-14.75		-15.70		-16.84		-18.34
45.00	170.172	339.744	39.839	41.387	22.256	17.793	14.240	9.312	9.632	5.283
		-13.62		-14.75		-15.71		-16.84		-18.36
62.00	212.266	468.092	49.693	57.023	27.761	24.514	17.762	12.830	12.014	7.278
		-13.62		-14.75		-15.70		-16.84		-18.34
83.33			60.935	76.640	34.041	32.948	21.780	17.244	14.732	9.783
				-14.75		-15.70		-16.83		-18.37

Table D5. Power law shear stress and shear rate at the wall and the difference between the shear rate at the wall as power law and the shear rate at the wall approximated to Newtonian, for 1.5 % Methocel: $\eta = 1.33$ and $n = 0.75$.

K $v_p \times 10^4$ (m/s)	0.950		0.852		0.773		0.682		0.568	
	τ_w pl	$\dot{\gamma}_w$ pl	τ_w pl	$\dot{\gamma}_w$ pl	τ_w pl	$\dot{\gamma}_w$ pl	τ_w pl	$\dot{\gamma}_w$ pl	τ_w pl	$\dot{\gamma}_w$ pl
		$\Delta \dot{\gamma}_{w1}$		$\Delta \dot{\gamma}_{w1}$		$\Delta \dot{\gamma}_{w1}$		$\Delta \dot{\gamma}_{w1}$		$\Delta \dot{\gamma}_{w1}$
1.667	8.651	12.141 -10.46	1.782	1.477 -11.51	0.944	0.633 -12.16	0.580	0.330 -13.03	0.377	0.186 -13.98
16.67	48.646	121.413 -10.46	10.008	14.745 -11.36	5.302	6.322 -12.12	3.255	3.298 -13.01	2.121	1.863 -14.22
45.00	102.449	327.748 -10.46	21.076	39.804 -11.36	11.168	17.067 -12.12	6.855	8.904 -13.03	4.466	5.029 -14.24
62.00	130.284	451.564 -10.46	26.803	54.841 -11.36	14.202	23.514 -12.12	8.718	12.267 -13.02	5.680	6.929 -14.23
83.33	162.629	606.917 -10.46	33.457	73.708 -11.36	17.728	31.603 -12.12	10.882	16.487 -13.02	7.090	9.313 -14.23

Table D6. Power law shear stress and shear rate at the wall and the difference between the shear rate at the wall as power law and the shear rate at the wall approximated to Newtonian, for Corn Syrup: $\eta = 2.67$ and $n = 1.00$

K $V_p \times 10^4$ (m/s)	0.950		0.852		0.773		0.682		0.568	
	τ_{wpl}	$\dot{\gamma}_{wpl}$	τ_{wpl}	$\dot{\gamma}_{wpl}$	τ_{wpl}	$\dot{\gamma}_{wpl}$	τ_{wpl}	$\dot{\gamma}_{wpl}$	τ_{wpl}	$\dot{\gamma}_{wpl}$
		$\Delta\dot{\gamma}_{w1}$		$\Delta\dot{\gamma}_{w1}$		$\Delta\dot{\gamma}_{w1}$		$\Delta\dot{\gamma}_{w1}$		$\Delta\dot{\gamma}_{w1}$
1.667	29.025	10.871	3.49	1.307	1.483	0.566	0.776	0.287	0.427	0.160
		0.00		0.00		0.00		0.00		0.00
16.67	290.252	108.709	34.898	13.070	14.835	5.556	7.660	2.869	4.266	1.598
		0.00		0.00		0.00		0.00		0.00

Table D7. Herschel-Bulkley shear rate at the wall, approximated to power law shear rate and the difference between the two shear rates for 2.0 % Kelset:
 $\eta = 27.0$, $n = 0.5$ and $\tau_0 = 8.8$.

K	0.852			0.773			0.682			0.568		
	$\dot{\gamma}_w$ HB	$\dot{\gamma}_w$ p1	$\Delta\dot{\gamma}_w$	$\dot{\gamma}_w$ HB	$\dot{\gamma}_w$ p1	$\Delta\dot{\gamma}_w$	$\dot{\gamma}_w$ HB	$\dot{\gamma}_w$ p1	$\Delta\dot{\gamma}_w$	$\dot{\gamma}_w$ HB	$\dot{\gamma}_w$ p1	$\Delta\dot{\gamma}_w$
$V_p \times 10^4$ (m/s)												
1.667	2.123	2.221	4.62	1.000	0.903	-9.70	0.580	0.509	-12.24	0.374	0.319	-14.71
16.67	19.127	22.301	16.59	8.579	9.069	5.71	4.726	5.112	8.17	2.872	3.201	11.46
45.00	50.654	60.201	19.00	22.417	24.481	9.21	12.184	13.802	13.28	7.280	8.643	18.72
62.00	69.325	82.946	19.65	30.648	33.73	10.06	16.602	19.015	14.53	9.876	11.908	20.58
83.33	92.811	111.479	20.11	40.938	45.334	10.74	22.115	25.557	15.56	13.108	16.005	22.10

Table D8. Herschel-Bulkley shear rate at the wall, approximated to power law shear rate at the wall, and the difference between the two shear rates for 1.5 % Kelset: $\eta = 9.1$, $n = 0.6$ and $\tau_0 = 9.746$.

K	0.852			0.773			0.682			0.568		
	$\dot{\gamma}_w$ HB	$\dot{\gamma}_w$ p1	$\Delta\dot{\gamma}_w$	$\dot{\gamma}_w$ HB	$\dot{\gamma}_w$ p1	$\Delta\dot{\gamma}_w$	$\dot{\gamma}_w$ HB	$\dot{\gamma}_w$ p1	$\Delta\dot{\gamma}_w$	$\dot{\gamma}_w$ HB	$\dot{\gamma}_w$ p1	$\Delta\dot{\gamma}_w$
$V_p \times 10^4$ (m/s)												
1.667	2.434	2.023	-16.89	1.257	0.989	-21.32	0.795	0.600	-24.53	0.557	0.407	-26.93
16.67	18.649	20.317	8.94	8.746	9.932	13.56	5.070	6.022	18.78	3.276	4.089	24.82
45.00	47.709	54.843	14.95	21.690	26.813	23.62	12.171	16.256	33.56	7.583	11.036	45.54
62.00	64.934	75.562	16.37	29.293	36.941	26.11	16.291	22.393	37.46	10.044	15.208	51.41
83.33	86.443	101.555	17.48	38.753	49.651	28.12	21.395	33.266	55.48	13.071	20.437	56.35

Table D9. Herschel-Bulkley shear rate at the wall, approximated to power law shear rate at the wall, and the difference between the two shear rates for 1.0 % Kelset: $n = 5.2$, $n = 0.4$ and $\tau_0 = 2.409$.

K $V_p \times 10^4$ (m/s)	0.852				0.773				0.682				0.568			
	$\dot{\gamma}_w$ HB	$\dot{\gamma}_w$ p1	$\dot{\gamma}_w$ p1	$\Delta \dot{\gamma}_w$	$\dot{\gamma}_w$ HB	$\dot{\gamma}_w$ p1	$\dot{\gamma}_w$ p1	$\Delta \dot{\gamma}_w$	$\dot{\gamma}_w$ HB	$\dot{\gamma}_w$ p1	$\dot{\gamma}_w$ p1	$\Delta \dot{\gamma}_w$	$\dot{\gamma}_w$ HB	$\dot{\gamma}_w$ p1	$\dot{\gamma}_w$ p1	$\Delta \dot{\gamma}_w$
1.667	2.598	2.380	-	8.39	1.237	1.109		-10.35	0.723	0.636		-12.03	0.469	0.405		-13.65
16.67	22.824	23.902		4.72	10.433	11.138		6.76	5.854	6.387		9.10	3.632	4.067		11.98
45.00	59.704	64.532		8.09	26.956	30.064		11.53	14.932	17.240		15.46	9.124	10.978		20.32
62.00	81.613	88.909		8.94	36.721	41.424		12.81	20.270	23.749		17.16	12.333	15.124		22.63
83.33	108.96	119.495		9.67	48.904	55.672		13.84	26.909	31.924		18.64	16.313	20.328		24.61

Table D10. Herschel-Bulkley shear stress at the wall, approximated to power law shear stress at the wall, and the difference between the two shear stresses for 2.0 % Kelset: $\eta = 27.0$, $n = 0.5$ and $\tau_0 = 8.8$.

K $V_p \times 10^4$ (m/s)	0.852			0.773			0.682			0.568		
	τ_w HB	τ_w p1	$\Delta\tau_w$	τ_w HB	τ_w p1	$\Delta\tau_w$	τ_w HB	τ_w p1	$\Delta\tau_w$	τ_w HB	τ_w p1	$\Delta\tau_w$
1.667	48.136	38.628	-19.75	35.800	25.157	-29.73	29.361	17.655	-39.87	25.307	12.242	-51.63
16.67	126.883	101.407	-20.08	87.881	61.087	-30.49	67.495	39.691	-41.19	54.56	25.303	-53.62
45.00	200.793	160.289	-20.17	136.637	94.707	-30.69	103.045	60.247	-41.53	81.650	37.434	-54.15
62.00	233.606	186.436	-20.19	158.275	109.630	-30.73	118.812	69.366	-41.62	93.649	42.811	-54.29
83.33	268.913	214.561	-20.21	181.555	125.686	-30.77	135.773	79.176	-41.69	106.552	48.595	-54.39

Table D11. Herschel-Bulkley shear stress at the wall, approximated to power law shear stress at the wall, and the difference between the two shear stresses for 1.5 % Kelset: $\eta = 9.1$, $n = 0.6$ and $\tau_0 = 9.746$.

K	0.852			0.773			0.682			0.568		
	τ_w HB	τ_w p1	$\Delta\tau_w$	τ_w HB	τ_w p1	$\Delta\tau_w$	τ_w HB	τ_w p1	$\Delta\tau_w$	τ_w HB	τ_w p1	$\Delta\tau_w$
$V_p \times 10^4$ (m/s)												
1.667	25.264	20.314	-19.59	20.187	14.523	-28.06	17.676	11.109	-37.15	16.149	8.400	-47.98
16.67	62.400	49.591	-20.53	43.174	30.273	-29.88	33.848	20.354	-39.87	28.291	13.701	-51.57
45.00	102.258	81.014	-20.77	67.396	46.908	-30.40	50.506	31.317	-37.99	40.432	19.066	-52.84
62.00	121.054	95.836	-20.83	78.785	54.734	-30.53	58.299	34.420	-40.96	46.070	21.569	-53.18
83.33	141.900	112.273	-20.88	91.408	63.411	-30.63	66.923	35.762	-46.56	56.289	24.355	-56.73

Table D12. Herschel-Bulkley shear stress at the wall, approximated to power law shear stress at the wall, and the difference between the two shear stresses for 1.0 % Kelset: $\eta = 5.2$, $n = 0.4$ and $\tau_0 = 2.409$.

K	0.852			0.773			0.682			0.568		
$V_p \times 10^4$ (m/s)	τ_w HB	τ_w pl	$\Delta\tau_w$	τ_w HB	τ_w pl	$\Delta\tau_w$	τ_w HB	τ_w pl	$\Delta\tau_w$	τ_w HB	τ_w pl	$\Delta\tau_w$
1.667	10.027	8.142	-18.80	8.071	5.823	-27.85	6.977	4.345	-37.72	6.250	3.160	-49.44
16.67	20.579	16.636	-19.16	15.694	11.203	-28.62	12.953	7.907	-38.96	11.120	5.425	-51.21
45.00	29.579	23.491	-19.28	21.830	15.531	-28.85	17.743	10.763	-39.34	15.001	7.235	-51.77
62.00	32.658	26.350	-19.32	24.386	17.334	-28.92	19.737	11.952	-39.44	16.614	7.987	-51.93
83.33	36.364	29.331	-19.34	27.055	19.217	-28.97	21.816	13.193	-39.53	18.295	8.773	-52.05

Table D13. Values of the experimental parameters for 1.0 % Methocel.

Ri cm	n	Vpi, Vpj $\times 10^4$ m/s	η New Pa·s	η pl Pa·s ⁿ	τ w pl Pa	$\dot{\gamma}$ w pl s ⁻¹	τ w New Pa	$\dot{\gamma}$ w New s ⁻¹	$\Delta \dot{\gamma}$ w1 %	$\Delta \tau$ w1 %
1.0	0.953	16.67 83.33	0.859 0.797	0.857 0.857	1.370 6.354	1.636 8.178	1.373 6.368	1.598 7.988	-2.32 -2.32	0.21 0.21
	0.843	62.00 16.67	0.699 0.859	0.853 0.852	4.123 1.362	6.490 1.745	4.156 1.373	5.943 1.598	-8.42 -8.42	0.79 0.79
	0.302	83.33 45.00	0.797 1.227	2.512 2.513	5.966 4.958	17.595 9.502	6.368 5.291	7.988 4.313	-54.60 -54.60	6.73 6.73

Best Vp combinations: 83/16, 62/16

Table D14. Values of the experimental parameters for 1.0 % Methocel.

Ri (cm)	n	Vpi, Vpj $\times 10^4$ m/s	η New (Pa·s)	η pl (Pa·s ⁿ)	τ_w pl (Pa)	$\dot{\gamma}_w$ pl (s ⁻¹)	τ_w New (Pa)	$\dot{\gamma}_w$ New (s ⁻¹)	$\Delta \dot{\gamma}_{w1}$ %	$\Delta \tau_{w1}$ %
1.2	0.988	83.33 45.00	0.598 0.603	0.614 0.614	8.579 4.668	14.411 7.782	8.583 4.669	14.341 7.744	- 0.49 - 0.49	0.04 0.04
	0.806	62.00 45.00	0.567 0.603	0.818 0.818	5.991 4.628	11.825 8.583	6.045 4.667	10.670 7.744	- 9.77 - 9.77	0.90 0.90
	0.900	83.33 16.67	0.598 0.703	0.744 0.744	8.547 2.007	15.043 3.009	8.583 2.016	14.341 2.869	- 4.67 - 4.66	0.42 0.42
	0.836	62.00 16.67	0.567 0.703	0.773 0.773	6.001 2.001	11.608 3.121	6.045 2.016	10.670 2.869	- 8.08 - 8.08	0.74 0.74

Best Vp combinations: 83/45, 83/16, 62/16

Table D15. Values of the experimental parameters for 1.0 % Methocel.

Ri (cm)	n	Vpi, Vpj x 10 ⁴ m/s	η New (Pa s)	η pl (Pa s ⁿ)	τ_w pl (Pa)	$\dot{\gamma}_w$ pl (s ⁻¹)	τ_w New (Pa)	$\dot{\gamma}_w$ New (s ⁻¹)	$\Delta \dot{\gamma}_w$ %	$\Delta \tau_w$ %
1.36	0.5899	83.33 45.00	0.304 0.391	1.003 1.003	8.288 5.762	35.881 19.377	8.441 5.870	27.774 14.998	-22.59 -22.60	1.85 1.88
	0.915	62.00 45.00	0.381 0.391	0.475 0.475	7.846 5.854	21.443 15.563	7.867 5.870	20.665 14.998	- 3.63 - 3.63	0.27 0.27
	0.732	83.33 16.67	0.304 0.468	0.660 0.660	8.353 2.571	32.032 6.408	8.441 2.598	27.774 5.556	-13.29 -13.29	1.06 1.06
	0.843	62.00 16.67	0.381 0.468	0.573 0.573	7.825 2.585	22.188 5.966	7.867 2.598	20.665 5.556	- 6.86 - 6.87	0.53 0.53
	0.820	45.00 16.67	0.391 0.468	0.589 0.589	5.832 2.582	16.351 6.057	5.870 2.598	14.998 5.556	- 8.27 - 8.27	0.65 0.65

Best Vp combinations: 62/45, 62/16, 45/16

Table D16. Values of the experimental parameters for 1.0 % Methocel.

Ri (cm)	n	Vpi, Vpj $\times 10^4$ m/s	η New (Pa s)	η pl (Pa s ⁿ)	τ_w pl (Pa)	$\dot{\gamma}_w$ pl (s ⁻¹)	τ_w New (Pa)	$\dot{\gamma}_w$ New (s ⁻¹)	$\Delta\dot{\gamma}_w$ %	$\Delta\tau_w$ %
1.50	0.7208	83.33	0.404	1.167	26.215	74.953	26.420	65.336	-12.83	0.78
		16.67	0.634	1.167	8.219	14.994	8.283	13.070	-12.83	0.78
	0.6515	62.00	0.401	1.362	19.291	58.482	19.491	48.612	-16.88	1.03
		16.67	0.634	1.362	8.198	15.724	8.283	13.070	-16.88	1.03
	0.3681	45.00	0.338	2.590	11.638	59.271	11.937	35.283	-40.47	2.57
		16.67	0.634	2.590	8.075	21.957	8.283	13.070	-40.47	2.57

Best Vp combinations: 83/16, 62/16, 45/16

Table D17. Values of the experimental parameters for 2.0 % Methocel.

Ri (cm)	n	Vpi, Vpj $\times 10^4$ m/s	Pi, Pj (Pa/m)	η_i, η_j (Pa.s ⁿ)	$\dot{\gamma}_w$ pl (s ⁻¹)	τ_w pl (Pa)	τ_w New (Pa)	$\Delta\dot{\gamma}_{w1}$ %
1.0	0.7092	83.33	15650.51	15.931	9.623	79.363	80.685	-16.99
		45.00	10111.78	15.934	5.197	51.276	52.131	-17.00
	0.5844	83.33	15812.99	19.504	10.846	78.551	80.685	-26.35
		16.67	6172.13	19.497	2.170	30.660	31.493	-26.35
	0.4544	62.00	11375.05	19.677	9.579	54.935	57.237	-37.96
		16.67	6258.79	19.665	2.575	30.227	31.493	-37.95
	0.5069	45.00	10297.58	19.583	6.442	50.347	52.131	-33.05
		16.67	6220.96	19.571	2.387	30.416	31.493	-33.04

Best Vp combinations: 83/45, 83/16, 45/16

Table D18. Values of the experimental parameters for 2.0 % Methocel.

Ri (cm)	n	Vpi, Vpj $\times 10^4$ m/s	Pi, Pj (Pa/m)	η_i, η_j (Pa.s ⁿ)	$\dot{\gamma}_w$ pl (s ⁻¹)	τ_w pl (Pa)	τ_w New (Pa)	$\Delta \dot{\gamma}_{w1}$ %
1.2	0.5769	62.00	23341.19	16.786	14.214	77.614	79.512	-24.93
		16.67	10939.94	16.785	3.822	36.376	37.266	-24.93
	0.7036	45.00	21894.29	15.466	9.224	73.843	74.962	-16.05
		16.67	10884.35	15.463	3.417	36.710	37.266	-16.04

Best Vp combinations: 45/16, 62/16

Table D19. Values of the experimental parameters for 2.0 % Methocel.

Ri (cm)	n	Vpi, Vpj $\times 10^4$ m/s	Pi, Pj (Pa/m)	η_i, η_j (Pa.s ⁿ)	$\dot{\gamma}_{w\ pl}$ (s ⁻¹)	$\tau_{w\ pl}$ (Pa)	$\tau_{w\ New}$ (Pa)	$\dot{\Delta\gamma}_{w1}$ %
1.36	0.2569	83.33	25864.96	19.274	61.719	55.583	58.399	-55.00
		45.00	22078.08	19.274	33.330	47.445	49.849	-55.00
	0.3768	83.33	25737.78	13.202	47.280	56.448	58.399	-41.26
		16.67	14033.83	13.200	9.458	30.779	31.843	-41.26
	0.5873	62.00	30203.91	9.825	26.689	67.614	68.879	-22.57
		16.67	13963.32	9.824	7.176	31.258	31.843	-22.57
	0.4512	45.00	21929.75	11.869	22.593	48.454	49.849	-33.62
		16.67	14008.43	11.868	8.369	30.951	31.843	-33.62

Best Vp combinations: 62/16, 45/16, 83/16

Table D20. Values of the experimental parameters for 2.0 % Methocel.

Ri (cm)	n	Vpi, Vpj $\times 10^4$ m/s	Pi, Pj (Pa/m)	η_i, η_j (Pa.s ⁿ)	$\dot{\gamma}_w$ pl (s ⁻¹)	τ_w pl (Pa)	τ_w New (Pa)	$\Delta \dot{\gamma}_{w1}$ %
1.50	0.9203	83.33	89149.39	2.603	67.510	125.634	125.886	- 3.22
		45.00	50562.67	2.603	36.457	71.255	71.399	- 3.22
	0.2559	83.33	89673.84	34.487	138.053	121.700	125.886	-52.67
		62.00	83138.85	34.487	102.716	112.831	116.712	-52.67
	0.3997	83.33	89493.86	19.306	102.9133	123.050	125.886	-36.51
		16.67	47034.63	19.305	30.588	64.671	66.161	-36.51
	0.4321	62.00	82946.41	17.820	73.739	114.275	116.712	-34.08
		16.67	47020.13	17.820	19.826	64.779	66.161	-34.08

Best Vp combinations: 83/45, 62/16, 83/16

Table D21. Values of the experimental parameters for 1.0 % guar gum.

Ri (cm)	n	Vpi, Vpj $\times 10^4$ m/s	Pi, Pj (Pa/m)	η_i, η_j (Pa.s ⁿ)	$\dot{\gamma}_w$ pl (s ⁻¹)	τ_w pl (Pa)	τ_w New (Pa)	$\Delta\dot{\gamma}_{w1}$ %
1.00	0.6962	45.00	2343.841	3.884	5.252	12.325	12.541	-17.87
		83.33	3739.196	3.884	9.725	18.927	19.259	-17.86
	0.3183	62.00	2814.440	5.835	12.539	13.051	13.884	-52.60
		45.00	2542.133	5.837	9.101	11.788	12.541	-52.61
	0.5717	83.33	3779.026	4.755	11.000	18.728	19.295	-27.38
		16.67	1505.505	4.753	2.200	7.461	7.673	-27.38
	0.4515	62.00	2760.450	4.792	9.626	13.321	13.884	-38.26
		16.67	1525.446	4.792	2.588	7.361	7.673	-38.26
	0.4945	45.00	2480.58	4.776	6.549	12.096	12.541	-34.14
		16.67	1517.621	4.774	2.426	7.400	7.673	-34.13

Best Vp combinations: 83/45, 83/16, 45/16

Table D22. Values of the experimental parameters for 1.0 % guar gum.

Ri (cm)	n	Vpi, Vpj $\times 10^4$ m/s	Pi, Pj (Pa/m)	η_i, η_j (Pa.s ⁿ)	$\dot{\gamma}_w$ pl (s ⁻¹)	τ_w pl (Pa)	τ_w New (Pa)	$\dot{\Delta\gamma}_{w1}$ %
1.20	0.4720	83.33	6021.53	4.623	21.628	19.726	20.404	-33.69
		45.00	4502.37	4.623	11.680	14.749	15.256	-33.70
	0.8629	62.00	5848.37	2.442	11.439	19.997	20.119	- 6.72
		45.00	4433.28	2.441	8.302	15.164	15.256	- 6.72
	0.4880	83.33	6016.04	4.456	21.157	19.759	21.404	-32.21
		16.67	2743.38	4.456	4.232	9.010	9.304	-32.21
	0.5870	62.00	5904.61	4.170	14.021	19.648	20.119	-23.90
		16.67	2730.68	4.170	3.770	9.086	9.304	-23.90
	0.4980	45.00	4495.80	4.425	11.276	14.789	15.256	-31.32
		16.67	2741.88	4.425	4.177	9.019	9.304	-31.32

Best Vp combinations: 62/45, 62/16, 45/16

Table D23. Values of the experimental parameters for 1.0 % guar gum.

Ri (cm)	n	Vpi, Vpj $\times 10^4$ m/s	Pi, Pj (Pa/m)	η_i, η_j (Pa.s ⁿ)	$\dot{\gamma}_w$ pl (s ⁻¹)	τ_w pl (Pa)	τ_w New (Pa)	$\Delta \dot{\gamma}_{w1}$ %
1.36	0.2549	83.33	6055.84	4.551	61.699	13.015	± 3.674	-54.99
		45.00	5175.55	4.551	33.319	11.123	11.186	-54.99
	0.6415	83.33	5989.25	1.399	34.126	13.468	13.674	-18.61
		62.22	4952.61	1.395	25.391	11.137	11.307	-18.61
	0.3565	83.33	6032.52	3.297	48.700	13.174	13.674	-42.97
		16.67	3397.37	3.295	9.742	7.419	7.701	-42.97
	0.2924	62.00	5000.21	3.633	41.687	10.813	11.307	-50.43
		16.67	3405.41	3.633	11.208	7.633	7.701	-50.43
	0.4195	45.00	5145.38	3.007	23.618	11.328	11.686	-36.50
		16.67	3390.62	3.005	8.749	7.465	7.701	-36.50

Best Vp combinations: 83/62, 45/16, 83/16

Table D24. Values of the experimental parameters for 1.0 % guar gum.

Ri (cm)	n	Vpi, Vpj x 10 ⁴ m/s	Pi, Pj (Pa/m)	η_i, η_j (Pa.s ⁿ)	$\dot{\gamma}_w$ pl (s ⁻¹)	τ_w pl (Pa)	τ_w New (Pa)	$\Delta\dot{\gamma}_{w1}$ %
1.50	0.2895	62.00 16.67	19998.87 13675.34	7.271 7.272	95.605 25.705	27.223 18.616	28.088 19.207	-49.15 -49.15

Table D25. Values of the experimental parameters for 1.5 % guar gum.

Ri (cm)	n	Vpi, Vpj $\times 10^4$ m/s	Pi, Pj (Pa/m)	η_i, η_j (Pa.s ⁿ)	$\dot{\gamma}_w$ pl (s ⁻¹)	τ_w pl (Pa)	τ_w New (Pa)	$\Delta \dot{\gamma}_{w1}$ %
1.0	0.1154	83.33	9474.403	25.906	40.930	39.759	44.603	-80.48
		62.00	9156.043	25.905	30.453	38.423	43.105	-80.48
	0.2972	83.33	9075.061	17.742	17.813	41.756	44.603	-55.16
		45.00	7556.990	17.743	9.619	34.771	37.142	-55.16
	0.4650	62.00	8555.126	14.600	9.420	41.428	43.105	-36.91
		45.00	7371.737	14.602	6.837	35.697	37.142	-36.92
	0.1691	83.33	9331.245	22.920	28.871	40.475	44.603	-72.33
		16.67	7107.580	22.918	5.776	30.830	33.974	-72.33
	0.1812	62.00	8989.670	22.772	20.192	39.255	43.105	-70.57
		16.67	7085.499	22.771	5.429	30.940	33.974	-70.57
	0.0896	45.00	7956.705	24.302	28.141	32.772	37.142	-84.67
		16.67	7278.076	24.298	10.424	29.977	33.974	-84.67

Best Vp combinations: 62/45, 83/45, 62/16, 83/16

Table D26. Values of the experimental parameters for 1.5 % guar gum.

Ri (cm)	n	Vpi, Vpj $\times 10^4$ m/s	Pi, Pj (Pa/m)	η_i, η_j (Pa.s ⁿ)	$\dot{\gamma}_w$ pl (s ⁻¹)	τ_w pl (Pa)	τ_w New (Pa)	$\dot{\Delta\gamma}_{w1}$ %
1.2	0.2828	62.00	13086.54	16.967	23.151	41.257	43.754	-53.91
		16.67	9027.36	16.969	6.225	28.460	30.182	-53.91
	0.3825	45.00	13098.22	15.643	13.425	42.244	44.140	-42.32
		16.67	8956.41	15.639	4.973	28.886	30.182	-42.31

Best Vp combinations: 45/16, 62/16

Table D27. Values of the experimental parameters for 1.5 % guar gum.

Ri (cm)	n	Vpi, Vpj $\times 10^4$ m/s	Pi, Pj (Pa/m)	η_i, η_j (Pa.s ⁿ)	$\dot{\gamma}_w$ pl (s ⁻¹)	τ_w pl (Pa)	τ_w New (Pa)	$\Delta \dot{\gamma}_{w1}$ %
1.36	0.1532	83.33	14081.62	14.809	92.290	29.621	31.633	-69.91
		16.67	11004.40	14.809	18.462	23.148	24.720	-69.91
	0.2239	45.00	13696.45	13.067	36.660	29.269	30.883	-59.09
		16.67	10963.22	13.064	13.581	23.428	24.720	-59.09

Best Vp combinations: 45/16, 83/16

Table D28. Values of the experimental parameters for 1.5 % guar gum.

Ri (cm)	n	Vpi, Vpj x 10 ⁴ m/s	Pi, Pj (Pa/m)	η_i, η_j (Pa.s ⁿ)	$\dot{\gamma}_w$ pl (s ⁻¹)	τ_w pl (Pa)	τ_w New (Pa)	$\dot{\Delta\gamma}_{w1}$ %
1.5	0.1847	83.33	32255.10	16.633	179.410	43.378	45.218	-63.58
		45.00	28785.11	16.633	96.885	38.711	40.353	-63.58
	0.6446	62.00	35189.57	3.568	58.411	49.108	49.614	-16.78
		45.00	28621.08	3.568	42.395	39.941	40.353	-16.78

Best Vp combinations: 62/45, 83/45

Table D29. Values of the experimental parameters for 1.5 % Methocel.

Ri (cm)	n	Vpi, Vpj x 10 ⁴ m/s	Pi, Pj (Pa/m)	η_i, η_j (Pa.s ⁿ)	$\dot{\gamma}_w$ pl (s ⁻¹)	τ_w pl (Pa)	τ_w New (Pa)	$\Delta \dot{\gamma}_{w1}$ %
1.0	0.4954	83.33	1354.943	1.921	12.108	6.609	6.851	-34.03
		62.00	1170.275	1.921	9.009	5.708	5.917	-34.03
	0.8670	83.33	9633.42	1.054	8.598	6.806	6.851	- 7.10
		45.00	770.72	1.053	4.643	3.987	4.014	- 7.11
	0.8897	83.33	1313.80	1.017	8.479	6.814	6.851	- 5.78
		16.67	313.62	1.017	1.696	1.627	1.635	- 5.78
	0.9785	62.00	1129.61	1.022	6.008	5.911	5.917	- 1.09
		16.67	312.20	1.022	1.616	1.634	1.635	- 1.08
	0.9039	45.00	769.13	1.018	4.540	3.995	4.014	- 5.01
		16.67	313.372	1.017	1.682	1.628	1.635	- 4.99

Best Vp combinations: 62/16, 45/16, 83/16

Table D30. Values of the experimental parameters for 1.5 % Methocel.

Ri (cm)	n	Vpi, Vpj $\times 10^4$ m/s	Pi, Pj (Pa/m)	η_i, η_j (Pa.s ⁿ)	$\dot{\gamma}_w$ pl (s ⁻¹)	τ_w pl (Pa)	τ_w New (Pa)	$\Delta\dot{\gamma}_{w1}$ %
1.2	0.8359	83.33	3009.523	1.034	15.602	10.273	10.349	- 8.08
		62.00	2350.275	1.034	11.608	8.023	8.082	- 8.08
	0.8022	83.33	3012.798	1.112	15.952	10.254	10.349	-10.10
		45.00	1837.636	1.112	8.614	6.254	6.312	-10.10
	0.7712	62.00	2354.970	1.169	12.094	7.995	8.082	-11.78
		45.00	1839.300	1.169	8.778	6.244	6.312	-11.78
	0.8807	83.33	3005.710	0.937	15.207	10.296	10.349	- 5.70
		16.67	728.220	0.936	3.042	2.495	2.507	- 5.70
	0.8908	62.00	2346.870	0.929	11.273	8.043	8.082	- 5.35
		16.67	728.090	0.929	3.031	2.495	2.507	- 5.34
	0.9294	45.00	1830.988	0.910	8.007	6.294	6.312	- 3.29
		16.67	727.290	0.910	2.966	2.500	2.507	- 3.28

Best Vp combinations: 45/16, 62/16, 83/16

Table D31. Values of the experimental parameters for 1.5 % Methocel.

Ri (cm)	n	Vpi, Vpj $\times 10^4$ m/s	Pi, Pj (Pa/m)	η_i, η_j (Pa.s ⁿ)	$\dot{\gamma}_w$ pl (s ⁻¹)	τ_w pl (Pa)	τ_w New (Pa)	$\Delta \dot{\gamma}_{w1}$ %
1.36	0.1384	83.33	2884.98	3.195	100.427	6.046	6.475	-72.34
		62.00	2769.85	3.195	74.721	5.805	6.217	-72.34
	0.797	83.33	2829.20	0.419	30.744	6.425	6.475	- 9.66
		45.00	1731.44	0.419	16.602	3.932	3.963	- 9.66
	0.8052	83.33	2828.85	0.409	30.588	6.428	6.475	- 9.20
		16.67	773.96	0.409	6.119	1.759	1.772	- 9.20
	0.9553	62.00	2710.59	0.338	21.032	6.208	6.217	- 1.74
		16.67	772.43	0.338	5.655	1.769	1.772	- 1.75
	0.8103	45.00	1731.01	0.407	16.432	3.935	3.963	- 8.73
		16.67	773.86	0.407	6.087	1.759	1.772	- 8.72

Best Vp combinations: 62/16, 45/16, 83/16

Table D32. Values of the experimental parameters for 1.5 % Methocel.

Ri (cm)	n	Vpi, Vpj $\times 10^4$ m/s	Pi, Pj (Pa/m)	η_i, η_j (Pa.s ⁿ)	$\dot{\gamma}_w$ pl (s ⁻¹)	τ_w pl (Pa)	τ_w New (Pa)	$\dot{\Delta\gamma}_{w1}$ %
1.5	0.6815	83.33	21550.48	1.553	77.451	30.104	30.389	-15.64
		62.00	17617.13	1.553	57.626	24.609	24.842	-15.64
	0.7896	83.33	21533.87	1.038	72.508	30.228	30.389	- 8.63
		16.67	6043.38	1.038	14.305	8.483	8.528	- 8.63
	0.8139	62.00	17603.54	0.971	53.370	24.711	24.842	- 8.92
		16.67	6043.38	0.971	14.350	8.483	8.528	- 8.92
	0.4237	45.00	9143.31	2.407	54.495	12.584	12.863	-35.25
		16.67	6062.05	2.407	20.187	8.343	8.528	-35.26

Best Vp combinations: 83/16, 62/16

Table D33. Values of the experimental parameters for high sucrose corn syrup.

Ri (cm)	n	Vpi, Vpj $\times 10^4$ m/s	Pi, Pj (Pa/m)	η_i, η_j (Pa.s ⁿ)	$\dot{\gamma}_w$ pl (s ⁻¹)	τ_w pl (Pa)	τ_w New (Pa)	$\Delta \dot{\gamma}_{w1}$ %
1.0	0.7908	83.33	421.74	0.379	9.039	2.163	2.186	-11.62
		16.67	118.15	0.379	1.808	0.606	0.612	-11.62
	0.4859	62.00	229.62	0.381	9.141	1.117	1.160	-34.98
		16.67	121.28	0.381	2.458	0.590	0.612	-34.98

Best Vp combinations: 83/16, 62/16

Table D34. Values of the experimental parameters for high sucrose corn syrup.

Ri (cm)	n	Vpi, Vpj $\times 10^4$ m/s	Pi, Pj (Pa/m)	η_i, η_j (Pa.s ⁿ)	$\dot{\gamma}_w$ pl (s ⁻¹)	τ_w pl (Pa)	τ_w New (Pa)	$\Delta\dot{\gamma}_{w1}$ %
1.2	0.8565	83.33 62.00	516.58 401.02	0.169 0.169	15.447 11.493	1.768 1.372	1.778 1.380	- 7.16 - 7.16
	0.8228	83.33 16.67	517.22 137.54	0.183 0.183	15.718 3.144	1.764 0.469	1.778 0.473	- 8.76 - 8.76
	0.8152	62.00 16.67	401.59 137.57	0.184 0.184	11.738 3.156	1.369 0.469	1.380 0.473	- 9.10 - 9.10
	0.6005	45.00 16.67	251.82 138.65	0.210 0.210	10.066 3.729	0.840 0.462	0.859 0.473	-23.07 -23.06

Best Vp combinations: 83/62, 83/16, 62/16

Table D35. Values of the experimental parameters for high sucrose corn syrup.

Ri (cm)	n	Vpi, Vpj $\times 10^4$ m/s	Pi, Pj (Pa/m)	η_i, η_j (Pa.s ⁿ)	$\dot{\gamma}_w$ pl (s ⁻¹)	τ_w pl (Pa)	τ_w New (Pa)	$\Delta\dot{\gamma}_{w1}$ %
1.36	0.4341	83.33	527.46	0.227	42.913	1.163	1.198	-35.28
		62.00	463.90	0.227	31.929	1.023	1.054	-35.28
	1.061	83.33	521.93	0.036	27.091	1.201	1.198	2.50
		45.00	271.25	0.036	14.630	0.624	0.623	2.50
	0.7136	83.33	524.26	0.099	32.360	1.185	1.198	-14.17
		16.67	166.26	0.099	6.474	0.376	0.380	-14.17
	0.7765	62.00	460.63	0.091	23.104	1.045	1.054	-10.56
		16.67	166.10	0.091	6.212	0.377	0.380	-10.56
	0.4975	45.00	273.65	0.133	21.248	0.608	0.623	-29.41
		16.67	166.985	0.133	7.871	0.371	0.380	-29.41

Best Vp combinations: 83/45, 62/16, 83/16

Table D36. Values of the experimental parameters for high sucrose corn syrup.

Ri (cm)	n	Vpi, Vpj $\times 10^4$ m/s	Pi, Pj (Pa/m)	η_i, η_j (pa.s ⁿ)	$\dot{\gamma}_w$ pl (s ⁻¹)	τ_w pl (Pa)	τ_w New (Pa)	$\Delta \dot{\gamma}_{w1}$ %
1.5	0.7798	83.33	5016.12	0.248	72.761	7.034	7.078	-10.20
		62.00	3983.26	0.248	54.138	5.586	5.620	-10.20
	1.129	83.33	5007.63	0.067	61.991	7.098	7.078	5.40
		45.00	2496.49	0.067	33.476	3.539	3.528	5.40
	1.141	83.33	5007.63	0.064	62.053	7.098	7.078	5.29
		16.67	797.31	0.064	12.414	1.130	1.127	5.29

Best Vp combinations: 83/16, 83/45, 83/16

Table D37. Values of the experimental parameters for 1.25 % Kelset.
 $Ri = 1.0 \text{ cm}$

n HB	η_{HB} (Pa.s ⁿ)	τ_o (Pa)	$\tau_w HB$ (Pa)	$\dot{\gamma}_w HB$ (s ⁻¹)	V _{pi} , V _{pj} x 10 ⁴ m/s	n pl	$\eta_{i,j pl}$ (Pa.s ⁿ)	$\tau_w pl$ (Pa)	$\dot{\gamma}_w pl$ (s ⁻¹)	$\Delta \dot{\gamma}_{w2}$ %
0.5	15.95	3.906	61.073	12.846	83.33	0.718	17.926	90.566	9.551	-25.65
			30.412	2.762	16.67		17.914	28.512	1.911	-30.82
			53.460	9.653	62.00	0.464	18.073	51.202	9.431	- 2.30
			30.412	2.762	16.67		18.075	27.839	2.536	- 8.19
			46.379	7.091	45.00	0.315	18.512	37.217	9.173	29.36
			30.412	2.762	16.67		18.511	27.215	3.398	23.03

Best Vp combinations: 62/16, 45/16, 83/16

Table D38. Values of the experimental parameters for 1.25 % Kelset.
Ri = 1.2 cm

n HB	η_{HB} (Pa.s ⁿ)	τ_o (Pa)	$\tau_w HB$ (Pa)	$\dot{\gamma}_w HB$ (s ⁻¹)	Vpi, Vpj x 10 ⁴ m/s	n pl	η_{pl} (Pa.s ⁿ)	$\tau_w pl$ (Pa)	$\dot{\gamma}_w pl$ (s ⁻¹)	$\Delta \dot{\gamma}_{w2}$ %
0.6	10.75	2.068	65.302	19.168	83.33	0.322	14.704	43.054	28.208	47.16
			26.755	3.997	16.67		14.701	25.651	5.643	41.18
			55.186	14.335	62.00	0.433	13.483	46.002	16.984	18.48
			26.755	3.997	16.67		13.479	26.028	4.567	14.25
			46.070	10.474	45.00	0.547	12.419	45.298	10.665	1.83
			26.755	3.997	16.67		12.417	26.318	3.951	- 1.51

Best Vp combinations: 45/16, 62/16, 83/16

Table D39. Values of the experimental parameters for 1.25 % Kelset.
 $Ri = 1.5 \text{ cm}$

n HB	η_{HB} (Pa.s ⁿ)	τ_o (Pa)	$\tau_w HB$ (Pa)	$\dot{\gamma}_w HB$ (s ⁻¹)	n pl	Vpi, Vpj x 10 ⁴ m/s	η_{pl} (Pa.s ⁿ)	$\tau_w pl$ (Pa)	$\dot{\gamma}_w pl$ (s ⁻¹)	$\Delta \dot{\gamma}_{w2}$ %
0.4	7.250	4.955	52.766	111.682	0.618	83.33	5.615	85.296	81.355	-27.16
			30.728	23.827		16.67	5.614	31.523	16.275	-31.70
			47.592	83.872	0.321	62.00	11.194	47.224	89.003	6.12
			30.728	23.827		16.67	11.194	30.989	23.931	0.43
			42.632	61.568	0.396	45.00	9.368	46.197	56.109	- 8.66
			30.728	23.827		16.67	9.367	31.169	20.785	-12.77

Best Vp combinations: 62/16, 45/16, 83/16

Table D40. Values of the experimental parameters for 1.5 % Kelset.
Ri = 1.0 cm

n HB	η_{HB} (Pa.s ⁿ)	τ_o (Pa)	$\tau_w HB$ (Pa)	$\dot{\gamma}_w HB$ (s ⁻¹)	Vpi, Vpj x 10 ⁴ m/s	n pl	η_{pl} (Pa.s ⁿ)	$\tau_w pl$ (Pa)	$\dot{\gamma}_w pl$ (s ⁻¹)	$\Delta \dot{\gamma}_{w2}$ %
0.6	12.325	4.697	58.228 42.422	11.562 6.453	83.33 45.00	0.613	14.424 14.424	61.067 41.849	10.517 5.679	- 9.04 -11.99
			58.228 26.489	11.562 2.585	83.33 16.67	0.590	14.971 14.968	60.940 23.562	10.779 2.156	- 6.77 -16.58
			49.916 26.489	8.728 2.585	62.00 16.67	0.485	15.072 15.068	44.064 23.304	9.142 2.458	4.75 4.90
			42.422 26.489	6.453 2.585	45.00 16.67	0.576	14.982 14.978	41.707 23.530	5.911 2.190	- 8.39 -15.29

Best Vp combinations: 62/16, 83/16, 83/45

Table D41. Values of the experimental parameters for 1.5 % Kelset.
 $Ri = 1.2 \text{ cm}$

n HB	η_{HB} (Pa.s ⁿ)	τ_o (Pa)	$\tau_w HB$ (Pa)	$\dot{\gamma}_w HB$ (s ⁻¹)	Vpi, Vpj x 10 ⁴ m/s	n pl	η_{pl} (Pa.s ⁿ)	$\tau_w pl$ (Pa)	$\dot{\gamma}_w pl$ (s ⁻¹)	$\Delta \dot{\gamma}_{w2}$ %
0.6	9.200	3.735	58.790 50.127	19.725 14.828	83.33 62.00	0.713	8.155 8.151	16.947 12.609	61.375 49.683	-14.11 -14.96
			58.790 42.311	19.725 10.903	83.33 45.00	0.623	9.976 9.974	18.266 9.864	61.002 41.540	- 7.40 - 9.53
			50.127 42.311	14.828 10.903	62.00 45.00	0.540	11.454 11.457	14.757 10.711	49.057 41.268	- 0.48 - 1.76
			58.790 25.738	19.725 4.277	83.33 16.67	0.482	13.788 13.784	21.339 4.269	60.258 27.741	8.18 - 0.19
			50.127 25.738	14.828 4.277	62.00 16.67	0.430	14.300 14.303	17.145 4.610	48.504 27.585	15.62 7.78
			42.311 25.738	10.903 4.277	45.00 16.67	0.394	14.714 14.712	40.637 27.473	13.168 4.878	20.78 14.05

Best Vp combinations: 83/16, 62/45, 83/45, 62/16

Table D42. Values of the experimental parameters for 1.5 % Kelset.
 $Ri = 1.36 \text{ cm}$

n HB	η_{HB} (Pa.s ⁿ)	τ_o (Pa)	$\tau_w HB$ (Pa)	$\dot{\gamma}_w HB$ (s ⁻¹)	Vpi, Vpj x 10 ⁴ m/s	n pl	η_{pl} (Pa.s ⁿ)	$\tau_w pl$ (Pa)	$\dot{\gamma}_w pl$ (s ⁻¹)	$\Delta \dot{\gamma}_{w2}$ %
0.6	5.05	0.505	43.695 30.417	35.768 19.391	83.33 45.00	0.399	8.709 8.709	39.894 31.190	45.169 24.392	26.28 25.79
			36.711 30.417	26.657 19.391	62.00 45.00	0.549	6.062 6.062	37.642 31.566	27.780 20.163	4.21 3.98
			43.695 17.093	35.768 7.258	83.33 16.67	0.407	8.519 8.518	39.930 20.746	44.592 8.921	24.67 22.91
			36.711 17.093	26.657 7.258	62.00 16.67	0.445	8.068 8.067	37.352 20.815	31.302 8.416	17.42 15.96
			30.417 17.093	19.391 7.258	45.00 16.67	0.411	8.459 8.458	31.228 20.753	23.920 8.861	23.35 22.08

Best Vp combinations: 45/62, 62/16, 45/16

Table D43. Values of the experimental parameters for 1.5 % Kelset.
 $Ri = 1.5 \text{ cm}$

n HB	η_{HB} (Pa.s ⁿ)	τ_o (Pa)	$\tau_w HB$ (Pa)	$\dot{\gamma}_w HB$ (s ⁻¹)	Vpi, Vpj x 10 ⁴ m/s	n pl	η_{pl} (Pa.s ⁿ)	$\tau_w pl$ (Pa)	$\dot{\gamma}_w pl$ (s ⁻¹)	$\Delta \dot{\gamma}_{w2}$ %
0.4	9.15	6.40	60.253	84.037	62.00	0.356	12.331	59.507	83.411	- 0.75
			53.992	61.699	45.00		12.331	53.094	60.540	- 1.88
			60.253	84.037	62.00	0.359	12.212	59.539	81.996	- 2.43
			38.967	23.90	16.67		12.216	37.142	22.046	- 7.76
			53.992	61.699	45.00	0.361	12.207	53.146	59.108	- 4.20
			38.967	23.90	16.67		12.210	37.158	21.896	- 8.38

Best Vp combinations: 62/45, 62/16, 45/16

Table D44. Values of the experimental parameters for 2.0 % Kelset.
 $Ri = 1.0 \text{ cm}$

n HB	η_{HB} (Pa.s ⁿ)	τ_o (Pa)	$\tau_w HB$ (Pa)	$\dot{\gamma}_w HB$ (s ⁻¹)	Vpi, Vpj x 10 ⁴ m/s	n pl	η_{pl} (Pa.s ⁿ)	$\tau_w pl$ (Pa)	$\dot{\gamma}_w pl$ (s ⁻¹)	$\Delta \dot{\gamma}_{w2}$ %
0.6	29.10	7.18	111.923	8.454	62.00	0.663	28.678	108.604	7.454	-11.83
			94.256	6.214	45.00		28.679	87.822	5.410	-12.94
			111.923	8.459	62.00	0.519	34.782	107.154	8.733	3.30
			56.790	2.433	16.67		34.764	54.151	2.348	- 3.49
			94.256	6.214	45.00	0.473	34.927	86.195	6.758	8.75
			56.790	2.433	16.67		34.906	53.867	2.503	2.89

Best Vp combinations: 62/16, 45/16, 45/62

Table D45. Values of the experimental parameters for 2.0 % Kelset.
 $Ri = 1.2 \text{ cm}$

n HB	η_{HB} (Pa.s ⁿ)	τ_o (Pa)	$\tau_w HB$ (Pa)	$\dot{\gamma}_w HB$ (s ⁻¹)	Vpi, Vpj $\times 10^4 \text{ m/s}$	n pl	η_{pl} (Pa.s ⁿ)	$\tau_w pl$ (Pa)	$\dot{\gamma}_w pl$ (s ⁻¹)	$\Delta \dot{\gamma}_{w2}$ %
0.6	23.10	6.805	102.475	10.681	45.00	0.411	36.380	103.667	12.811	19.94
			122.076	14.572	62.00		36.371	118.216	17.651	21.13
			143.823	19.436	83.33	0.471	29.831	126.913	21.661	11.45
			60.928	4.133	16.67		29.828	59.489	4.333	4.85
			122.076	14.572	62.00	0.528	28.658	119.670	14.992	2.88
			60.928	4.133	16.67		28.658	59.820	4.031	-2.47
			102.475	10.681	45.00	0.566	27.915	105.280	10.445	-2.21
			60.928	4.133	16.67		27.910	60.013	3.869	-6.38

Best Vp combinations: 62/16, 45/16, 83/16

Table D46. Values of the experimental parameters for 2.0 % Kelset.
 $Ri = 1.36 \text{ cm}$

n HB	η_{HB} (Pa.s ⁿ)	τ_o (Pa)	$\tau_w HB$ (Pa)	$\dot{\gamma}_w HB$ (s ⁻¹)	V_{pi}, V_{pj} x 10 ⁴ m/s	n pl	η_{pl} (Pa.s ⁿ)	$\tau_w pl$ (Pa)	$\dot{\gamma}_w pl$ (s ⁻¹)	$\Delta \dot{\gamma}_{w2}$ %
0.6	9.20	1.678	56.514 80.705	19.594 36.028	45.00 83.33	0.569	10.523 10.523	57.362 81.441	19.715 36.508	0.62 1.33
			32.231 80.705	7.392 36.028	16.67 83.33	0.421	16.402 16.404	40.876 80.528	8.735 43.667	18.18 21.20
			32.231 67.980	7.392 26.889	16.67 62.00	0.517	14.333 14.333	41.191 81.204	7.715 28.693	4.37 6.71
			32.231 56.514	7.392 19.594	16.67 45.00	0.330	18.785 18.786	40.502 56.201	10.274 27.734	38.99 41.54

Best Vp combinations: 45/83, 62/16, 83/16

Table D47. Values of the experimental parameters for 2.0 % Kelset.
 $Ri = 1.5 \text{ cm}$

n HB	η_{HB} (Pa.s ⁿ)	τ_o (Pa)	$\tau_w HB$ (Pa)	$\dot{\gamma}_w HB$ (s ⁻¹)	V_{pi}, V_{pj} x 10 ⁴ m/s	n pl	η_{pl} (Pa.s ⁿ)	$\tau_w pl$ (Pa)	$\dot{\gamma}_w pl$ (s ⁻¹)	$\Delta \dot{\gamma}_{w2}$ %
0.4	22.45	7.994	122.53 85.753	58.791 22.327	45.00 16.67	0.344	29.020 29.017	119.568 84.951	61.238 22.685	4.16 1.60

MICHIGAN STATE UNIV. LIBRARIES



31293009930979